

THESIS FOR THE DEGREE OF DOCTOR OF PHILOSOPHY

FUNCTIONAL FIBER BASED MATERIALS FOR MICROSYSTEM
APPLICATIONS

CARL ZANDÉN



CHALMERS

Department of Microtechnology and Nanoscience (MC2)

CHALMERS UNIVERSITY OF TECHNOLOGY

Göteborg, Sweden 2014

Functional Fiber Based Materials for Microsystem Applications

CARL ZANDÉN

ISBN 978-91-7597-082-0

Copyright ©Carl Zandén, 2014.

Doktorsavhandlingar vid Chalmers tekniska högskola

Ny serie nr 3763

ISSN 0346-718X.

Technical Report MC2-287

ISSN 1652-0769

CHALMERS UNIVERSITY OF TECHNOLOGY

Department of Microtechnology and Nanoscience - MC2

BioNano Systems Laboratory

SE-412 96 Göteborg, Sweden

Phone +46 (0) 31 772 1000

Abstract

This thesis explores the integration of functional electrospun micro- and nanofiber based materials in two fields of microsystem technology: fibrous scaffolds as cell culture substrates and fiber-reinforced metal matrix composites as thermal interface materials (TIMs).

Electrospun structures have been found to carry great potential as biomimicking microenvironments for future tissue engineering and cell culture applications. In the first part of this thesis, electrospun polyurethane fiber architectures have been fabricated, characterized and studied as cell culture scaffolds. The effects of plasma treatment, as a physical surface modification of the electrospun scaffold interface, are characterized and demonstrated to improve the possibility for human embryonic stem cell culture expansion. Electrospun scaffolds with specific fiber diameters are shown to allow maintenance of astrocytes with complex morphologies, limit up-regulation of protein expression related to astrocyte stress and activation, and to facilitate the formation of three-dimensional neuronal networks. Taken together, these findings indicate that electrospun scaffolds can be used to complement or improve traditional *in vitro* culture methods. To enable detailed studies of the interplay between physical and chemical cues for cells in controlled microenvironments, a method to integrate electrospun structures with microfluidic systems was devised.

Thermal interface materials have been identified by the semiconductor industry as one of the major bottlenecks in the heat dissipation for high power density devices. The second part of this thesis presents the development of a novel metal matrix composite TIM technology utilizing fiber reinforcements formed through electrospinning. Employed as a TIM, the composite structure relies on heat conduction through its continuous metal phase, while the fiber network modifies the thermo-mechanical properties. Three specific implementations have been developed: Polyimide fibers with an indium matrix and a tin-silver-copper (SnAgCu) alloy matrix, and carbonized mesophase-pitch based fibers with a SnAgCu alloy matrix. To facilitate liquid phase infiltration of the indium matrix into the polyimide fibers, a chemical reduction based method for coating Ag nanoparticles on the fiber surface was developed. Using the same Ag coating, the SnAgCu composite was fabricated and demonstrated to exhibit a reduced elastic modulus, which indicates the potential to lower the thermally induced stress when bonding materials with thermal expansion mismatch. The expected increase in thermal conductivity when switching from polymer to carbonized fibers is found to be limited, and improved methods to reduce the thermal contact resistance at the matrix-fiber interface are needed. Measurements of low thermal contact resistances ($< 1 \text{ Kmm}^2/\text{W}$) and high thermal conductivities ($\sim 20 \text{ W/mK}$) show that the composite architectures are promising candidates for future applications when compared to both existing and other emerging TIM technologies.

Keywords: electrospinning, electrospun fibers, scaffold, plasma surface modification, cell-scaffold interaction, microfluidic system, electronic packaging, thermal management, thermal interface material, metal matrix composite.

List of Publications

Appended Papers

This thesis is based on the work contained in the following papers:

A Surface characterisation of oxygen plasma treated electrospun polyurethane fibres and their interaction with red blood cells

C. Zandén, M. Voinova, J. Gold, D. Mörsdorf, I. Bernhardt and J. Liu

European Polymer Journal, vol. 48, no. 3, pp. 472-482, 2012.

B Stem cell responses to plasma surface modified electrospun polyurethane scaffolds

C. Zandén, N. Hellström Erkenstam, T. Padel, J. Wittgenstein, J. Liu and H. G. Kuhn,

Nanomedicine: Nanotechnology, Biology, and Medicine, vol. 10, no. 5, pp. 949–958, 2014.

C Bioactive 3D cell culture system minimizes cellular stress and maintains the in vivo-like morphological complexity of astroglial cells

T. B. Puschmann, C. Zandén, Y. de Pablo, F. Kirschhoff, M. Pekna, J. Liu and M. Pekny

Glia, vol. 61, no. 3, pp. 432–440, 2013.

D A novel method for three-dimensional culture of central nervous system neurons

T. B. Puschmann, Y. de Pablo, C. Zandén, J. Liu and M. Pekny

Tissue Engineering Part C: Methods, vol. 20, no. 6, pp. 485–492, 2014.

E A method to integrate patterned electrospun fibers with microfluidic systems to generate complex microenvironments for cell culture applications

P. Wallin, C. Zandén, B. Carlberg, N. Hellström Erkenstam, J. Liu and J. Gold,
Biomicrofluidics, vol. 6, no. 2, 024131 (18 pp.), 2012.

- F Fabrication and characterization of a metal matrix polymer fibre composite for thermal interface material applications**
C. Zandén, X. Luo, L. Ye, and J. Liu
Proceedings of the 19th International Workshop on THERMal INvestigations of ICs and Systems, IEEE, pp. 286–292, 2013.
- G A new solder matrix nano polymer composite for thermal management applications**
C. Zandén, X. Luo, L. Ye, and J. Liu
Composites Science and Technology, vol. 94, pp. 54-61, 2014.
- H A carbon fiber solder matrix composite for thermal management of microelectronic devices**
M. Murugesan, C. Zandén, X. Luo, L. Ye, V. Jokubavicius, M. Syväjärvi and J. Liu
Journal of Materials Chemistry C vol. 2, no. 35, pp. 7184-7187, Aug. 2014.

Other Contributions

- A Evaluation of new and improved thermal interface materials and surface roughness effect on thermal interface resistance**
C. Zandén, B. Carlberg, P. Melin, L. Olsen and J.Liu
Proceedings – The International 3rd Swedish Production Symposium, pp. 88–96, 2009.
- B Future Emerging Packaging Technology Using Carbon Nanotubes**
J. Liu, Y. Qin, C. Zandén, Y.Fu, T. Wang and L. Ye
ELTE 2010 & 34th IMAPS-CPMT, 2010.
- C Surface Properties of Electrospun Polyurethane-based Elastomer Networks for Biomedical Applications**
C. Zandén, M. Voinova, C. Wang, D. Mörsdorf, I. Bernhardt, J.Gold and J.Liu
Poster Symposium C Hybrid Materials Conference, Paris, March 7–9, 2011.
- D Electrospun polyurethane-based elastomer fibers for biomedical applications**
C. Zandén, M. Voinova, C. Wang, D. Mörsdorf, I. Bernhardt, J.Gold and J.Liu
European Cells and Materials, vol. 21. Suppl. 1, 2011.
- E Boron nitride nanofiber and indium composite based thermal interface materials for electronics heat dissipation applications**
X. Luo, Y. Zhang, C. Zandén, M. Murugesan, Y. Cao, L. Ye, and J. Liu
Journal of Materials Science and Engineering Materials in Electronics, vol. 25, no. 5, pp. 2333–2338
- F Thermal Performance Characterisation of Nano Thermal Interface Materials after Power Cycling**
S. Sun, L. Xin, C. Zandén, B. Carlberg, L. Ye, and J. Liu
Proceedings - Electronic Components and Technology Conference, ECTC, pp. 1426-1430, 2012
- G HB-EGF affects astrocyte morphology, proliferation, differentiation and the expression of intermediate filament proteins**
T.B. Puschmann, C. Zandén, I. Lebkuechner, C. Philippot, Y. de Pablo, J. Liu, and M. Pekny
Journal of Neurochemistry, vol. 128, no. 6, pp. 878-889, 2014.

Abbreviations

3D	Three-dimensional
APU	Accelerated processing unit
ATP	Adenosine triphosphate
ATR-FTIR	Attenuated total reflection - Fourier transform infrared spectroscopy
BLT	Bond-line thickness
BME	Benzoin methyl ether
CA	Contact angle
CF	Carbon fiber
CNT	Carbon nanotube
CNS	Central nervous system
CPU	Central processing unit
CTE	Coefficient of thermal expansion
CVD	Chemical vapor deposition
DMAB	Dimethylamine borane
DNA	Deoxyribonucleic acid
DUV	Deep ultraviolet light
ECM	Extra cellular matrix
eGFP	Enhanced green fluorescent protein
GFAP	Glial fibrillary acidic protein
hESC	Human embryonic stem cell
IC	Integrated circuit
ICT	Information and communication technology
IHS	Integrated heat spreader
ITRS	International Technology Roadmap for Semiconductors
KOH	Potassium hydroxide
LDH	Lactate dehydrogenase
LMAs	Low melting point alloys
MMC	Metal matrix composite
nSC	Neural stem cell
PI	Polyimide
PDL	Poly-d-lysine
PDMS	Polydimethylsiloxane
PoLam	Poly-L-ornithine and laminin
PU	Polyurethane
RNA	Ribonucleic acid
SAC	Tin silver copper
SEM	Scanning electron microscopy
SMNPC	Solder matrix nano polymer composite
STIM	Solder based thermal interface material
TEM	Transmission electron microscopy
TIM	Thermal interface material
XPS	X-ray photoelectron spectroscopy

Contents

Abstract	iii
List of Publications	v
1 Introduction	1
1.1 Background	1
1.1.1 Scaffolds for Biomedical Applications	2
1.1.2 Thermal Management of Microelectronics	4
1.2 Scope and Outline	6
2 Electrospinning	9
2.1 Electrostatic Drawing of Fibers	10
2.2 Process Variations	14
2.3 Applications	16
3 Electrospun Scaffolds for Cell Culture	19
3.1 Cell-Substrate Interactions	22
3.1.1 Stem Cells and Neural Cells	23
3.1.2 Electrospun Polyurethane Scaffolds and Surface Modifications	26
3.2 Stem Cell Response on Plasma Surface Modified Electrospun Scaffolds	36
3.3 Topographical Reactions of Neural Cells on Electrospun Scaffolds .	49
3.4 Integration of Patterned Electrospun Structures in Microfluidic Sys-	
tems	62
4 Thermal Interface Materials in Microelectronics Packaging	69
4.1 Heat Transfer Across Interfaces	69

4.2	Thermal Interface Materials	73
4.2.1	Conventional Materials	73
4.2.2	Emerging Technologies	76
4.3	Metal Matrix Composite Thermal Interface Material	81
4.3.1	Development and Fabrication	81
4.3.1.1	Concept	81
4.3.1.2	Fabrication	82
4.3.1.3	Evaluation of Thermal Properties	92
4.3.2	Indium Matrix and Polyimide Fiber Composite	94
4.3.3	Solder Alloy Matrix and Polyimide Fiber Composite	97
4.3.4	Solder Alloy Matrix and Carbon Fiber Composite	104
4.3.5	Summary and discussion	109
5	Conclusions and Outlook	115
	Acknowledgements	118
	References	119

Chapter 1

Introduction

1.1 Background

Advanced materials enabled through fabrication processes with precise control at the micro- and nanoscale are playing an increasingly dominant part in the development of new technologies relevant to most aspects of our lives, from biomedical implants to energy production. At small scales, the importance of material surfaces and interfaces cannot be overstated, and seemingly unaffiliated fields can merge to face similar challenges and use common solutions. In both nature and engineering, material based solutions often make use of the surface and interface characteristics that are inherent to micro- and nano-sized fibers. Natural fibrous structures are prevalent throughout complex and living organisms and are utilized for a range of critical functions. Some examples include the supportive and guiding fibrous structures in and around cells and tissue in the body, the hierarchical and fiber-like barbs and barbules of duck feathers rendering superhydrophobic characteristics, and the thermally insulating role of hair and fur. Certainly these examples bear resemblance to engineered materials, where woven and non-woven fibers are applied as reinforcement in composites, water permeable membranes in filters, as well as water-repellent and insulating fabrics in clothes. This thesis explores the integration of electrospun fiber based materials and related interfaces in two microsystem applications: fiber scaffolds for biomedical applications and fiber based metal matrix composites for thermal management of electronics.

At a first glance, these two applications may appear quite far apart, with one belonging in life–science, whereas the other connects to the sterile world of electronics. However, when viewed from a basic perspective, the challenges are not distinctly different. The common denominator is the use of electrospinning to utilize the novel properties of electrospun materials, particularly the inherent spatial organization. In both cases, the fiber surface requires modification to be fully functional, with the difference being the order of magnitude of the surface energies. On one hand, the relevant interface for the scaffolds is towards cells and water, which have surface energies of the order of $\sim 10^2$ mJ/m². On the other hand, the fibers in the composite are interfaced towards metal alloys with surface energies which are one order of magnitude larger, i.e. $\sim 10^3$ mJ/m². Additionally, there are similarities with respect to the concept of wetting and infiltration. For the scaffold it is important to allow for H₂O wetting and cellular attachment/infiltration, while the composite forming relies on wetting and infiltration of metal alloys.

1.1.1 Scaffolds for Biomedical Applications

In the field of tissue engineering and regenerative medicine, an essential goal is to be able generate different types of healthy functional tissue using *in vitro* based processes. The generated tissue is then envisioned to be inserted into the body wherever needed, as a new way to actively treat diseases or trauma. In particular, the combination of stem cells with suitable supporting material structures, i.e. scaffolds, is considered to be a highly promising strategy for engineering tissue [1, 2]. Stem cells are particularly interesting as they can be expanded indefinitely and stimulated to undergo processes to become virtually any cell type in the body. One of the key aspects to form tissue constructs of a specific type using stem cells, is that the cells need to be seeded in the appropriate niche microenvironment. It has been proven that the extrinsic factors exerted by the scaffolds chemical, mechanical and topographical character are significant factors affecting stem cell behavior and fate, i.e. adhesion, proliferation, differentiation and migration [3]. In this regard, scaffold design can play a crucial role in the formation of stem cell based tissue and the effectiveness of the regenerative process [4]. Consequently, to exploit useful consequences of cell–material interactions, it is important to understand in

detail how stem cells respond to different scaffolds characteristics.

Another area where scaffolds are of potential future importance, is within the field of cell culture. Cell culture was developed in order to better understand single cell types and study their isolated response to different events, such as trauma or treatments. These *in vitro* based studies have been common laboratory practice in thousands of laboratories since the middle of the 20th century [5, 6]. Even though *in vitro* cell culture research has contributed to a substantial portion of the knowledge we have today, it is not without complications. Unfortunately, research results obtained from *in vitro* experiments often do not predict the outcome of *in vivo* experiments [7]. One of the major causes of this discrepancy is the inadequate representation of cells in highly artificial two-dimensional cell culture systems, currently used for *in vitro* experimentation [8]. More sophisticated *in vitro* cell culture systems are therefore needed to improve the reliability of research data obtained during the *in vitro* phase of biomedical research and testing of drug target candidates. With an increasing awareness of this, there has been a growing interest in scaffolding materials and related methods that can evolve traditional *in vitro* cell culture to better mimic the anatomy and physiology of their native tissue. Related to this, a trend in cell culture is to move towards so called three-dimensional (3D) cell culture scaffolds, which are essentially material constructs that can provide support for 3D cellular organization *in vitro*.

There is a wide range of scaffolds directed towards both tissue engineering and 3D cell culture applications, with certain overlap. Most scaffolds are made from fiber-based or porous polymeric material structures [5]. Due to the possibility to fabricate biomimetic artificial matrices with morphological similarities to the fibrillar structures of the *in vivo* extra cellular matrix, electrospun materials have emerged as promising candidates for both tissue engineering and cell culture applications. A large number of studies related to electrospun fiber based scaffolds, targeting various forms of tissue, such as cardiovascular, osseous, cartilage and nervous tissue, have been carried out.

The central nervous system (the brain and the spinal cord) is the most complex structure in the human body and shows very limited capacity to recover from injury or disease [9]. Substantial attention is therefore directed towards stem cell and scaffold based therapies that could be used to assist in nervous tissue repair.

An equally important aspect in the treatment of trauma and diseases is to advance our understanding of the processes and functions of individual neural cell types in nervous tissue, such as neurons and astrocytes. This could be alleviated by *in vitro* cell culture scaffolds that capture important *in vivo* features for these cell types otherwise lost when cells are transferred to standard two-dimensional culture systems. Using such *in vitro* cell culture scaffolds, could potentially refine our understanding of cellular processes and result in more precise and earlier insights on the effects from new experimental drugs, leading to faster development of new or enhanced treatments. In this thesis, we have explored the use of electrospun fiber scaffolds and related topographies in the context of culturing cells, primarily related to neural tissue.

1.1.2 Thermal Management of Microelectronics

The rapid pace of development in microelectronics over the last decades, has led to some of the most influential technological and societal advances in the modern era. To continue coping with the progressive demands of improved performance, device miniaturization and extended functionality, both the semiconductor and the ICT industry are in constant pursuit to increase integration densities across the IC and packaging levels. However, enhanced computational power and more compact device designs, comes at the cost of increased power dissipation and/or higher power densities [10]. As most of the input power is ultimately converted to heat, the requirements on thermal management is becoming increasingly challenging.

Today, thermal dissipation is considered one of the main bottlenecks for further development of many high performance micro- and power-electronic systems. The general prognosis is that the power densities will continue to rise within the foreseeable future [11]. Addressing the thermal management issues has therefore been posed by the industry consortia iNEMI and ITRS as a field of research priority [12–14]. New and innovative materials and packaging technologies for improved thermal dissipation are expected to play key roles in order to further advance the performance and achieve sufficient reliability of systems based on semiconductors. This is true, going from handheld devices (\sim mW) to massive data centers (\sim GW).

On the IC level, while increasing the computational power, the associated in-

crease in power dissipation can be limited by using scaled down and more effective transistors and IC architectures. For microprocessors, the emerging next generations, targeting the 14 and 10 nm nodes and using the low leakage fin-FET based transistor technology will have reduced levels of power consumption compared to current generations. The multi-core architectures for CPUs and APUs have allowed for increased computational power while limiting the power densities to around 1 W/mm^2 , deviating from the earlier exponentially growing trend [15]. Nevertheless, as transistor density and total number of transistors increase, a net effect of higher power densities is to be expected. Of additional concern, is that the power dissipation in modern chip architectures is typically non-uniform and focused to functional areas. In such regions of the die, the local power densities can reach up to $3\text{--}10 \text{ W/mm}^2$ [16, 17]. These, so called hotspots, are problematic since the overall reliability is typically constrained by the hottest region on the IC, rather than the average temperature [10].

To advance performance and functionality without relying on reduced feature scaling, significant effort is focused on increasing packaging density by integration of multiple functionalities such as ICs and related passive circuits into single packages. Towards this end, the stacking of ICs, so called three-dimensional integration, using vertical interconnects, is seen as a promising path to reduce footprint and interconnect paths for higher bandwidth, lower latency and lower power consumption. However, stacking several heat generating ICs, brings an additional set of complications and generally intensifies the thermal management challenges to new levels.

On top of these challenges, is that the traditional engineering based solutions for increasing the thermal dissipation are approaching their limits. Air-cooled heat sinks, which are the most common cooling solutions, are already an order of magnitude larger than the chip itself and still provide inadequate heat removal capability for future needs. Continued development towards larger and more powerful cooling solutions is not a viable strategy, as it features more bulky systems and higher power consumption for active cooling. As a matter of fact, the power consumption of the active cooling solutions is becoming an issue felt by the IT-industry. Data centers have been reported to consume 50-100 % additional energy solely dedicated to active cooling and thermal dissipation. Consequently, the thermal issues has

now become a major factor preventing higher data rates [15].

Moreover, in the hardware design of electronics system, it is often attractive to move towards passive cooling solutions. Primarily, as they do not rely on moving mechanical parts to maintain function, but also from a power consumption perspective. The problem is that natural convection is coupled with a larger thermal resistance going from the heatsink to the ambient, compared to forced convection. Therefore, to keep the total thermal resistance within functional limits, the thermal resistance from the heat generating components to the heatsink, has to be reduced.

Several aspects that are crucial for maintaining the microelectronics industry's momentum currently rely on innovative development of new process and material technologies that can alleviate the thermal management issues. From a material perspective, this includes: moving to new semiconductor materials with higher conductivity and higher heat resistance compared to silicon, such as GaN [18] and SiC [19]; more effective thermoelectric materials for thermoelectric local hot spot cooling; utilization of carbon allotropes as light and highly thermally conductive materials [20–23]; and developing new thermal interface materials (TIMs) with lower thermal resistance and reliable performance. TIMs have been identified by the ITRS [11, 13] as one of the main bottlenecks to reduce the junction-to-ambient thermal resistance. In this thesis, we present the development of a novel metal matrix composite technology incorporating electrospun fibers, aimed towards meeting current and future requirements on thermal performance and thermo–mechanical reliability for TIMs in microelectronic systems.

1.2 Scope and Outline

This thesis concerns the processing, characterization and utilization of material structures based on micro- and nanofibers fabricated using electrospinning within two fields: Electrospun scaffolds with surface modifications for *in vitro* 3D cell culture and tissue engineering applications, and electrospun fiber–reinforced metal matrix composites for thermal interface material applications.

Chapter 2 describes the electrospinning technique, its process details and variations, as well as a few of the many interesting potential applications.

Chapter 3 presents results on the fabrication, characterization and implementation of electrospun polyurethane (PU) fiber architectures and their imposed effects on a few different cell types, predominantly associated with neural tissue. Firstly, detailed characterization of plasma surface modifications on PU fiber networks and related effects on subsequently seeded stem cells, are presented. Secondly, electrospun PU fibers with physically adsorbed protein coatings are studied as *in vitro* scaffolds for primary neural cells. Finally, the integration of patterned electrospun PU topographies into microfluidic systems is demonstrated and discussed.

Chapter 4 is devoted to the development of a novel metal matrix polymer composite technology incorporating electrospun fiber networks. After introducing the reader to some of the boundary conditions at the thermal interfaces in microelectronics, and reviewing current and emerging material solutions, the fabrication of the MMC technology is presented. Three implementations of the technology is developed, evaluated and compared to conventional interface materials and other TIM technologies still in research.

Chapter 5 concludes the thesis and a brief future outlook is given.

Chapter 2

Electrospinning

In essence, electrospinning is the process of electrostatic drawing out and collection of fibers, typically polymeric, from a solution or melt onto a grounded collector. The process of electrospinning, or electric-field induced spinning, was recognized early in the 1900s, when the first related patents were deposited. However, it was not until about two decades ago, when the process was evidenced to enable formation of high added-value organic micro and nanomaterial, that the interest for electrospinning was completely renewed. This "rediscovery" of electrospinning is commonly attributed to Reneker et al. [24] who demonstrated and argued for its potential to form continuous fibers with diameters in the micro- and nanometer range. Since then, electrospinning has been explored as a method to compose non-woven fibrous assemblies for a broad range of applications, involving both technical and life science directions (for reviews on the subject see [25–32]).

Electrospinning is a top-down method and one among several ways to form fibers in the micro and nanoscale range, such as drawing, template synthesis, phase separation, chemical vapor deposition, melt blowing and self-assembly [33]. However, in comparison to these methods, electrospinning offers some key features that makes it attractive. First and foremost, it stands out among the other methods due to its scalability. Importantly, this can alleviate the transfer of promising lab research findings into industrial processes, which permits realization of end-products that have impact outside the scientific community. In addition, the combination of scalability and allowing for controlled preparation of non-woven, long,

continuous fibers into hierarchical fiber architectures, offered by electrospinning renders unique and powerful opportunities that are not easily accessible through other methods. In general, electrospun nonwoven fiber meshes (also referred to as membranes, mats, webs and networks) are characterized by high spatial interconnectivity, high porosity, an intrinsic three-dimensional topography and an associated large surface-to-volume ratio. The process parameters that govern the formation and morphology of electrospun fibers will be addressed in the following section.

2.1 Electrostatic Drawing of Fibers

There are many specific implementations of electrospinning based fabrication [27], but the basic principles of operation are largely the same [34]. The process relies on the balanced interaction between cohesive forces and the electrostatic forces induced on charged entities in a solution. In a conventional electrospinning setup (figure 2.1), the solution is fed through a syringe equipped with a metal cannula/nozzle connected to a high voltage source, typically in the range of 5–50 kV. When a pendent drop of the solution accumulates at the cannula orifice it forms a convex meniscus, due to the surface tension and the excess charges, primed through the voltage supply, that will start to gather at the apex of the liquid cone. As the repellent forces of the positive charges overcome the surface tension of the viscous solution, a jet erupts, in what is called a Taylor cone, and travels towards the grounded collector. While travelling towards the collector any instability subjected to the jet beam will render an uneven surface charge distribution causing a whipping or spinning motion due to the Coulombic repulsion. The result of the spinning motion is extensive stretching that leads to severe thinning of the cross section of the liquid beam, typically by 4–6 orders of magnitude. The width of the ejected jet in combination with the number of stages of bending and stretching action that occurs, determines the resulting diameters of the collected fibers. As the solution jet travels towards the collector, the solvents evaporate, and dry polymer fibers are deposited on the collector. Depending on the degree of solvent evaporation during spinning, the collected fiber network may display fused splices and joints at fiber intersections and crossovers. The evaporation rate of the

solvent is governed by several factors, both external and intrinsic to the solvent. Many of the properties that effect the evaporation, such as vapor pressure, boiling point, enthalpy and heat of vaporization, are related to the molecular weight of the solvent. The rate of evaporation of the solvent is also higher whilst travelling in the jet because of the repulsion between similarly charged solvent molecules.

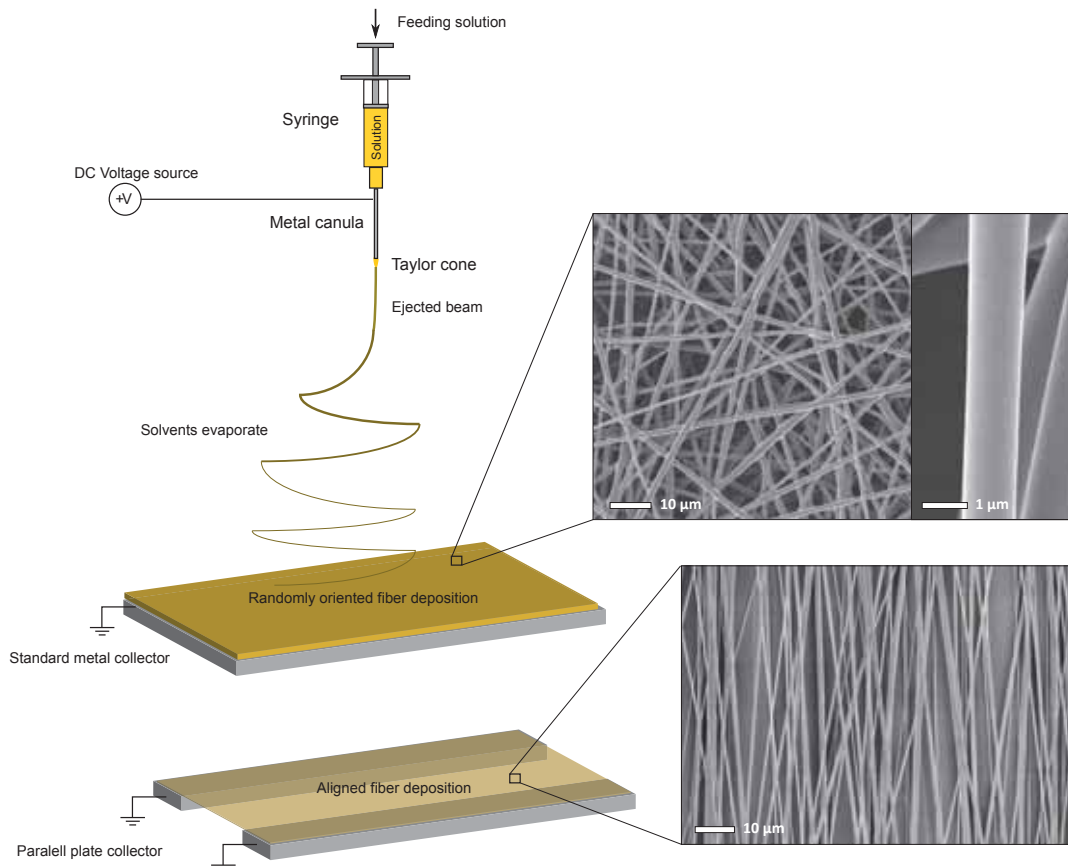


Figure 2.1: Schematic of a typical electrospinning process.

In case the viscosity and/or surface tension of the solution are not tuned to counterbalance the stretching action of the electric field, the solution will break into smaller constituents in the form of discrete droplets. Thus, for a continuous electrospinning operation, the polymer content needs to be sufficiently high to cause a molecular chain entanglement that prevents the electrically driven jet from breaking into droplets. The transition between a stable jet and discrete

droplets can also occur if the surface tension has a dominant influence in the solution, as it strives towards minimizing the exposed surface area. This balance between solution viscosity and surface tension is typically observed experimentally as an emerging bead formation on the collected fibers while decreasing polymer concentration in the spinning solution. Below a certain threshold for the polymer concentration, the outcome will be spraying of solution droplets onto the collector. This related process is called electro-spraying.

The parameters that affect the fiber formation during electrospinning can be classified into three groups: solution parameters, processing conditions and ambient conditions. Out of these, the solution properties (viscosity, surface tension, electrical properties, vapour pressure, boiling point which are dependent on polymer molecular concentration/weight/solubility, solvent conductivity/dielectric constant/vapour pressure/boiling point, number of ions in the solution) have the most significant influence on the fiber morphology and need to be balanced within a certain range for fiber formation to occur [35]. Once these parameters are within a functional range, the solution viscosity is the primary factor determining the resulting fiber diameter. This effectively by limiting the extent of elongation of the solution during flight. The solution viscosity is influenced by the degree of molecular chain entanglement, which in turn is dependent on polymer molecular weight/solubility and concentration. Thus, the most straightforward way to control the fiber diameter, for a given soluble polymer, is by adjusting the polymer concentration in the solution. Another way to adjust the outcome of the process is to increase the electrical conductivity of the solution by adding ions, for instance through a small amount of salt or ionic surfactant. As a result of an increased conductivity, the number of charges that are carried by the solution is higher, thereby increasing the stretching of the electrospinning jet. Within a small range, a higher conductivity of the solution tends to yield fibers of smaller diameter and can be utilized to enable spinning of solutions with low polymer concentration by reducing the bead formation. Solutions with significant concentration of conductive particles are often challenging to electrospin.

The basic processing conditions that are important in the electrospinning process are the supplied voltage, feeding rate, orifice diameter, type of collector and distance between needle and collector. Higher voltage and resulting electric field

cause a larger volume of solution to be drawn from the Taylor cone and will affect the deposition morphology of the fibers, with a tendency towards reducing the fiber diameter. To certain extent, higher voltage has also been reported to induce a greater crystallinity in the fiber [35]. For a given voltage, a stable and continuous fiber formation is achieved by feeding the solution at a rate that corresponds to the speed of which the material is ejected. Typically a lower feeding rate is desirable as the jet will then contain less solvents, and avoid the fibers of fusing together upon deposition due to residual solvents. Fiber merging is also more common when the distance between the orifice and collector is low. The type of collector can be used to control the alignment, but also affects the morphology in terms of fiber mat density distribution and porosity. Common ways to achieve fiber alignment is by using a rotating drum collector or by using separated parallel conductive collector surfaces. The fiber mat porosity is affected by the number of residual charges that is present on the deposited fibers, as they repel additional incoming fibers. Consequently the local ability of the collector to transport away residual charges will affect the porosity and fiber mat deposition. In the functional range, changing orifice diameter has a limited effect on the spinning process, even though a smaller orifice can lead to a reduction in the fiber diameter, as the surface tension of a smaller droplet is increased.

The impact of ambient conditions on electrospinning, such as temperature, humidity and pressure, are not extensively characterized. The reported results tend to depend on the specific polymer-solvent system investigated [36, 37]. However, a general effect is that higher temperature lowers the solution viscosity and increase the evaporation rate. Volatile solvents will also dry more rapidly at low humidity, which can cause rapid solidification of the electrospinning solution and be disruptive of the process. The humidity has been reported to affect the fiber formation through condensing on the surface of the jet due to the cooling from the rapid evaporation of volatile solvents. High relative humidity has also been found to result in pores on the fibers [38]. Additionally, humidity have been shown to significantly affect the fiber diameter, where the direction of the change can go either way depending on the chemical and molecular interactions with the solvent-polymer system.

All in all, as illustrated by the multiple and interrelated factors affecting the

process, electrospinning is a difficult technique to master. On the contrary, it is comparably straight forward technique in its simplest form, and requires relatively basic hardware. In fact, simple electrospinning is also considered theoretically well understood and modelling work has contributed to a more in-depth understanding of the influence of different processing parameters. Nevertheless, the field is largely dominated by creative experimental work to probe and assess the potential of the fiber architectures that can be formed. In the next section, a brief outlook on interesting variations of the basic electrospinning that further extend the basic processing capabilities is given. This is followed by a short review on some recent prominent implementations of electrospun fibers to illustrate the diversity of possible applications.

2.2 Process Variations

The most common process variations of electrospinning is to use a custom design of the collector and/or the solution delivery configuration. In terms of collectors, there are several configurations that can produce aligned fibers, each with its strengths and weaknesses. Seemingly the most commonly used aligning collectors are based on spinning drums, wire drums, tubes or discs, that rotate at high RPM. The high speed rotation causes the fibers to deposit in alignment with the direction of rotation. For small tube collectors, there are also additions of knife-edge electrodes that enables deposition of thicker layers of fibers, which are otherwise limited. This enables the formation of free standing macroscopic tubes consisting of electrospun fibers. The static collector alternatives to deposit aligned fibers are in the form of parallel electrodes or separated blades in a line. These collectors allows for highly aligned fibers but are limited regarding the length of the fibers and the thickness of the fiber mat that can be collected, especially compared to rotating collectors. On the other hand, the static alternatives offers comparably easy transfer from the collector surface or direct spinning onto custom substrates. For rotating collectors, fiber mat transfer can be problematic as there tends to be residual stress in the fibers. This residual stress comes from additional stretching from the rotating action during deposition and causes the mat to contract/deform once released from the collector surface.

Going from controlled alignment of fibers in one direction, to multiple directions, there are reports on using arrays of counter electrodes to manipulate the electric field, which cause alignment between each electrode in a pattern formation. However, this technique of alignment is quite limited with regards to the achievable thickness and area of consistent patterning. For an even higher degree of control of the fiber deposition, while sacrificing process scalability, is the near-field electrospinning process [39]. Near-field electrospinning is a form of serial direct writing of single fibers at a short distance ($\sim 500 \mu\text{m}$) to the collector using a small tip ($\sim 10 \mu\text{m}$) as spinneret.

Another way to manipulate the electric field to control the electrospinning jet and affect the fiber deposition, is to position additional auxiliary electrodes along the jet path at same polarity as the electrospinning jet. Primarily this is seen in the form of rings around the electrospinning nozzle, that acts to limit the area onto which fiber are deposited. To mitigate collection of continuous fiber mats at larger scale, conveyor belts and roll-to-roll collectors can be employed. Another interesting option for sustained fiber deposition is to collect fibers into a water bath, while allowing a portion of the mat to be continuously rolled up onto an external roll. This enables the fabrication of continuous mats without the use of a carrier substrate.

In terms of solution delivery configurations there are multiple ways to form the initial protrusion in the solution, wherein charges can accumulate, and eventually cause eruption into a jet towards the collector. By far the most common configuration is to use a metal nozzle or cannula attached on a solution container along with a feeding mechanism, for instance a syringe along with a syringe pump. A variation of this is specially designed orifices with multiple openings along the same axis from different solution containers, that enables formation of core-shell fibers, through so called co-axial electrospinning. Instead placing multiple nozzles in parallel is a way to co-electrospin different polymers into interwoven networks or alternatively to increase the rate of fiber deposition.

As an alternate route to using needles, it is possible to commence electrospinning directly from a larger solution bath, where the protrusions is formed directly on the solutions surface. Aside from the natural or random occurrence, the initial protrusion formation in the electrospinning solution can then be assisted by an

underlying geometry, by actively introducing bubbles in the solution, or by applying a magnetic field. Spinning directly from a solution bath is an effective way of scaling the productivity of the electrospinning process, but generally offers less precise control of the fiber diameter.

To-date there is a number of equipment manufacturers that offer electrospinning equipment with capability of continuous fabrication of fiber mats both for lab-scale and commercial production. Currently the commercial applications are limited, mainly to filter applications, and the scientific community constitutes the major customers on the electrospinning equipment market [31]. However, as some of the emerging applications for electrospinning and related products reach higher technology readiness levels, this can be expected to change over a not so distant future.

2.3 Applications

The range of potential applications for electrospun materials is quite remarkable. The versatility of the process enables electrospinning to be a potential starting point for material based solutions to problems which are initially quite different. To illustrate this to the reader, we will briefly go through a number of examples in recent literature, going all the way from electrospun materials as anode materials in batteries, via the use in composites and wearable sensors, to wound dressings, implants and finally scaffolds for cell culture.

Starting with materials in batteries, Zhou et al. [40] reported on the synthesis of an ultra-uniform nanohybrid anode material for Li-ion batteries by electrospinning. Their initial material was a solution of polyacrylonitrile in dimethylformamide with suspended tin-oxide nanoparticles. After electrospinning and stabilization, the collected fibers were carbonized to form hybrid fibers, i.e. carbon nanofibers with tin-oxide content. The benefit with using electrospun material as electrode material were stated to primarily come from its open and interconnected structure. When used as an anode material, the open structure enabled the material to accommodate for the mechanical strain from the volume expansion, that occurs during lithium insertion, while preserving high electrical conductivity through the continuous fiber network.

For composite application, Jiang et al. [41] utilized electrospun nylon nanofibers as a reinforcement in a thermosetting plastic matrix and managed to improve the tensile strength and toughness significantly. They also noted a drastic effect on the improvement of properties depending on the wetting procedure used between the matrix resin and the reinforcing fibers.

For stretchable electronics, e.g. wearable sensors and electronic skin, polymer based transistors using electrospun fibers were recently reported by Shin et al [42]. The transistors were formed using Au nanosheets as electrodes, electrospun semiconducting polymer fibers as the active channels, with ion-gel polyelectrolyte as the dielectric layer. The structure was formed on top of electrospun polystyrene based fiber mat as substrate. They found that the network structure of the ion-gel and electrospun substrate lead to transistors with high mechanical stability under severe stretching events, and that the performance was retained for over 1000 stretching cycles.

To enable self-powered electronics that directly interface with the human body, flexible design, lightweight and self-powered operation are properties which are highly sought for. In this context, Persano et al. [43] fabricated large area flexible piezo-electric material from aligned electrospun mats, and found that the structure of the material resulted in outstanding piezoelectric characteristics, which enable ultra-high sensitivity to pressure differences.

From wearable electronics to assisting the healing process, Chen et al. [44] prepared wound dressings based on electrospun polyurethane fibers with silver nanoparticles. The wound dressings was found to have an improved wound healing rate compared to other wound dressings, due to its excellent antimicrobial activity, high specific surface, and its porosity that allowed for high water transmission rate and fluid drainage ability.

From interfacing with the human body on the outside to the inside, the use of electrospun fibers as a cellular scaffolds was recently demonstrated for the first time in clinical surgery on humans. Jungebluth et al. [45] replaced an airway with a artificially created analogous where the surface was covered with electrospun fibers that had been seeded with stem cells in a bioreactor. Their conclusions was that it is possible to use bio-artificial scaffolds as a treatment for complex airway defects. In the report, one of the key factors for the successful clinical outcome was

mentioned as the bioreactor reseeded of the stem cells, hinting of the importance of the scaffold.

However, clinical trials on humans using stem cells and scaffolds are still an exception for the majority of tissue and cell types. On the road towards better understanding of how electrospun scaffolds affect stem cells and also differentiated cell types, there are many studies conducted *in vitro* and *in vivo* on cultured and animal derived cells. For instance, Fon et al. [46] recently investigated the ability of aligned electrospun scaffolds with encapsulated proteins to direct the migratory pathway of neuroblasts in rats. They found that the scaffold was able to support neuroblast migration along the intended direction and that there were indications of differentiation of the neuroblasts into neurons. On a similar topic, Binan et al. [47] studied the cell survival and differentiation of neural stem cells on electrospun fibers in combination with controlled release of substances that influence differentiation. They found the combination of the topographical cues emanating from the electrospun fiber scaffolds and controlled delivery of chemically instructive cues could enhance the differentiation into motor neuronal lineages and promote neurite outgrowth. Their findings was believed to be a step further towards improved strategies for peripheral nerve injury repair.

Chapter 3

Electrospun Scaffolds for Cell Culture

One of the major driving forces for the exploration and development of electrospinning technology is its wide potential in the biomedical field. This is reflected in the exponential increase of the number of peer reviewed articles on electrospinning related technology with biomedical relevance during the last 15 years [48]. Depending on application, commonly electrospun materials are of biodegradable and/or biocompatible nature [49], including both natural and synthetic polymers such as collagen [50], silk fibroin [51, 52], cellulose [53], PE [54], PLLA [55], PCL [56], PLGA [57, 58], PVA [59], PS [60], PET [61] and PU [44, 62–64]. The suggested applications for these electrospun materials range from wound dressing and biomolecule filtration, to scaffolds for 3D cell culture and complex tissue engineering.

Seemingly the most promising biomedical use of electrospun scaffolds are within the field of tissue engineering and regenerative medicine. Ultimately aiming to help generate implantable functional tissue, organs or support regeneration of damaged or dis-functional tissue, tissue engineering holds great promise in allowing clinical treatments beyond what was previously feasible. Up until now, extensive efforts combining fabrication and detailed characterizations of the substrates, along with studies of cellular behaviour have lead to improved appreciation of how surface properties affect the biological response [65]. Commonly targeted tissues include

cardiovascular [63, 66], osseous (bone) [67], epidermis (skin) [68], muscular [69] and nervous tissue.

The ideal scaffold based implant for replacing or regenerating tissue should, in addition to biological compatibility of the structure with the host cells and tissue, present a number of characteristics. There is a general consensus in literature, that it is desirable for scaffold based implants to mimic and incorporate key features of the extra cellular matrix (ECM) found *in vivo* [6]. Important features are porosity, pore size, and mechanical properties, while containing the suitable chemical cues and exhibiting a topology that allows for a spatial organization appropriate for the targeted tissue. In this respect, electrospinning has attracted substantial attention as a method to generate fibrous scaffolding structures with morphological characteristics bearing resemblance to the ECM [54, 70]. More specifically, as a synthetic analogue to the morphology of fibrillar collagen and elastin components of ECM. Additional characteristics that makes electrospun scaffolds attractive, are their high porosity, interconnected pores, high specific surface as well as the morphological control that the electrospinning process admits. For a cell scaffold *in vitro*, high porosity and interconnected pores facilitates the transport of gases, nutrients and regulatory factors that are basic for cell survival and function. An interconnected pore structure also allows for cell–cell interactions, as opposed to isolated cell clusters, which would result from a closed pore structure. A high surface area–to–volume ratio can increase the number of cells that can adhere and also offer better possibility to incorporate biomolecules. The possibility for controlling fiber alignment during electrospinning is considered useful as a mechanical cue to direct tissue growth, cellular orientation and migration.

Albeit promising, several challenges for electrospun scaffolds are still subjects for further exploration. This includes cellular infiltration, detailed knowledge of the effects on the cells from the topographical and chemical interface that the scaffolds presents, and how to best modify the fiber surfaces using additional processing technologies. The incorporation of cells into electrospun scaffolds can be problematic due to the generally small pore size and several routes to deal with this has been investigated. One example is alternating electrospinning deposition with cell seeding [71]. Other suggestions include inclusion of large fibers to increase pore size and sacrificial fiber layers that dissolve after cellular infiltration [72]. The

interface between the cells and the scaffold is a crucial factor governing the cellular response. Commonly used surface modification strategies to promote favorable interactions include plasma surface treatment, protein grafting and physical adsorption of proteins. As the family of receptors that mediate cell-matrix adhesion, vary depending on cell type, so does the conditions for increasing the cell adhesion to a surface. Consequently, the most suitable method to coat or surface modify electrospun scaffolds will depend on target cell type. Also the chemical microenvironment, e.g. the cell culture media, can influence the surface interactions, as additional components may aggregate at the interface between the native scaffold surface and the cell membrane.

Despite the considerable knowledge base built up over the years, the understanding of cellular processes at the interface towards synthetically prepared materials can still be regarded to be in its infancy [73]. Continued research is required to discern the impact of different surface characteristics and how they may be utilized for biomedical engineering. The following sections present work performed in a multidisciplinary environment, aiming to further explore the effects of electrospun scaffold based microenvironments on cellular response. First, in section 3.1, we introduce relevant concepts and earlier research on extrinsic factors affecting cell behavior, stem cells, neural cells, electrospun PU and plasma surface modifications. Here we also include characterization of the effects of oxygen (O_2) plasma on morphology, surface chemistry and wettability of electrospun PU networks (corresponding to Paper A). This initial study contributes to the understanding of how the O_2 plasma modification acts on fibrous PU material systems and is relevant for the design and fabrication of electrospun fibers with controlled physical properties. Following this, in section 3.2, we investigate how a few different plasma surface modifications of electrospun PU scaffolds affects the response of human embryonic stem cells (hESCs) and neural stem cells (nSCs) (corresponding to Paper B). Next, the topographical reactions of neural cells, more specifically astrocytes and neurons, are studied (corresponding to Paper C and D). Our findings indicate that specific implementations of electrospun scaffolds may be able to take traditional *in vitro* cell culture a step further by allowing experiments in an environment that better captures important aspects of the *in vivo* situation. Finally, in section 3.4 we explore a route to integrate electrospun fibers with microfluidic channels to en-

able further elaboration on the effects of electrospun structures on cell behaviour (corresponding to Paper E). The developed system platform offers the possibility to study cell responses when simultaneously subjected to extrinsic topographical and chemical cues. More specifically, in the form of patterned electrospun topographies defined through direct photolithography, in combination with chemical gradients, achieved with a gradient generating network.

3.1 Cell-Substrate Interactions

Cells, tissue and organs are undeniably complex systems. Each cell contain numerous nano and microscale internal structures that continuously orchestrates a multitude of different processes. Macroscopically, we can observe the results of these processes, for instance in the form of what proteins the cells express, when and how they proliferate (divide to multiply), differentiate (specialize) and initiate apoptosis (programmed cell death) [74]. Ultimately individual cellular actions of different cell types, act together in a symphony to make up the different forms of functional tissue and organs. In addition to the intrinsic factors that regulate individual cell fate and behavior, cells are inherently sensitive to extrinsic signals from their surrounding micro-environment. It has been well-established that extrinsic physical stimuli influence crucial aspects of cell development and physiology [75–78]. Within the biomedical field, there is growing interest in utilizing fabrication techniques which can manipulate and enable defined material formation on the micro and nanoscale and thus offer possibilities to control aspects of material-cell-interactions.

The ECM is a mesh-like organisation of fibrillar proteins and glycosaminoglycans (polysaccharides) and a part of connective tissue. Throughout the body the ECM provides a structurally and biochemically supportive surrounding for cells. There are several different cell types that secret ECM components (eg. fibroblasts, chondrocytes, and osteoblasts) and the local composition depends on the cells in the specific tissue type [79]. The components of the ECM were originally hypothesized to primarily assist in the control of cellular attachment and growth. However, studies performed a few decades ago [80] identified that the fibrillar structures in the native ECM (fiber diameters of 10–500 nm [74, 81]) also exerted

effects on neuronal cell shape and could direct migration. It was suggested that there was a contact guidance mechanism leading to an increased probability of axons to follow along fibrils. This spurred on an interest to examine cell response on surfaces with well-defined topographies. The possibility to study this in more detail was improved through advances in micro-fabrication technologies allowing, for instance, greater control over grooved structures, that could be used to mimic the topography of ECM fibrils. With further studies it became increasingly clear that topographical variations on the micro and nano-scale can affect cell behaviour, even though the specific response is dependent on cell type as well as simultaneous cell-cell interactions [75]. Through continued efforts it has been shown that virtually all essential functions, such as attachment, growth, proliferation, migration and differentiation, are affected by the complete niche microenvironment comprising all physical and chemical factors. However, the properties of the surface onto which the cells adhere have in many instances been found to be particularly important [78, 82]. Mechanical cues have been shown useful to convey control over cell characteristics, especially in synergy with other surface cues [73]. Additionally nano- and microtopography have been identified to promote cell attachment and guide the lineage of differentiating stem cells. As a continued direction within this field of research, the opportunities offered by the electrospinning technique to move from topographies based on grooves defined through standard micro- and nanofabrication processes into three-dimensional fibrillar porous constructs with spatial connectivity, are considered attractive.

3.1.1 Stem Cells and Neural Cells

The common property of all stem cells are that they can divide indefinitely and have the ability to differentiate into more specialised cell types. There are many different stem cells, but they can be conceptually divided into embryonic and adult stem cells. Embryonic stem cells can be derived from the inner cell mass of a blastocyst, at an early stage of embryonic development. These cells are pluripotent, which mean that they can essentially differentiate into all cell types in the human body after a number of differentiation steps. Adult stem cells are found in post-natal tissue in the body, and are generally capable of differentiating into a more

limited number of different cell types, typically within their specific organ or tissue. The capability of unlimited renewal for adult stem cells is still under discussion [83], and they are difficult to distinguish from progenitor cells that only divide a limited number of times. An example of such cells are neural stem cells/neural progenitor cells, which differentiate into cells in neural tissue.

Neural tissue in the CNS consists primarily of neurons and neuroglial cells. The brain is estimated to contain about 10^{11} neurons (sensory, motor, autonomic etc.) which corresponds to about 15 % of the total number of cells in our brain [84]. Generally, neurons have one single axon accompanied by numerous smaller dendrites, projecting from the cell body. They process and transmit electrical and chemical signals, and connect to other neurons via synapses, forming neural networks. For neuroglial cells, the most abundant sub-population in the human central nervous system is the astrocytes. The "astro"-part in their name originates from having a characteristic star-shape-like appearance in the CNS and there are ~ 1.4 astrocytes for every neuron in the human neocortex [85]. Traditionally, astrocytes were considered to mainly act as part of the supportive tissue for neurons ("glia" is derived from gliok which is essentially greek for glue). However, findings over the last two decades have redefined this view and established that astrocytes also execute more advanced functions, such as Ca^{2+} -based signalling and releasing transmitters to modulate a host of important brain functions [86]. This and other subsequent discoveries have turned astrocytes into a crucial area of research in the field of neuroscience. Astrocyte responses are, for instance, involved in neurodegenerative diseases, such as ALS, Parkinsons, Alzheimers, and Huntingtons disease, but also CNS trauma. Even though much remains to explore, a hint of the importance of astrocytes, is that the ratio of astrocytes to neurons in the mammalian brain increase with brain complexity [85]. This is not only true comparing to amidst different animals, but also among human individuals. One prominent example of this, is the reported observations from dissections of Einsteins brain. The main difference found comparing tissue from one of the most brilliant minds of our time to samples from normal brain tissue, was the incredibly high number of glial cells. On average, Einsteins brain was found to have approximately twice as many glial cells compared to what is considered average [87]. Additionally, the size and complexity of the astrocytes appear to be linked to more evolved brain

functions when comparing to other species. It has for instance been shown that the astrocytes in the human neocortex are ~ 2.5 -fold larger in diameter and have processes that extend 10-fold more than that of rodents [88].

Being able to control the differentiation of stem cells is an important part in the future of stem cell based therapies. For instance, when expanding hESC lines it is important to prevent or restrict differentiation, in order to ensure enough cells can be created in a reasonable time and limiting contamination from differentiation into unwanted cell types. On the other hand, when applying the expanded cells from culture to form specific functional tissue, the target is shifted towards ensuring that the stem cell source can differentiate into the right cells for the intended tissue type. The differentiation processes of both hESCs and nSCs are influenced by the microenvironment in which the cell resides. The scaffold surface and morphology constitute a part of the motifs that can potentially act both to prevent and drive the differentiation into certain lineages. Exerting control of differentiation and other cellular processes through material design are expected to be an important tuning parameter in the design of scaffolds for stem cell therapies. This is believed to be true, even though the relative effects from the topographical cues and surface properties of the electrospun scaffold compared to chemical cues in the media are still not that well studied. Nonetheless, several studies have reported how different features of electrospun scaffolds affect differentiation of stem cells. For instance, Low et al. [89] found that synergistic effects from topographical cues and scaffold-mediated protein, that bind to specific DNA sequences, enhanced the neuronal differentiation of nSCs so that they could generate functional neurons. Another example is Wang et al. [90] who studied neural precursors, derived from hESCs, on electrospun silk fibers and found that aligned fiber topography promoted neuronal differentiation. From our group, earlier work has shown that use of electrospun PU substrates can affect the differentiation of hESCs. The next section will shortly introduce electrospun PU and then continue exploring its potential as a culture substrate for stem cells after surface modifications.

3.1.2 Electrospun Polyurethane Scaffolds and Surface Modifications

PU are extensively applied within both industrial engineering such as coatings, adhesives, engineering materials and biomedical applications. From a biomaterial perspective, PU is comparably well-studied and have been widely used in applications such as implants, blood-contact materials, infusion pumps, heart-valves, bandages, blood dialyzers and cardiovascular catheters [91–93]. The popularity of PUs stems from typically favorable mechanical, thermal and chemical characteristics in combination with biocompatibility and moderate blood compatibility [94]. Several more recent studies have shown that PU based materials in electrospun form is promising as a scaffolding material for tissue engineering. Rockwood et al. [95] created biodegradable scaffolds with electrospun micro sized PU fibers and showed that it presented useful mechanical properties and degradation profile for soft tissue engineering. Meng et al. [96] investigated the effects of an electrospun PU fiber and MWCNT (multi-wall carbon nanotube) composite and found that the structure can provide extracellular signals causing enhanced proliferation and stimulate the extracellular collagen secretion of vascular endothelial cells. Chen et al. [97] fabricated electrospun membranes from thermoplastic PU and collagen blends and found that endothelial cells grew favourably on the mats, which also allowed certain cellular infiltration through migration into the scaffolds. Their study also indicated that electrospinning PU was a viable approach to mimic native extracellular matrix for tissue engineering, despite the lack of intermolecular bonds between the scaffold and collagen coating.

Previous work in our group has demonstrated the potential of electrospun PU in tissue engineering related to the adult nervous system. By employing electrospun PU scaffolds as bio-mimetic substrates for hESCs during proliferative and differentiative conditions, it was shown that the substrate topography assisted in directing the cells towards a neuronal fate [98]. Indeed the result agrees with many other studies in literature, suggesting that the geometrical and topological organization provides extrinsic physical cues that affect hESC proliferation, differentiation and morphology [58, 99–101]. Nevertheless, based on these results, it was deemed of further interest to continue exploring the use of electrospun PU scaffolds. As a

continuation, there was a need to address the surface properties of electrospun PU in order to improve the scaffold-cell interface for attachment. We therefore sought to find how the surface of the scaffold could be modified, what effects such modification would have on the scaffold properties and how this translated to changes in cell behavior and fate. As with most synthetic polymeric materials, PU also presents intrinsic surface characteristics that are unfavorable for cell adhesion and require functionalisation or surface modification [102]. One particularly critical aspect of the surface properties for PU is the low surface energy, typically associated with a hydrophobic response and poor adhesion. Generally, increasing the surface energy is beneficial for many applications ranging from technical [103, 104] to biomaterials [105, 106] and cell-interactions [107].

Surface modification by exposing substrates to electrically ionized gases, i.e. plasmas, has been used quite extensively used for biomedical applications. One of the most common use is the treatment of the polystyrene surface in culture dishes [108]. Much of the interest in plasma surface treatments is because it allows modification of surface properties without affecting material bulk characteristics, through relatively straightforward and scale-able processing [105, 106, 109]. Generally, a plasma surface modification process acts on polymeric substrates through excitation, deionisation and dissociation events by physical bombardment of free radical species which insert, generate or remove functional groups at the surface. Plasma treatments is commonly adopted to modify the wettability of polymers through incorporation of O₂ species during or after exposure. This can be accomplished using e.g. argon or oxygen species, that increase the surface energy and modifies surface chemistry, typically concomitant with an increased surface roughness.

Our initial trials using O₂ plasma treatment on electrospun PU substrates indicated that the surface modification was capable of significantly enhancing the number of hESC that could attach, survive and proliferate (figure 3.1). We therefore directed our investigation towards discerning the possibilities and limitations regarding the use of plasma treatment as a modification of the electrospun fiber surface (corresponding to Paper A).

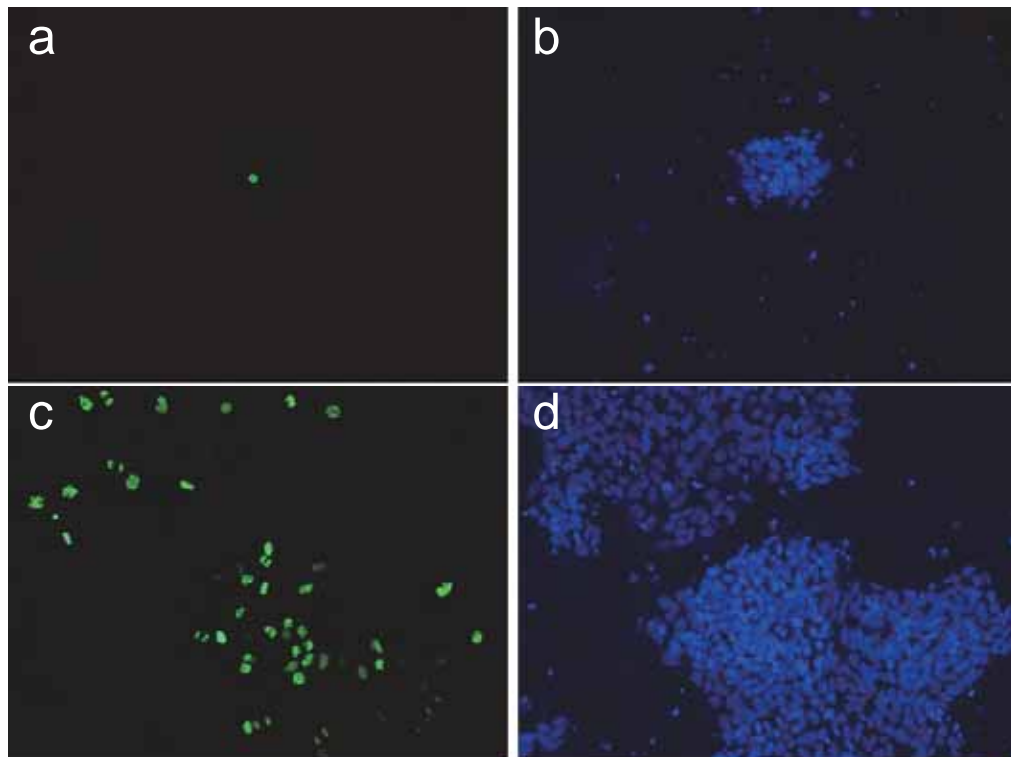


Figure 3.1: Initial trials with hESC grown under proliferative conditions during four days on pristine and O₂ plasma treated fibers. Cells grown on pristine fibers showing low cell counts (in blue) and low proliferation (green) (a, b). Cells grown on O₂ plasma treated fibers showing significantly increased number of proliferating cells and number of cells that survive. (c, d)

Effects of Oxygen Plasma on Electrospun Fibers

Oxygen plasma surface modification has been frequently applied to activate and enhance the surface properties of synthetic polymeric materials by enriching it with O₂ functionalities. For PU it has been demonstrated that O₂ plasma treatment is a useful method that can be utilised to improve surface energy, wettability and biocompatibility [110]. More specifically O₂ plasma treatment of PU films have been shown to decrease contact phase activation of the intrinsic coagulation cascade [111] and platelet adhesion [112] while increasing cell attachment [113] and collagen immobilisation through generation of peroxide groups (e.g. R-O-O-H) [114]. It has also been reported possible to optimise the plasma exposure conditions to create relatively high concentration of the generated functional groups on the surface of PU [115, 116].

For planar substrates, O₂ plasma treatment is typically associated with increased surface roughness, without affecting bulk properties or structural integrity. However, because the typical feature size of the electrospun material is nearly on the same scale as the induced roughness, additional consequences related to fiber diameter, porosity and network morphology are expected. It is therefore important to understand how parameters in the process can be tuned to allow well-controlled fabrication of fiber networks [27]. For instance, it has been shown that UV-ozone and ethylene oxide gas sterilisation of electrospun PU induce significant changes on topography and surface roughness [117]. Another example is O₂ ion beam surface modification of the near surface morphology for PU fibers that cause fibers to flatten, decrease in diameter and introduced new functional surface groups [118]. In a comparable manner the O₂ plasma treatment can also be anticipated to affect the structural integrity of electrospun PU through etching mechanisms. To the best of our knowledge there had been no earlier study elaborating on the effects of O₂ plasma treatment on important physical properties, such as morphology, surface chemistry and hydrophilicity of electrospun PU. The knowledge of explicit effects and optimised processing windows that could aid in the controlled fabrication of the desired fiber assemblies was thus limited.

Effect of Exposure Time on Electrospun Morphology

To investigate the effects of O₂ plasma, polyether based PU was electrospun using a solution of 11 wt% biocompatible aromatic polyether based PU resin in a 60:40 mixture of tetrahydrofuran and n,n-dimethylformamide, feed at a rate of 2 ml/h and applying a voltage of 18 kV. The resulting fibers, which had a diameter of approximately 1.3 μm , were collected in 30 μm thick films on glass coverslips and an O₂ plasma treatment using 100 W RF electrode power and 30 sccm O₂ gas flow was applied while varying exposure time.

SEM micrographs showing the evolution of the morphology from pristine condition up to 7 min O₂ plasma treated fibers are presented in figure 3.2. Detailed image analysis revealed that the fiber diameter etching rate effectively is approx. 300 nm/min during the first 30 s of treatment, leading to a decrease in average diameter of around 150 nm. Even though the etching rate between 1 and 3 min appear comparatively slow, below 50 nm/min, changes in network morphology start to be visible in SEM first after 3 min treatment, as the fibers become noticeably thinner and the surface roughness of individual fibers appear altered. The diameters were found to decrease from 1190 to 970 nm, with a standard deviation (SD) of 290 and 250 nm for pristine and 3 min plasma treated fibers, respectively, corresponding to an approximate rate of decrease in average fiber diameter of 70 nm/min (when integrated and averaged over time). The initially high etching rates which rapidly decrease is possibly due to a different composition of hard and soft segments present at the surface compared to the bulk. Assuming the fibers to be etched with a uniform rate, the etching rates corresponds to a removal of polymer in the range 2.5-0.8 nm/s which are comparable to values reported elsewhere [119] for similar power density and pressure. The overall impression throughout all observations is that the fibers are primarily subjected to etching in the top layers. Potentially this is due to a combination of shadowing effects and z-position in the plasma during exposure.

The effect of the plasma etching on the surface of single fibers grows more apparent after 5 min, as a rough texture emerges on the majority of the fibers. Also a minor population of fibers that are completely cut off can be seen at this point. A possible explanation for the emerging roughness is, again, the selective etching

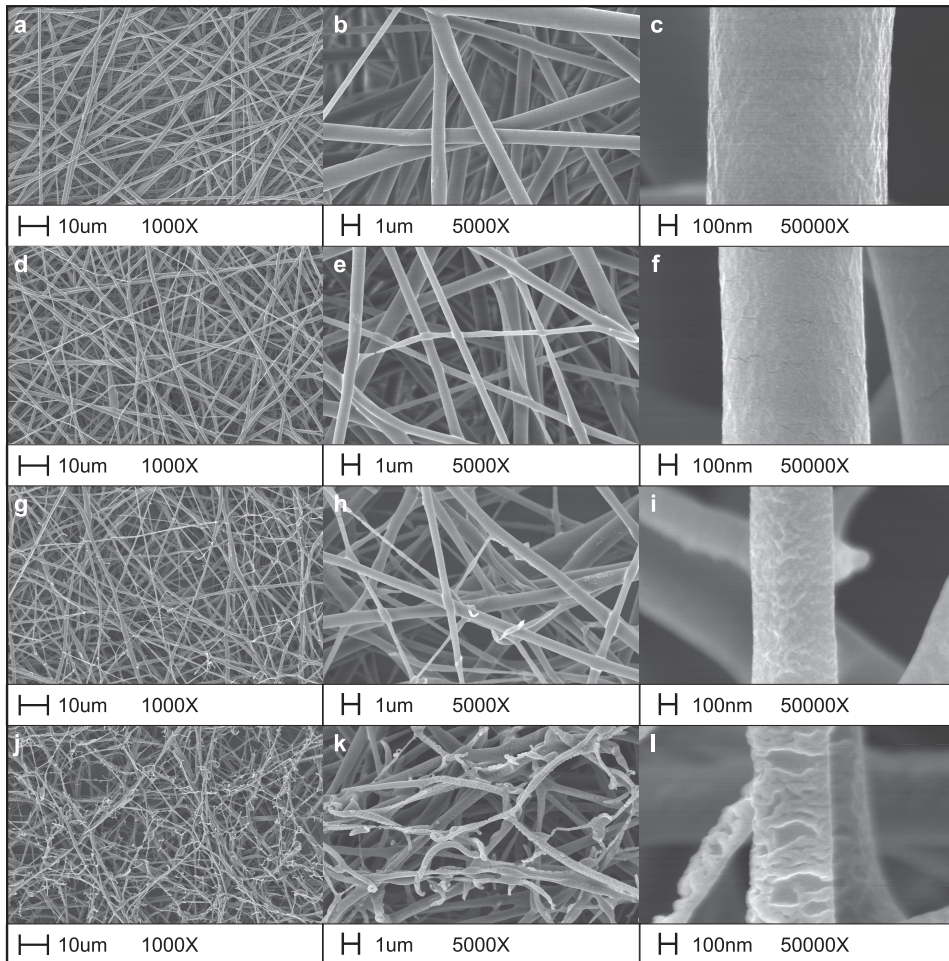


Figure 3.2: Effect of O_2 plasma treatment on electrospun PU morphology. (a-c) Pristine electrospun PU, (d-f) 3 min plasma treatment, (g-i) 5 min plasma treatment, (j-l) 7 min plasma treatment.

of soft and hard segments of the PU chains distributed in the fibers. Extending the treatment to 7 min completely degrades top laying fibers of the network as a large portion collapse to short ends, making it difficult to define meaningful data on fiber diameters for longer treatments than 5 min. Proceeding beyond 7 min was considered irrelevant since the useful fibrous morphology and the membrane itself essentially become completely degraded.

Indeed the morphological changes imposes limitations to the plasma processing windows for electrospun fibers. Considering the increased number of cut off fibers after 5 and 7 min this seems to occur when the fiber diameters have been reduced to $\sim 600\text{-}800$ nm, effectively $\sim 50\text{-}70$ % of their original dimension. The potential for the O_2 plasma to reduce fiber dimensions and alter surface texture before breakage is thus significant.

In terms of porosity the influence of plasma etching was limited (64-74 % going from pristine condition to 7 min O_2 plasma treatment) and the result is in agreement with porosities that has been reported for electrospun PU networks of other dimensions. Choi et al. measured the porosity to be in the range of 55-60 % using mercury porosimetry for fibers with a few microns in diameter [120]. Applying the same technique on electrospun fibers of diameters in the range of 200-500 nm, both Lee et al. [121] and Carlberg et al. [98] found the porosity to be 80 % and 86 %, respectively. As the diameters reported here are around one micron, it is sensible for the porosity to reside between the previously reported values.

Effect of Exposure Time on the Surface Chemical Composition

In order to determine and compare the surface elemental composition and amount of functional groups introduced on the electrospun fibers by the O_2 plasma, wide scan and high-resolution XPS spectra were recorded for various treatment times. Representative spectra are given in figure 3.3. From the wide-scan data it can be seen that the O_2 plasma treatment increases the overall O_2 content at the surface by approximately 5-7 atomic% units, while the carbon content is decreased by roughly the same amount. This corresponds to an increase of roughly 20-30 % O_2 content compared to the pristine fibers. The O_2 content initially increases

slightly with longer treatments and the maximum of ~ 27 atomic% corresponding to an O/C ratio of 0.39 is detected after 5 min. Both these values are similar to data presented by Sanchis et al. [110] who studied O₂ treated polyester based PU films and found maximum O₂ content to be 27 atomic% with an O/C ratio of 0.39. The reduction in O₂ content observed after 7 min as compared to 5 min can be explained by the fibers being cut off or becoming completely degraded which exposes underlying fibers that are initially shadowed to the plasma radicals and therefore have lower O₂ content.

To further investigate the state or binding configuration in which the increased O₂ content is present at the surface, high resolution spectra of the C 1s peak were acquired and Gaussian-Lorentzian functions were fitted to the spectral envelope. Studying the magnitudes of the C 1s sub-peak components in the HRXPS spectra of pristine and O₂ treated electrospun PU reveals that the chemical shift is towards carbon of higher binding energy. The two peak components that exhibit the largest increase represent functional groups containing double bonded O₂ in the form of carbonyl (C=O) at 288 eV and carboxyl (O-C=O) at 289.2 eV. Considering the ratios of the C=O / N-C-O and O-C=O peak towards the C-R peak (a combination of C-H and C-C), the increase of these groups are around 5-10 fold when compared to the pristine. The O₂ binding is believed to occur both at the soft segment and at or in-between the aromatic sites.

Water Contact Angles

Wettability measurements can to a high degree sense changes in the interfacial layers of a surface and reveal information about the surface energy that complements the data acquired with XPS. The static water contact angle (CA) for solution cast PU film was measured to $72^\circ \pm 4^\circ$, which is relative close to other reported findings of 73° [122], $61-67^\circ$ [123], $78^\circ \pm 3^\circ$ [124] and 87° [110]. Comparing cast PU with electrospun PU, shows that the wettability is strongly affected by the porous surface structure of the fiber network (figure 3.4a and b), which is in agreement with findings for other polymers [125]. The hydrophobic response is significantly amplified by the electrospun morphology as an effect of the resulting interface towards the water drop being a combination of multiple PU and air contact points

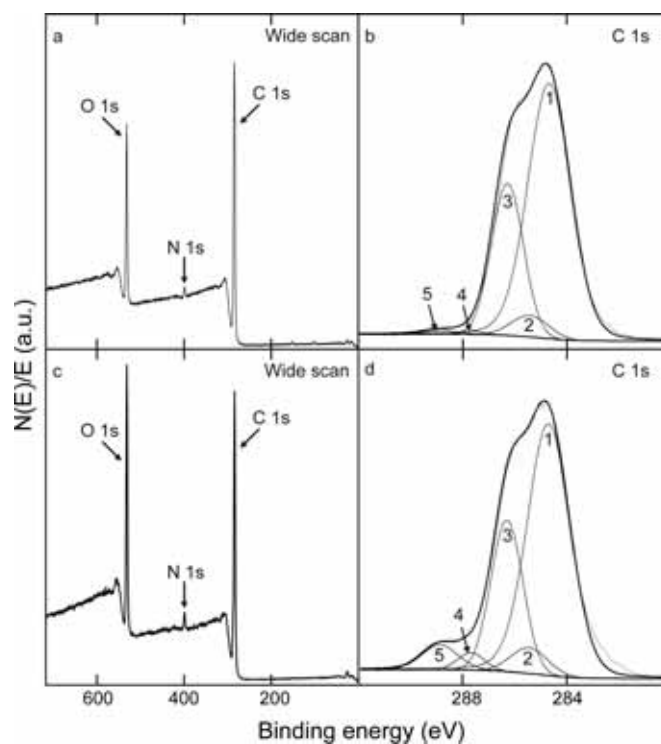


Figure 3.3: Representative XPS wide scans and C 1s core-level spectra showing the effect of the O_2 plasma treatment on the surface elemental composition. Comparing (a, b) pristine electrospun PU fibers and (c, d) O_2 plasma treated (1 min) electrospun PU fibers there are clear differences in the relative magnitude of the carbon and O_2 peaks. The C 1s spectra further reveals that it is primarily the peaks representing carbonyl (4) and carboxyl (5) that are responsible for the increased O_2 content.

[126]. Since the single fiber diameter and pore sizes are relatively small compared to the droplet, the behaviour can arguably be described by the Cassie equation for films comprising surface pores filled with air and water:

$$\cos(\theta_{\text{porous}}) = f_1 \cos(\theta_1) \pm f_2 \quad (3.1)$$

where θ_1 is the CA on a non-porous surface of the material and f_1 and f_2 are the area fractions of material and air(-) or water(+), respectively.

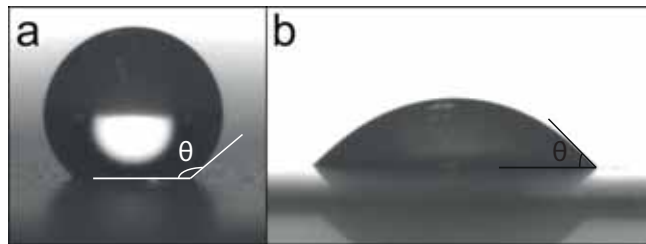


Figure 3.4: Representative images acquired during water CA measurements showing the hydrophobic response of pristine PU fibers (a), in contrast to the hydrophilic response after O₂ plasma (b).

The static CA on the pristine electrospun PU was measured to be 135°. Comparing this value to a theoretical estimation based on equation 3.1 (using the SEM estimation of the fiber area fraction and the CA for cast PU) it can be seen that the model underestimates the CA by more than 10°. Reversing the equation and using the measured CA on pristine fibers of 135° to estimate the area fraction results in an effective porosity of 78 % in the top layers. This indicates a higher porosity of the electrospun network than the estimation made from SEM image analysis.

All plasma treated samples were found to absorb water into the network at a rate varying from approximately 4-6 $\mu\text{l}/\text{min}$, with the trend being that longer treatment time lead to higher rates. The results shows that an increase in surface O₂ content and change in carbon binding states, as seen from XPS spectra, can produce a drastically different and more hydrophilic wetting behaviour for this type of fibrous substrates. In this context it is reasonable to ascribe the response to change in polarity or charged groups on the surface.

A correlation between water contact angles and cell interactions is commonly mentioned in the context of cell culture surfaces, and has been treated explicitly in literature. In an interesting work Tamada and Ikada [107] studied fibroblast cell adhesion relation to water contact angles ranging from 40° to 120° induced through plasma treatment on planar substrates from five different polymers. The reported results showed, with small variations, that the maximum cell attachment was achieved for a range of contact angles from roughly $55\text{--}75^\circ$, peaking slightly below 70° , regardless of polymer type. It was also stated that no relation between longer plasma treatment time and increased cell adhesion could be found. In fact, the results clearly demonstrated that further hydrophilization of the surface do not always improve adhesion. Nevertheless, applying a plasma treatment caused improvement above non treated surfaces on all polymers, even when the water contact angle was similar. It was speculated the reason could be related to increased total surface area through induced microscopic roughness and/or that functional groups, such as carboxyl groups, are favorable for cell attachment. Consequently, it is also relevant to compare alternative plasma gases to O_2 , as the specific gas will affect both the composition of functional groups and the resulting surface roughness.

After learning the effects from O_2 plasma on electrospun PU, we returned for a more elaborate investigation regarding the effects that the surface modification of the electrospun scaffolds can impose on seeded hESC and nSCs. However, recognizing the relation between water contact angle, surface chemistry, nanoscale morphology/roughness and cell attachment, we extended our studies to also include surface modification using argon and hydrogen plasma gases on both randomly oriented and aligned electrospun PU fibers (Paper B).

3.2 Stem Cell Response on Plasma Surface Modified Electrospun Scaffolds

The stem cell response on plasma surface modified electrospun scaffolds can be an important input to the development of functional scaffolds for tissue engineering and regenerative medicine. To our knowledge, there had been no previous studies

comparing the influence of different surface plasma modifications of electrospun PU fibers on cellular behavior. In an attempt to discern the potential of using plasma surface modification on electrospun scaffolds, we evaluated and compared how argon (Ar), oxygen (O₂) and hydrogen (H₂) plasma surface modifications on random and aligned electrospun PU affect the expansion, migration and differentiation of hESCs as well as postnatal rodent nSCs.

The fibrous scaffolds used for this study were electrospun using both a commercial electrospinning equipment and a custom built setup. The polymeric solutions for electrospinning were prepared by dissolving a biocompatible aromatic polyether based PU resin in a 60:40 mixture of tetrahydrofuran and n,n dimethylformamide and homogenized for 24 h. A small amount of benzoin methyl ether (BME) was also added. The resulting solution was then transferred to a syringe with a 21-gauge stainless steel cannula. Randomly oriented fiber membranes, $\sim 30 \mu\text{m}$ thick, were collected directly onto glass cover slips attached to the grounded collector. A feeding rate of 2 ml/h was used and a positive potential of 18 kV was applied to the stainless steel cannula at a distance of 18 cm. Aligned fibers were electrospun using the same spinning parameters, but using a custom fixture with parallel, separated and grounded electrodes, that forced the fibers to align uniformly as they deposited on the cover slips. After deposition, the samples were briefly exposed to DUV irradiation in order for the BME molecules to induce crosslinking between rigid macromolecular blocks of the segmented PU chains, resulting in fixation of the fiber networks to the glass substrate [127]. The plasma surface modification of the scaffolds was then applied with 100 W RF electrode power, 30 sccm gas flow, for 3 min at 13 Pa and 0.1 Pa as process and base pressure respectively. After the treatment the fibers were exposed to air for 10 min to allow for any remaining free radicals to settle.

The resulting morphology of the electrospun surfaces after the plasma surface modifications was investigated using SEM (figure 3.5). The primary observed effect was altered fiber surface texture and roughness, and three different morphologies were identified. For the Ar plasma treated samples, the texture consists of a grainy structure with an average grain diameter of $\sim 25 \text{ nm}$. The H₂ treatment results in fibers that appear smoother compared to the native case. In contrast, the O₂ plasma gives rise to a high surface roughness consisting of larger random elongated

granular structures.

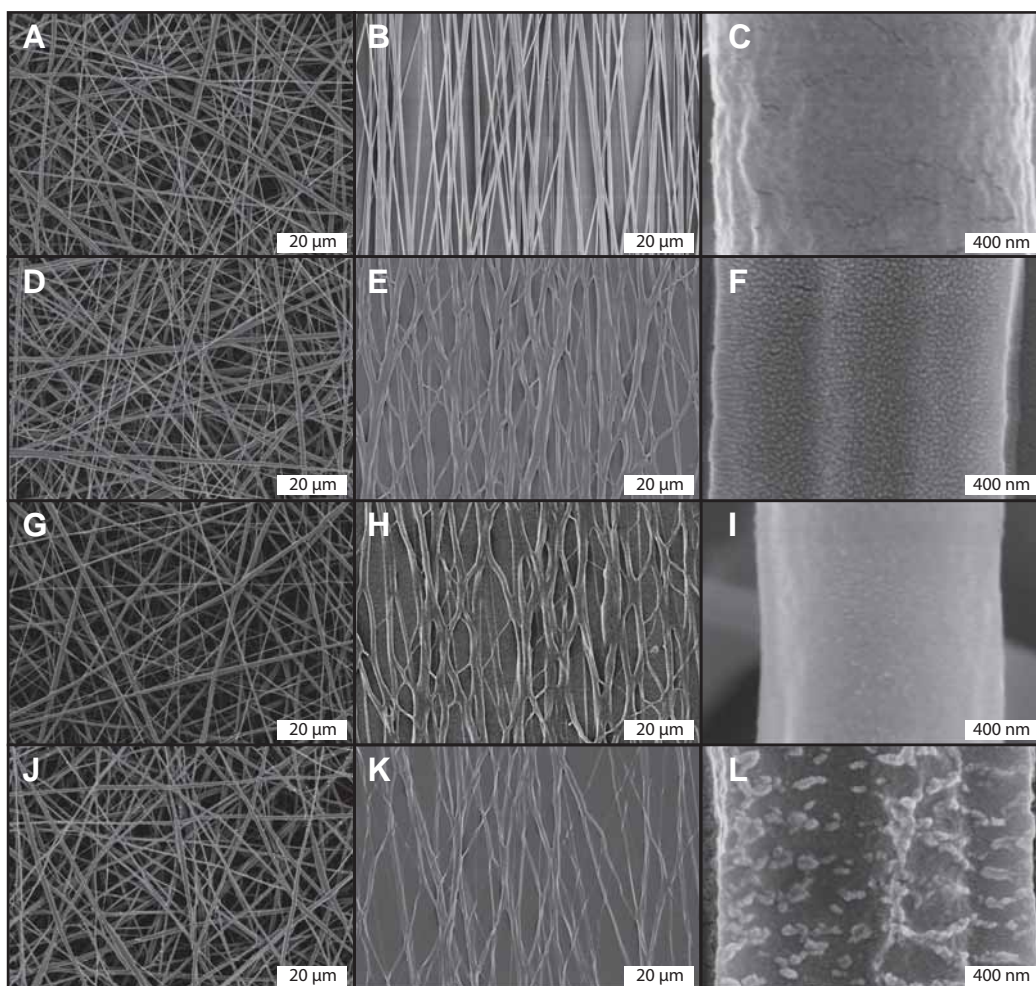


Figure 3.5: Effect of plasma surface modification on scaffold and single fiber morphology. SEM of (A-C) native fibers and (D-F) Ar, (G-I) H₂ and (J-L) O₂ plasma surface modified fibers.

For both the random and aligned fiber networks, the plasma treatments leave the overall network structure largely unaffected. A reduced average fiber diameter was observed on the O₂ plasma samples, which was in agreement with our previous studies. No significant reductions of average fiber diameter were found for the Ar and H₂ treatments.

Through image analysis of the collected SEM images, the porosities of the

randomly oriented fiber scaffolds were estimated to be $67\pm 4\%$, $66\pm 6\%$, $66\pm 6\%$ and $69\pm 3\%$, for Native, Ar, H₂ and O₂ treated samples respectively. The pores size distributions in the top layers of the scaffolds were found similar for all randomly oriented fiber scaffolds (figure 3.6). The majority of the pores were found to have an area below 15 μm^2 up to maximum area of approximately 45 μm^2 .

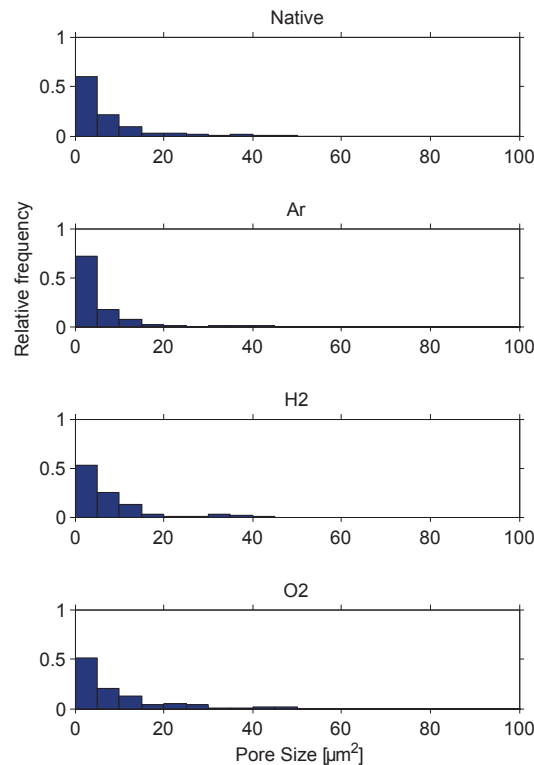


Figure 3.6: Pore size distribution of the randomly oriented fiber scaffolds

To determine and compare the surface elemental composition and amount of functional groups introduced on the fiber surfaces from the plasma surface modifications, wide scan and high-resolution XPS spectra were recorded. The Oxygen/Carbon (O/C) ratio was found to increase nearly 40 % from the O₂ plasma modification as compared to the native fiber condition (table 3.1). In contrast, the O/C ratio decreased by 10 and 30 % for H₂ and Ar plasma modification respectively. In addition, the H₂ plasma was found to reduce the amount of surface

Table 3.1: Surface elemental composition from XPS wide-scan.

Sample	Atomic percentage [%]			O/C ratio
	O 1s	N 1s	C 1s	
Native	19.9	2.2	77.9	0.26
O ₂	25.5	2.9	71.7	0.36
H ₂	18.4	0.9	80.6	0.23
Ar	15.4	2.5	82.1	0.19

Table 3.2: Fraction of functional groups from high resolution XPS scan of C 1s peak.

Peak	Binding Energy (eV)	Chemical function	Relative Percentage			
			Native	O ₂	H ₂	Ar
1	285	C-R	65.0	58.0	67.8	66.7
2	285.75	C-N	3.8	4.6	4.9	3.7
3	286.61	C-O-C	29.5	28.2	20.8	16.9
4	288	C=O or N-C-O	0.6	3.2	5.0	3.2
5	289.2	O-C=O	1.1	6.0	1.5	1.2

exposed nitrogen, while the O₂ and Ar gas tend to increase it slightly.

In terms of specific functional groups, the differences between the treatments are further emphasized by the C 1s core level spectra (figure 3.7) and the corresponding relative percentages from Gaussian curve-fitting (table 3.2). The main feature of the O₂ treatment is a large increase in the number of carboxyl groups (O-C=O) on the surface. As seen from the peaks at 289.2 eV, these are much less pronounced for the other samples. The H₂ and Ar treatments show similar spectra which are characterized by a significantly reduced contribution from the peaks related to the ether linkages (C-O-C) at 286.6 eV. Compared to the native condition, the number of surface exposed carbonyl (C=O) groups is higher for all the treated samples. The H₂ plasma treatment lead to the highest concentration of carbonyl functionality.

The measurements of contact wetting angle showed that the all three plasma surface treatments modifies the wettability from the hydrophobic surface of the native electrospun fibers to a hydrophilic response. All three modifications showed similar wetting behavior and had an initial water contact angle close to 50°. Within

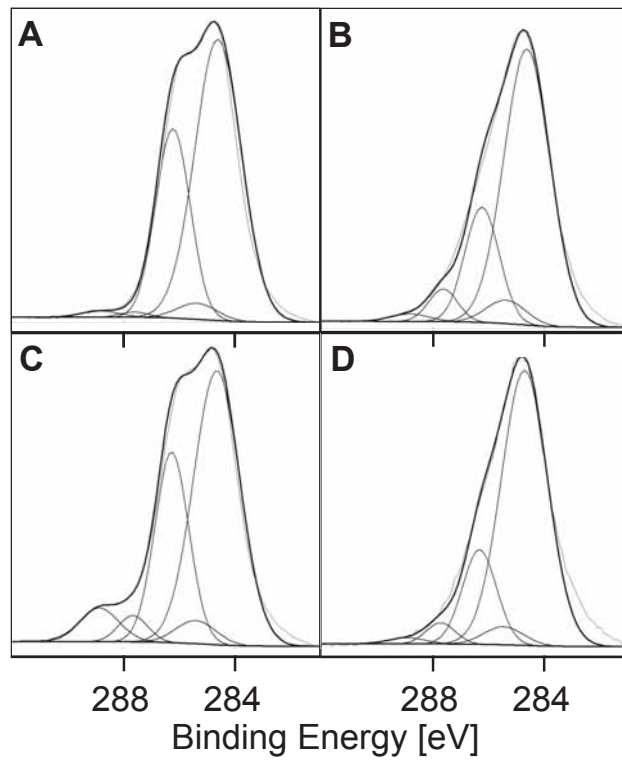


Figure 3.7: Effect of plasma surface modification on surface chemistry. C 1s core-level spectra of (A) native fibers and (B) H₂ (C) O₂- and (D) Ar plasma surface modified fibers.

a few minutes the water penetrated into the modified networks, while the water drop remained on top for the native fibers.

In summary, the different plasma gases generate three variations of surface functionalities, which have potential to give rise to detectable differences on cellular behavior. The amount of O₂, particularly in the form of carbonyl and carboxyl functionalities, is of interest as it has been reported previously to be correlated with cell adhesion on PU [121, 128–130]. Thus, after characterizing the effects of the plasma surface modifications on the scaffold, we next sought to investigate the effect different treatments have on the expansion (i.e. both attachment and proliferation) of hESCs.

Expansion of hESC on surface modified electrospun PU

Prior to culture, the electrospun scaffolds with the different plasma treatments, were coated with a protein coating in accordance with recommendations from the stem cell line. hESCs were then seeded as a monolayer of single cells on the electrospun networks and allowed to grow under proliferative conditions using growth factors until confluency, which took about 3-4 days. Under these culture conditions, staining indicated that the cells retained their multipotency and was not driven into differentiation on any of the substrates. On randomly oriented fibers, all plasma treatments were found to dramatically improve the expansion capability of the seeded hESC, as compared to the native fibers. The observed increase in expansion was roughly 7-fold for Ar, 5-fold for H₂ and 4-fold for O₂ treated fibers (figure 3.8A). However, when expanding hESCs on aligned fiber surfaces, no improvements in expansion capability was observed from applying the plasma surface modifications (figure 3.8B).

For nSCs, migration, cellular alignment and differentiation is of high interest in order to repair damaged nervous tissue that requires directional composition. Recent studies have shown that both the orientation of the fibers as well as the diameter of the fibers can significantly influence the morphology, proliferation, phenotype and function of various cell types, including neuronal stem cells [62, 90, 131]. Additionally, increased surface roughness on the micro and nanoscale has been shown to alter cell differentiation and extracellular matrix production *in vitro*,

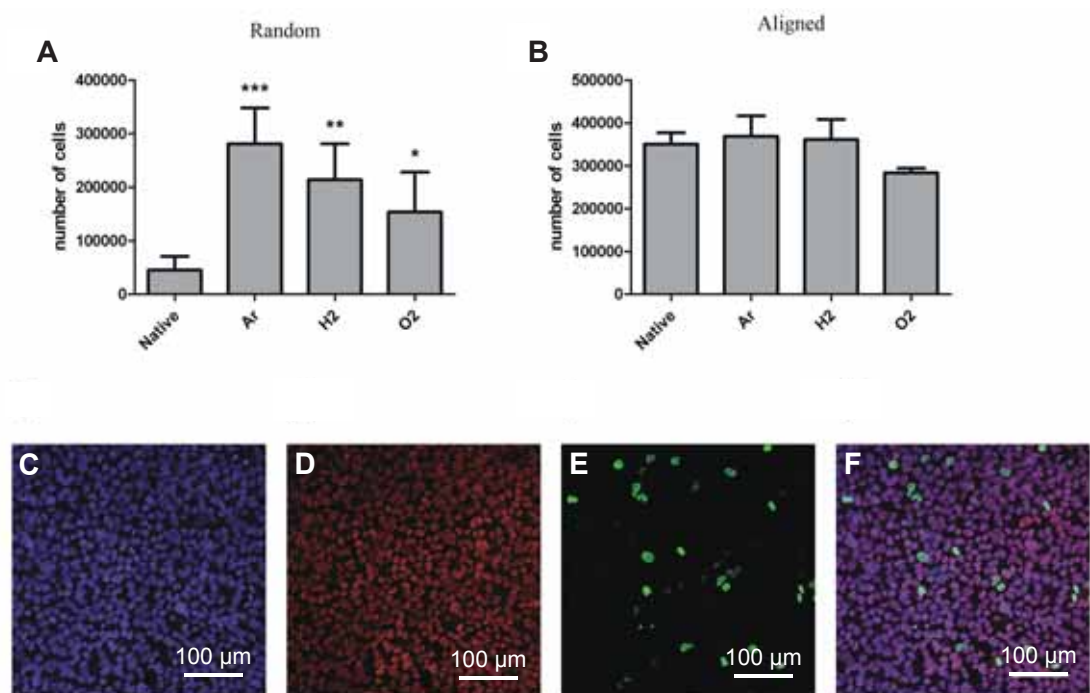


Figure 3.8: Quantification of hESC expansion on plasma treated electrospun PU networks. (A) Randomly oriented, plasma treated fibers significantly improve the expansion of hESCs, as compared to native fibers. (B) Cells cultured on aligned fiber substrates could be expanded equally well on native and plasma treated substrates. (C-F) Microphotograph of hESC growing under proliferative culture conditions. (C) DAPI (cell nuclei), (D) Oct-4 (marker for undifferentiated stem cell) (E) pHH3 (dividing cells) and (F) overlay of images shown in C-E. Data displayed are mean values with standard error of the mean, $n = 5$ in (A) and $n = 3$ in (B).

suggesting that it could determine cell fate *in vivo*[132]. Therefore, we proceeded to investigate whether the surface modifications of aligned fibers surfaces affect migration and differentiation of nSCs.

Migration and differentiation of NSCs on surface modified electrospun PU

Neural stem cells are often cultured as clusters of cells termed neurospheres. When culturing small ($\sim 100\text{-}150\ \mu\text{m}$ in diameter) neurospheres together with aligned fibers, individual cells were observed to start migrating out of the spheres. These cells preferentially migrated along the direction of the fibers, creating an oval-shaped halo around the original sphere. The cells remaining inside the neurosphere extended long, glial fibrillary acidic protein (GFAP)-positive bundle of processes along the direction of the fibers (figure 3.9). GFAP is a protein component of the cytoskeleton expressed by several different cells in the CNS, among these astrocytes. A quantification of the number of cells migrating along with the fiber, as compared to cells migrating perpendicular to the fiber is presented in figure 3.9, D-F. In addition, the average distance of migration was measured. We found that there was a highly significant effect on the angle of migration, where cells preferentially migrated along with the fiber as compared to perpendicular to the fiber (figure 3.9, D-F). However, differences between different plasma treatments were not statistically significant.

To investigate if the plasma surface modification affected the differentiation, NSC were seeded as single cells on both randomly oriented and aligned fiber substrates. After attachment and differentiation for 2 days, the cells were fixed, stained for a the immature neuronal marker -III-tubulin, and quantified. Differentiation was found largely unaffected by both plasma treatment and fiber alignment, as all samples displayed approximately that 5 % had differentiated into neurons. This result indicates that the NSC fates were mainly governed by growth factors and chemottractants in the media, rather than the scaffold related cues.

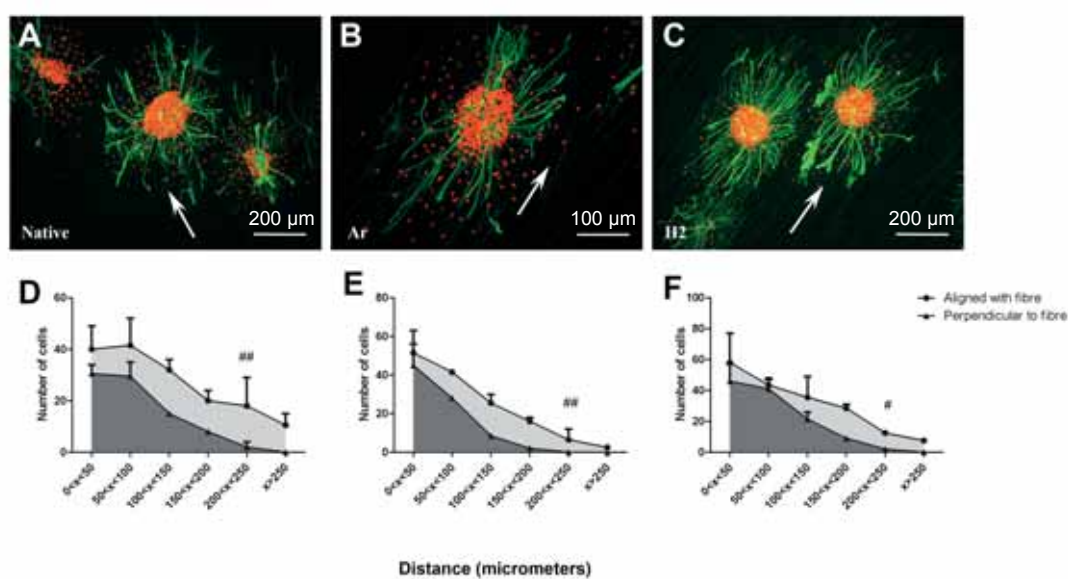


Figure 3.9: Effect of fiber orientation on cellular migration and process extension. (A-C) Microphotographs of neurospheres cultured on native, Ar- or H2-treated fibers. White arrow indicates the direction of the fiber. Cell nuclei are visualized in red, GFAP processes in green. (D-F) Cells preferentially migrated along the fiber direction on all substrates (D) native fibers, (E) Ar-treated fibers and (F) H2-treated fibers.

Summary and discussion

In summary, the plasma surface modifications generated three combinations of different surface functionalities and roughness, but with similar hydrophilicity. In our study, characterization of hESC cultured on both random and aligned electrospun PU shows that plasma surface modification of O₂, Ar and H₂ plasma drastically improves the possibility to expand hESC on randomly oriented fibers. These findings are in agreement with previous reports on enhancement of cell adhesion potential related to the degree of surface roughness and hydrophobicity [129].

Surface functional groups, such as hydroxyl (-OH), carboxyl (-COOH), carbonyl (C = O) and amino (NH₂), have been shown to affect the binding of cell-adhesive proteins, such as fibronectin and vitronectin, through changing the surface energy and charge [133]. O₂ and Ar plasma surface modification has specifically been reported to induce hydroxyl, carboxyl and carbonyl functionalities and also to improve attachment of unrestricted somatic SCs on planar PU surfaces [134]. The modified surface functionality is likely contributing to our observation of increased hESC adhesion on the Ar and O₂ plasma treated randomly oriented fibers. A similar effect also appears to be valid for the H₂ plasma treated fibers, even though this has not been reported earlier.

Moreover, the protein conformation onto various surface functionalities has earlier been shown to influence the proliferation and differentiation potential of stem cells [135]. We found the highest number of cells on Ar plasma treated samples, followed by H₂ and finally O₂ plasma, and that the cells remain in an undifferentiated state. Since the wettability of the three substrates was found to be similar, additional factors have likely influenced the expansion. Based on the differences between the plasma treatments, these additional factors could be due to the specific functional groups and the surface roughness of the individual fibers. Considering the results, it appears that the changes of surface functionality and roughness have a somewhat smaller, yet significant, influence on cell expansion, compared to that of surface energy. Argon plasma is here found to induce the more optimal combination of surface functionality and roughness for hESC expansion on random electrospun PU when compared to O₂ and H₂ plasmas.

Based on the observation that the changes induced from the Ar and H₂ plasma

treatment have similarities, can be seen as an indication that certain morphology of the nanoscale roughness may be more optimal for the cell expansion. Similar effects have been reported by several studies, where it has been suggested that nanoscale surface roughness can increase the opportunity for protein adsorption on scaffolds, which could facilitate stem cell attachment and growth [136, 137]. One example is Bao et al. [138], who found that scaffolds based on electrospun PLGA with a nanofibrillar morphology absorbed large amount of proteins, due to large surface area, and therefore could enhance human mesenchymal stem cells spreading and viability. Recently, Zamani et al. [139] studied fibrous scaffolds of different roughness and found nano-rough cylindrical fibers to be more favorable compared to smooth fibers for attachment, growth and proliferation of human neurons. This was also attributed to high surface area and roughness. Our results point in the same direction as other studies performed on human endothelial cells, which have shown that surface roughness, on the scale of 10-100 nm, can enhance the adhesion and growth of cells [140].

Unexpectedly, the improved cell expansion possibilities with plasma surface modifications on random fibers were not found for fiber substrates with aligned fibers. Instead the results showed negligible differences between the modified and native fiber surfaces. A possible explanation could be that parallel aligned fibers provide a more flat surface which is similar to a planar surface. Compared to the random fibers, exposing a higher micro scale roughness and limited area of contact due to the random stacking, the planar surface allows the cells to form a higher number of focal contact points. With a higher number of contact points, the properties of the specific surface may become less critical, which diminish the detectable effect of the plasma treatment in our measurements. This reasoning is also in agreement with the result that O₂ plasma treated samples, which show the largest micro scale roughness, leads to a somewhat lower cell expansion compared to the other plasma treatments.

Previous investigations have reported indications that the differentiation of stem cells can be affected by surface roughness as well as fiber alignment and diameter [141–143]. Some studies have found that substrates with aligned fiber morphology induce differentiation towards neural lineages of murine embryonic stem cells, while directing and improving neurite outgrowth. Massumi et al [141]

investigated the effect of surface roughness and fiber alignment on differentiation of mouse embryonic stem cells and found higher expression of ectoderm/neural markers indicating neural differentiation on some of the aligned substrates. It was argued that alignment is important for efficient neural differentiation, but that it also can be promoted by the surface roughness generated by the fiber scaffold. Xie et al [142] demonstrated that dissociated mouse embryonic stem cells can be induced to differentiate into specific neural lineages, when seeded onto electrospun fibrous surfaces. They found that aligned fibers could enhance this type of differentiation and also direct the associated neurite outgrowth. A few previous studies also show that a particular fiber diameter can assist to direct the differentiation of neural stem/ progenitor cells towards specific neural lineages. For instance, Christopherson et al. [144] studied electrospun fibers with varying fiber diameter and found that rat neural stem/progenitor cells under differentiation conditions on 750 and 1500 nm fibers result in an increased differentiation towards neuronal lineage. This was compared to fibers of smaller diameter, which instead lead to increased oligodendrocyte differentiation. Cells on smaller fiber diameter assumed cell morphology of glial lineage, whereas cells on larger fibers assumed morphology closer to that of differentiated neurons. It was also found that there was a significantly reduced adhesion and limited migratory capacity on larger fibers. In contrast to the study by Christopherson et al., Wang et al. [90] found that 400 nm fibers lead to increased neuronal differentiation of hESC-derived neural precursors compared to 800 nm fibers.

Even though several other studies have found significant effects of surface roughness on differentiation on flat substrates, our results indicate that the influence of surface roughness on individual electrospun fibers is small. In our hands, the percentage of differentiating cells remained relatively constant (approximately 5 % of the total number of cells) throughout the different surface conditions. With this said, it should be noted that the time provided for the cells to differentiate was relatively short, and therefore it is possible, but not likely, that more cells would have differentiated into neurons with longer differentiation times.

In our experiments, the two main effects observed on aligned fiber substrates were contact guided migration from neurospheres and GFAP-positive bundle of processes extending in the direction the fibers. This type of contact guidance

was not significantly affected by the altered fiber surface roughness and surface chemistry induced from the H₂ and Ar plasma modifications. Despite seeing clear effects on cell alignment from the fiber topographical cues, the fiber orientation and the plasma treatments were found not to affect the neuronal differentiation of the NSCs. A possible explanation is that the growth factors and chemottractants of the cell media, in this case, had a dominating influence on the differentiation compared to the topological cues induced from the electrospun topography.

Several groups have previously reported that cells [145] as well as axons [146, 147] orient themselves along the direction of underlying topographical cues imposed by electrospun fiber matrices. This result was also confirmed by our study, where the effect on migration preference, as well as the direction of process extension, was clearly observed. It appears as even though growth factors and other components in the cell media strongly influence differentiation, the fiber substrate provides a strong cue for cellular migration.

In parallel to our studies of the effects on hESC and neural stem cell behavior, as described above, we were also interested in the related question of how the topographical features would influence fully differentiated cells, i.e. specific neural cells. As mentioned earlier, electrospun scaffolds has been proposed as an alternative three-dimensional substrate to conduct *in vitro* based biological studies. Electrospun polystyrene substrates has, for instance, been suggested as a complement to traditional 2D polystyrene cell culture systems, based on results from muscle cell attachment and morphology [60].

3.3 Topographical Reactions of Neural Cells on Electrospun Scaffolds

Studying and isolating the intricate biological processes and functions of a single specific cell type among the vast array of other cells and their concomitant signalling *in vivo* is largely impossible with current technology. Adding to this are the many ethical considerations for both animal and human tissue that limit experiments from being conducted directly *in vivo*. To escape many of these issues and enable detailed investigations of individual cell types, *in vitro* based cell cul-

ture systems were developed. Today, *in vitro* based studies are used extensively in the biomedical area to improve fundamental understanding of different cellular processes and for biotechnical applications, such as drug testing and screening, preceding animal trials.

Conventional cell culture has traditionally been performed on planar substrates, typically from polystyrene or glass. Despite recognition of the fact that this type of system constitutes a highly artificial environment, two-dimensional surfaces have almost exclusively dominated the field of *in vitro* cell studies [6]. The unwanted consequences of using the standard planar culture substrates are altered cell morphology and function as well as gene and protein expression compared to the *in vivo* situation [148–150]. As mentioned earlier, this adds to the already difficult challenge of understanding and predicting cellular processes and responses *in vivo* based on results observed for cells *in vitro*. In the following section we present our results from investigating the use of electrospun PU fiber networks as scaffolds for *in vitro* culture of primary astrocytes and neurons.

Fiber based Microenvironment Maintaining Astrocyte Morphological Complexity

Aiming to improve *in vitro* cell culture systems, in a way that they that better capture the structural and functional complexity of cells *in vivo*, 3D culture scaffolds are of high current interest. Generation of such scaffolds, intended to provide 3D porous structural support for cells, have been demonstrated through various techniques, including for instance solid-free forming, solvent casting/particular leaching, phase separation, freeze-drying, two photon lithography and non woven electrospun meshes [60, 151] (for reviews see [5, 152–155]). Some of the most commonly used 3D culture substrates to date, are alginate based scaffolds [156], collagen gels [157] and hydrogels [158]. The main issues with these systems are their dense structure, that often hinders process extensions and partly distorts cell distribution, high volume of gel bound liquid, slow diffusion rates of nutrients and lack of the possibility to use cell type specific ECM coatings. Other systems with sponge-like or macroporous structure typically induce cell clustering and compartmentalization that prevent free cell–cell interactions. However, through its fibrous

and ECM-like features, electrospun fiber based scaffolds have the potential, to be tuned to escape some of these issues.

Suggestions on how to accomplish a biomimetic surface using electrospinning include direct spinning of collagen fibers [50, 159], adding peptides or proteins into the solution to be spun or by attaching ECM mimicking biomolecules on the fiber surface [160]. One of the issues with directly utilizing natural proteins, is that the procedures used to process the material, into an engineered form, often compromise its biological and structural properties. For example, Rho. et al. [159] reported that electrospun collagen needed to be crosslinked prior to use, as it swells and partially dissolves in water, making it difficult to use as a scaffold during *in vitro* culture. After observing relatively low human epidermal and oral keratinocyte adhesion onto uncoated electrospun and gluteraldehyde vapor-phase crosslinked collagen networks, compared to polystyrene surfaces, it was suggested that denaturalization of the collagen conformation had occurred. Coating the electrospun collagen with additional ECM proteins indicated that type I collagen and laminin were the functionally active proteins and required for significantly increased adhesion.

The strategy of adding short sequences of functional nucleotides or full ECM protein coatings to the surface, has been shown to promote cell-scaffold interactions on a variety of different fibrous materials. A specific comparison between adding laminin through covalent bonding, physical adsorption and incorporating it in the electrospinning solution of PLLA fibers, was performed by Koh. et al. [160]. They reported that cell viability was highest on the fibers with physically adsorbed and covalently bonded laminin. Fibers produced through adding laminin in the electrospinning solution presented slightly lower cell viability, but enhanced the nerve growth.

To investigate the potential topographically induced benefits employing electrospun fiber based *in vitro* culture system for astrocytes, multiple series of experiments were carried out. Initially, we investigated how fiber dimensions and alignment in combination with physically adsorbed protein coating affect astrocyte adhesion, survival, morphology and proliferation. The fiber diameters were varied from 400 nm up to several microns and produced by tuning polymer concentration of the spinning solution while aligned fiber substrates were fabricated using

parallel plate electrodes. Results indicated that fiber networks around diameters of $\sim 1.2 \mu\text{m}$ with random orientation allowed for the most complex cell morphology, with features similar to the *in vivo* appearance (figure 3.11). The astrocytes reacted to the underlying topography by following the contact guidance cues. In the case of aligned fibers, this lead to stretched morphologies, which is unnatural and hence an undesirable cell shape for *in vitro* astrocyte cultures. As expected, using electrospun PU without coating brought low astrocyte adhesion and survival. In contrast to our result for hESC attachment, no improvements in attachment of the astrocytes to plasma surface modified fibers could be observed, regardless of additional protein coating. Nevertheless, both poly-d-lysine (PDL) and Poly-L-ornothine plus laminin (PoLam) coated fibers displayed significant increase in the number of live cells (quantified through lactate dehydrogenase (LDH) levels and cell counts). The collected data implied that the cells favoured the PoLam coating on the electrospun PU, for which the resulting LDH levels and number of cells were similar to that of standard coated glass coverslip surface (figure 3.10).

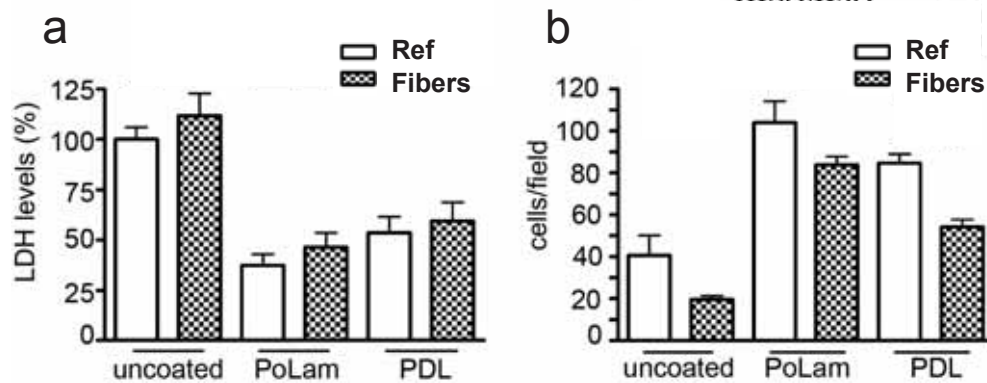


Figure 3.10: Cell survival and cell adhesion are comparable in the electrospun system and on standard culture surface. LDH levels (a) as a measure of cell death and cell adhesion (DAPI positive cells per field) (b), after 24 hours, on glass reference and electrospun fibers in non-coated condition and coated with PoLam or PDL.

Visualizing parts of the cytoskeleton by staining for GFAP and nestin, show that astrocytes on electrospun substrates have a different cytoskeletal morphology compared to astrocytes grown on the glass reference. Extensions that engulf the

fibers are observed in both fluorescence microscopy (figure 3.11) and in SEM after fixation (figure 3.12).

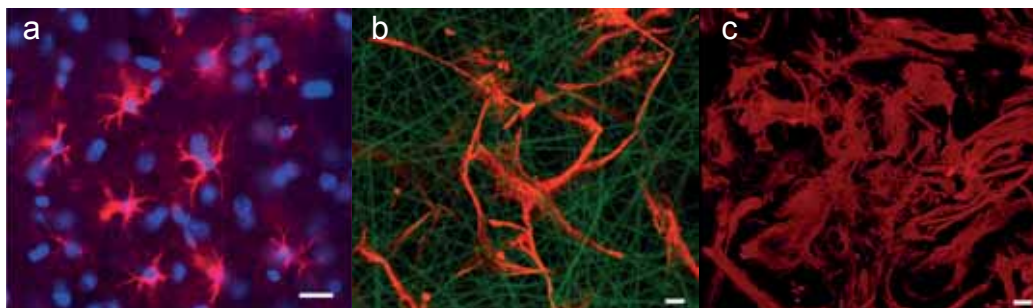


Figure 3.11: Immunohistochemical and immunocytochemical detection of astrocyte intermediate filament protein GFAP in cortical astrocytes in situ (a), for astrocytes cultured in the electrospun system (b) and on glass reference surface (c).

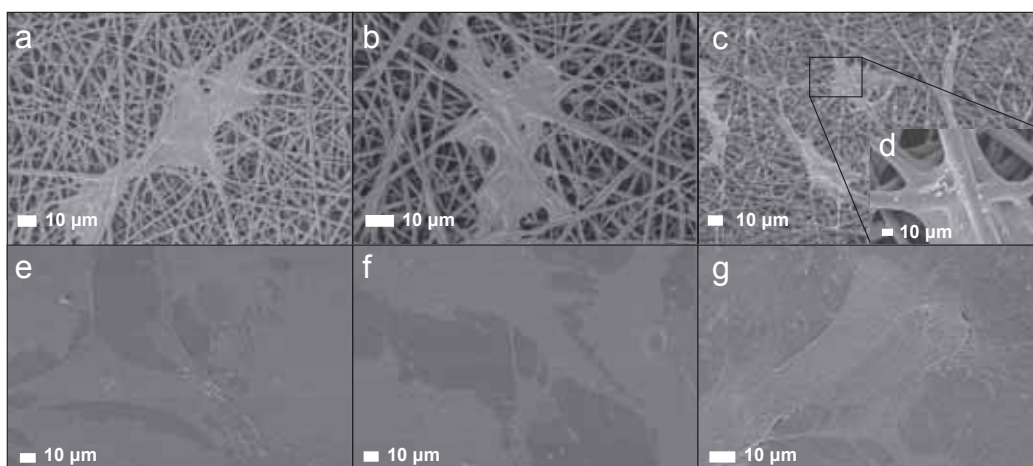


Figure 3.12: SEM micrographs of fixed astrocytes cultured on coated electrospun fibers (a, b, c, d) and standard culture surface (e, f, g).

To further clarify the morphological differences, astrocytes derived from transgenic animals that express the enhanced green fluorescent protein (eGFP) distributed throughout the entire cell body, were used. In this way it was possible to assemble and compare 3D reconstructions based on confocal images of single

astrocytes. The surface area and volume was found similar for the cells on both substrates, but the fibrous scaffold was again confirmed to support formation of a more complex cell morphology that retain certain features of the *in vivo* morphology. The similarity is quite discernible by comparing the *in vitro* grown cells to the morphology of astrocytes stained in a tissue section, i.e. *in-situ* (figure 3.13c).

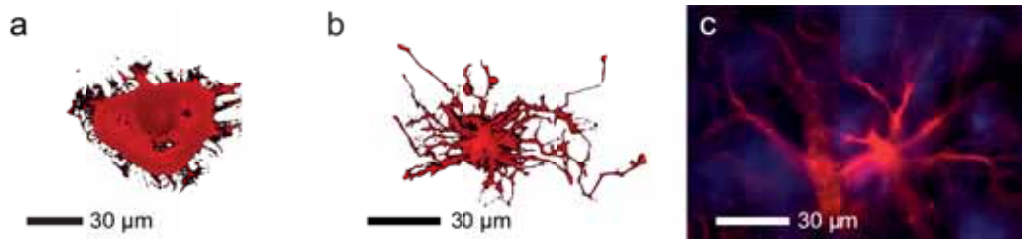


Figure 3.13: Single cell morphology of eGFP-expressing astrocytes cultured *in vitro* on glass (a) and on PoLam coated electrospun PU (b) by a 3D reconstruction of confocal images. Cells cultured on coated electrospun PU show complex cell morphologies which have similar features to astrocytes *in-situ* (c).

A drastic change in cellular morphology will affect the internal cellular structure, such as organelles and cytoskeleton, as well as the interface towards the scaffold, surrounding media and other cells. To further explore topographically related effects, Western blot analysis was used to determine the expression of protein markers related to cell stress and activation. Remarkably, the expression of all five proteins tested (GFAP, nestin, synemin, vimentin and HSP 70), was found to be reduced to fractions on the fiber substrates compared to the reference (figure 3.14). This means that astrocytes are far less reactive and stressed when grown on the PoLam coated electrospun PU network, which is of high relevance for *in vitro* culture systems.

Cellular stress has earlier been considered to be a consequence of two main aspects of *in vitro* cell culture; the cellular stress imposed by the artificial environment causing unnatural cell morphology and the presence of serum in the culture medium. As serum containing medium was used for both cultures on the electrospun and glass substrates our results points towards the reactivity of astrocytes *in vitro* is primarily a consequence of the cell forced into assuming an unnatural morphology.

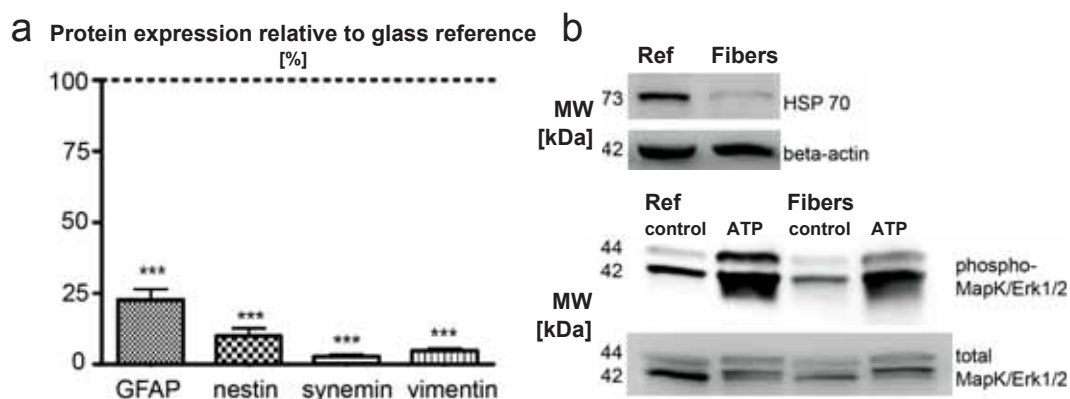


Figure 3.14: Comparison of western blot analysis showing reduced reactivity and cellular stress without affecting their responsiveness to activation. (a) Western blot analysis of intermediate filament proteins GFAP, nestin, synemin and vimentin (all known to be up-regulated upon astrocyte activation and cellular stress) in astrocytes cultured on PoLam coated electrospun fibers relative to the glass reference. (b) Western blot analysis of HSP70, a cellular stress marker, and phosphorylated MapK/Erk1/2, showing responsiveness, in astrocytes cultured on PoLam coated electrospun fibers and glass reference.

Another unwanted aspect of *in vitro* cell cultures, related to the reactive state of astrocytes, is hyper proliferation. Increased proliferation rates of astrocytes *in vivo* are most commonly associated with trauma or formation of cancerous tissue. For astrocytes grown on the electrospun fibers, measurements of two proliferation markers (Ki67 and EdU) showed significantly reduced proliferation compared to the reference, after three days into the cell culture. Importantly, it was also established that astrocytes on the electrospun fibers were still responsive to stimuli by confirming the initiation of a signalling cascade upon activation with ATP (figure 3.14b).

Moreover, comparing gene expression profiles, it was found that cells cultured on the fibers had distinct differences compared to the planar reference. Primary differences were again related to proliferation, cell shape and motility which further confirms the results of functional difference between the two culture systems.

In literature, there are several examples treating the effects of fibrous topographies on the response of astrocytes [161, 162]. Delgado-Rivera et al. [163] reported,

with similarity to this work, that a fibrous culture environment for astrocytes lead to *in vivo*-like stellate morphology and further claimed that this effect was enhanced by the presence of fibroblast growth factor. They also found that the astrocytes were more permissive to neurite outgrowth when co-cultured with neurons on the fibrous substrate compared to standard culture surfaces. Chow et al. [164] studied aligned and random fiber matrices and found that astrocytes displayed directional growth, controlled by the underlying matrix, which also agrees with the topographic guidance seen in our experiments. Recent results from Cao et al. [165] indicated that PCL based fibers with an average diameter of ~ 650 nm suppresses astrocyte proliferation and increases apoptosis, without altering cellular activation as compared to flat surfaces. In another study, Kim et al. [166] observed that electrospun PCL fibers containing spirulina (a pharmaceutical additive) alleviated astrocyte growth and activity compared to tissue culture plates. Both the two latter findings are of related character and in agreement with the result of reduced stress and activation related protein expression, as well as decreased hyper proliferation, found in our studies.

In contrast to conventional cultures, the electrospun topography induce complex cell morphologies which have similar features to astrocytes *in vivo* and suppress the undesirable over-expression of intermediate filament proteins associated with increased cellular stress levels and hyperproliferation. The combination of convenient liquid exchange and compatibility with standard culture methods, renders the electrospun fibers a broadly applicable system. Although the electrospun topography still represent an oversimplified mimicry of the *in vivo* situation, lacking a plethora of factors of chemical, temporal and spatial complexity, the system is seemingly capable to capture important features, that can be useful for basic studies of development and pathogenesis. Our findings thus provide additional arguments for using electrospun fiber based culture systems as a complement to classical conditional culture models in standard laboratory *in vitro* assays, such as protein and RNA/DNA assays, immunocytochemistry, live cell imaging and confocal imaging.

Electrospun scaffolds support formation of complex neuronal networks

The communication between neurons *in vivo* are based on cell-cell contacts in complex, three-dimensional and dynamic networks. Cell culture systems is a critical experimental platform to help understanding the involvement of neurons in neurodegenerative diseases, by studying cell-cell communication, synaptogenesis, and neural network plasticity. When using conventional culture systems based on flat substrates, the cell-cell contacts for neurons are forced into abnormal configurations and limited to extend processes in-plane. An additional problem when culturing neurons on conventional culture substrates is the high reactivity of the naturally occurring culture-contaminating glial cells. As neurons do not proliferate, while astrocytes do, astrocytes can take over the neuronal cultures. Based on our findings for astrocytes, a culture system for neurons using coated electrospun scaffolds, could potentially allow for cultured neurons to extend neurites out of plane and also minimize the number of contaminating astrocytes that release undesired stress factors. To study this, we first evaluated the viability of neurons on PDL-coated electrospun PU scaffolds based on fiber diameters of 450, 1350 and 2500 nm (figure 3.15) and compared these scaffolds with PDL-coated standard plastic surfaces. Results showed no differences in cell survival between coated 2D surfaces and the electrospun scaffolds with different diameters.

To mimic the networks of neuronal processes found *in vivo*, neurons must be placed in culture conditions that promote and support the outgrowth of neurites. Therefore, we investigated in which way the different topographies affect the outgrowth of neurite extensions of hippocampal neurons. After two days in culture, we observed that 51 ± 5 % of neurons had extended neurites when cultured on the 450 nm fibers, while only 23 ± 12 % and 23 ± 9 % on the 1350 and 2500 nm fibers, respectively (figure 3.16a). For the 2D control the percentage of neurons extending neurites was 32 ± 12 %. Thus, as the 450 nm fiber scaffold were found to best promote neurite outgrowth we limited further experiments to compare these to conventional 2D substrates.

The cells were observed to move about in the electrospun scaffolds, and were pushing and shuffling the nanofibers around to modulate their environment. This

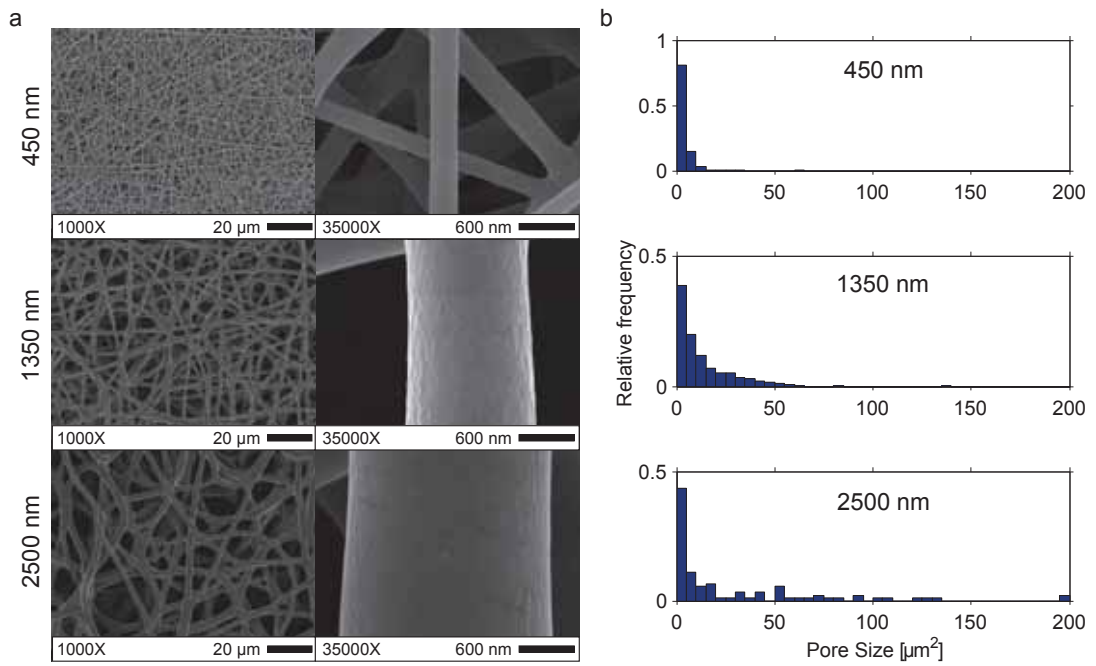


Figure 3.15: Scanning electron microscopy images of nanofiber scaffolds with 450, 1350 and 2500 nm fiber diameter (a) and their corresponding pore size distribution estimated through image analysis (b).

means that the state of crosslinking between fibers and their rigidity are important factors of the scaffolds that can influence cell behaviour and spatial organization. By using confocal microscopy, the neurite extension in the z-direction was quantified. The neurons grown on the 450 nm electrospun fibers was observed to extend their neurons up to 25 μm in the z-direction. Arguably, this is not enough for free and uninhibited three-dimensional growth. Nevertheless, it is still a significant improvement over the single cell layers present on the planar substrates (figure 3.16b). Consequently, through supporting the extension in the z-direction, the electrospun scaffold allowed the neurons to establish complex networks with cell-cell contacts in all three dimensions.

Moreover, western blot analysis of the neuronal cultures showed that the contaminating astrocytes on the electrospun fibers expressed lower levels of a reactive astrocyte marker, compared to the astrocytes on 2D substrates. After 7 days in neuronal cultures, immunocytochemistry indicated that a confluent monolayer of GFAP-positive astrocytes was present on the 2D substrates, while only a few such cells were present on the electrospun scaffold (figure 3.17). Both western blot analysis and labeling of proliferation markers confirmed a reduced astrocyte proliferation on the electrospun scaffold. Importantly, this means that the contaminating astrocytes will not take over neuronal cultures by proliferating.

To the best of our knowledge, there has not been any previous investigations whether electrospun PU nanofiber scaffolds are suitable for primary neuronal cell cultures and how neurite outgrowth and network formation are influenced by fiber diameter and scaffold porosity. Our findings indicate that fiber diameter and scaffold pore size has a large influence on neurite outgrowth, and that smaller fiber diameter scaffold promote longer neurite outgrowth. Neurons cultured within electrospun scaffolds are also found capable of extending neurites in all three dimensions, which is an important improvement over current 2D cell culture platforms. Additionally, we observed that the contaminating astrocytes in neuronal culture are less reactive on the electrospun scaffold, which is similar to the results obtained for individually cultured astrocytes, despite using a scaffold with smaller fiber diameters.

Surface topography has been reported earlier to affect neurite outgrowth. In a recent report, Qu et al. [167] showed that smaller fiber diameters (i.e. 400 nm)

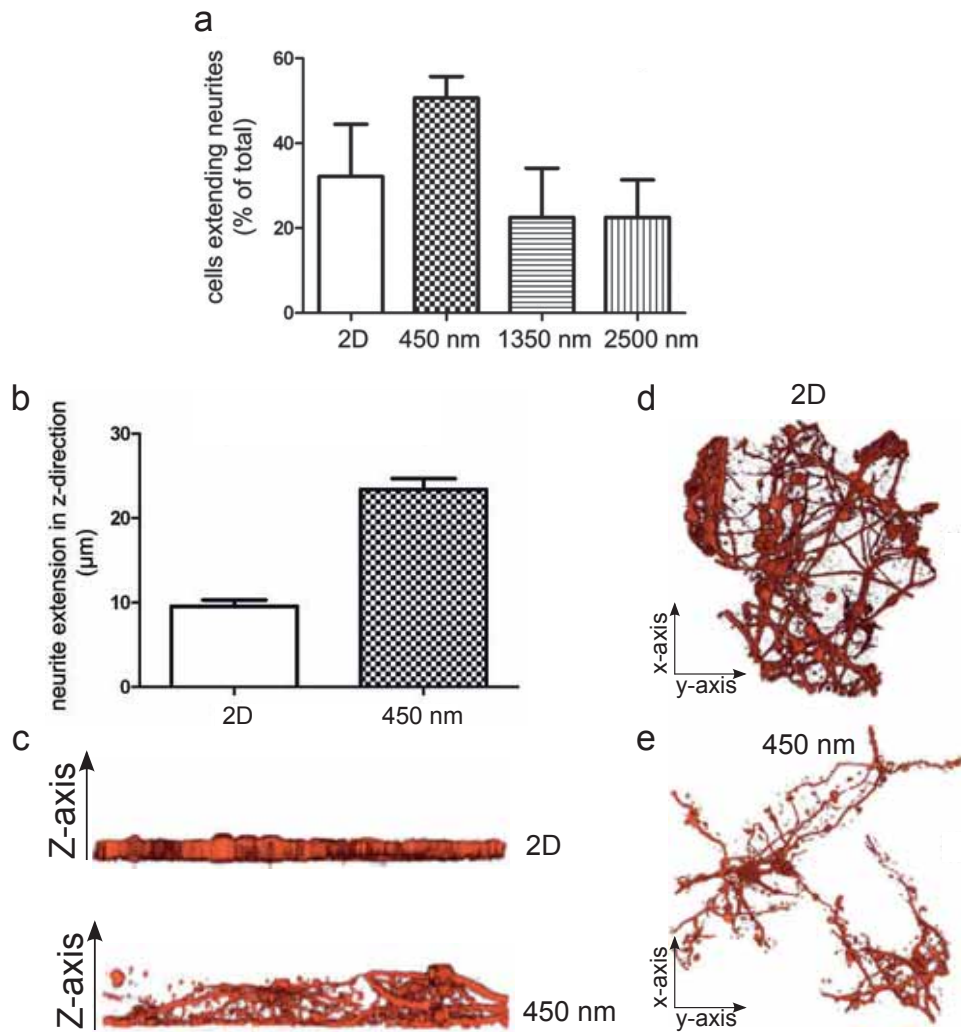


Figure 3.16: Comparison of the percentage of cells that extended neurites between scaffolds with different diameters and on 2D (a). Length of neurite extensions along the z-axis (b). Confocal 3D reconstruction of the neurite extensions along z-axis (c) and in the perpendicular x-y plane(d, e).

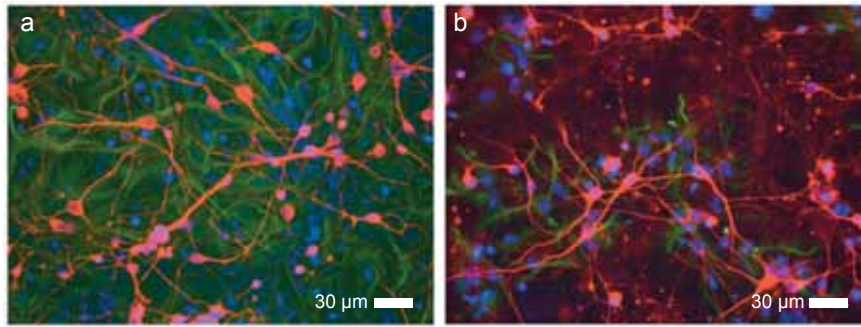


Figure 3.17: Representative immunocytochemistry pictogram of neuronal culture on 2D (a) and 450 nm electrospun fibers (b). The green staining corresponding to GFAP-positive cells indicate a monolayer of reactive astrocytes beneath the 2D neuronal culture, while only a few cells are GFAP positive on the electrospun fiber substrate.

were favorable compared to larger diameters, for the spreading of subventricular zone derived neurons and migration efficiency of astrocytes. In another study, Smeal et al. [168] found that the sensitivity to substrate curvature varied in a cell-type specific manner, indicating that adult and central nervous system neurons were less sensitive to substrate curvature compared to postnatal neurons. Their findings suggests that the surface geometry may not be a potent cue in directing the regeneration of already established neural networks. This, together with our own findings, generates questions regarding the interplay and the relative potency of different physical (i.e. topographical from fibers) and chemical cues (i.e. cell media).

Recognizing that there is a plethora of different combinations of fiber diameters, exposing different surface properties and with chemical surroundings, the number of possible studies required, e.g. to elucidate on specific conditions for a certain cell response, are considerable. To partly aid this situation for electrospun topographies, the next section presents a platform using microfabrication based integration of patterned electrospun fibers into microfluidic channels that can generate complex and scalable micro-environments with certain screening functionality.

3.4 Integration of Patterned Electrospun Structures in Microfluidic Systems

Microfluidics is a technology platform for liquid handling offering expanded possibilities, compared to traditional bulk media cell culture wells, for studying cell biology ranging from small populations down to single cells. In a typical system, handling of the liquid microenvironment is achieved through simulation aided design and use of microfabricated inlets, outlets, channels, valves, and chambers etc. in combination with an external pumping system. While controlling flow speeds and taking advantage of the diffusive nature of the soluble species in a laminar flow, accurate spatial and temporal definition of the chemical microenvironment can be achieved.

Cellular development and processes are, as previously stated, collective responses to a combination of chemical and physical cues. In-vitro systems that offer the possibility to generate and manipulate multiple factors of the cellular microenvironment are therefore attractive to the field of cell biology and in biotechnological applications, such as cancer research [169–171], drug screening [172], immunological studies [173] and regenerative medicine [171]. From the perspective of tissue engineering, control of chemical gradients of soluble cell-signalling molecules, such as growth factors, cytokines and chemokines, are important as they play a crucial role in many *in vivo* processes. Such signalling molecules may hence be exploited to induce certain desired behaviour, for instance in terms of migration and differentiation [174–176]. In this regard, microfluidic channels offer a particularly well-suited technology to control soluble cues in a microenvironment around cells, for example through formation of stable liquid gradients [177], fast switching of liquids [178] and temporal increase in concentration of relevant substances [179]. Integrating electrospun fibers in microfluidic system thus presents a platform which can combine bio-mimetic fibrillar surfaces with well defined chemical environments to study the interplay between extrinsic physical and chemical cues on cellular processes.

In literature, there are a few examples where electrospun materials have been introduced into microfluidic systems, typically by inserting and fixing fiber mats between the bottom substrate and the PDMS mold [121, 180–184]. Relying on

such methods of integration can be considered crude, but more importantly lack scalability as well as the possibility for effectively varying morphological parameters, such as fiber diameter and orientation, in a single system. Thus recognizing these limitations of earlier reported methods for integration of electrospun fibers, a more intricate microfabrication approach was developed to create a platform with significantly improved capabilities.

The strategy to introduce fibers in this work was to spatially define fibrous topographies on a substrate onto which microfluidic channels could be subsequently bonded. The spatial definition was based upon a patterning technique that relies on addition of a crosslinking agent (Benzoin Methyl Ether (BME), Sigma-Aldrich) to the electrospinning solution, followed by direct photolithographic definition of patterns. In general, the process is largely similar to standard photolithography using negative resist [127]. Upon deep ultraviolet (DUV) irradiation of the fiber network, utilizing a quartz mask, the BME molecules are subject to an α -cleavage type photodissociation and free radical formation inducing crosslinking between rigid macromolecular blocks of the segmented PU chains. This renders a significant reduction of the solubility of the exposed regions. For DUV exposure a standard mask aligner (KS MJB3, SUSS MicroTec AG, Germany) with a DUV light source (248 nm wavelength) was used. To achieve adequate degree of crosslinking, exposure was carried out for 5 minutes at an intensity of 1.5 mW/cm² (total dose 450 mJ/cm²). After crosslinking, and as the network was immersed in THF, the unexposed areas dissolved, leaving only the intended patterns on the substrate. Patterns were fully developed upon immersion in THF for approximately one minute, which was followed by rinsing in de-ionized water to remove unwanted solvent residues.

To construct complex geometries and hierarchical microstructures on a single substrate, the process of deposition, exposure and development can be repeated multiple times. Thus a strong advantage of the developed platform is that arbitrary fiber patterns can be combined with virtually any microfluidic network. To show the potential of this technique, three different fiber arrangements were demonstrated and combined with a gradient generating microfluidic network (figure 3.19).

The first pattern was a rectangular pad of dimensions 250x4000 μm^2 consist-

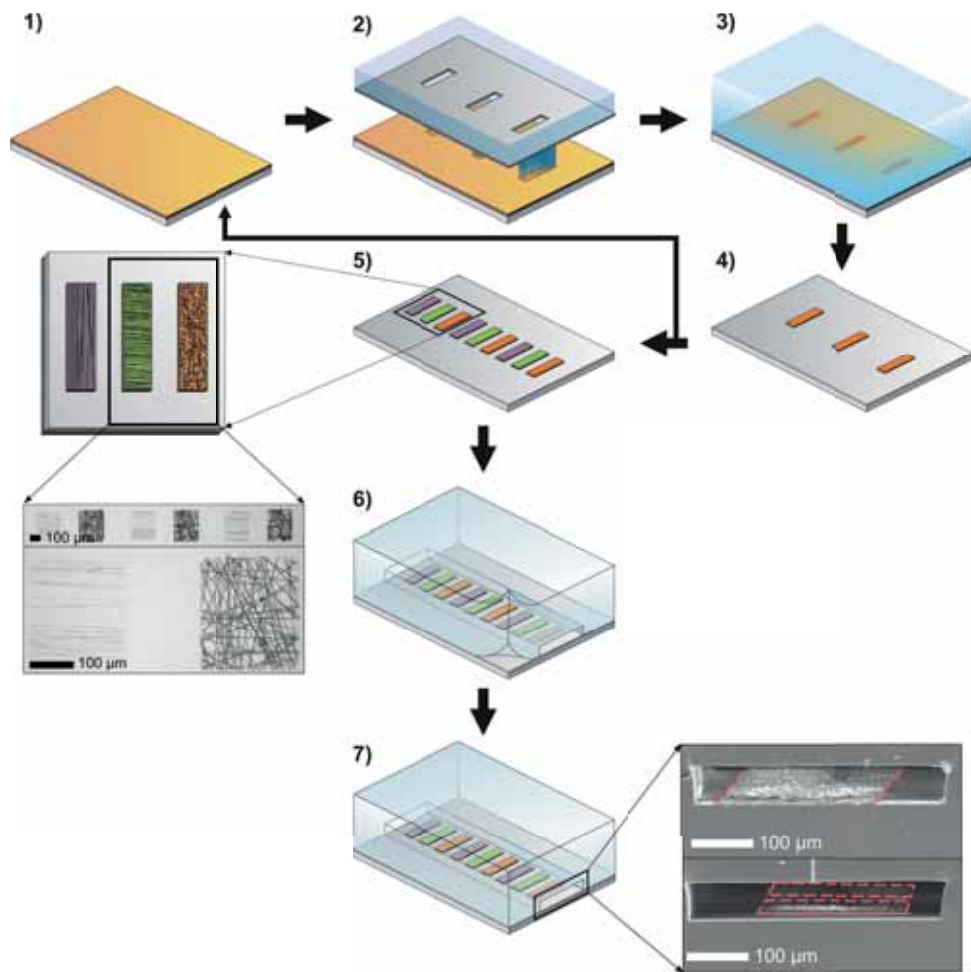


Figure 3.18: Schematic of the process steps to integrate spatially defined patterns of electrospun fibers within PDMS based microfluidic channels for cell assay applications. In short, 1) Polyurethane solution containing a crosslinking agent (BME) is electrospun directly onto a glass substrate; 2) the electrospun network is exposed to DUV through a quartz mask causing allowing the BME to form radicals which results in crosslinking of the fiber network rendering the fibers insoluble to THF; 3) development of the patterns by immersion in THF, dissolving the non-crosslinked areas, followed by rinsing in de-ionized water; 4) substrate is dried and the first layer is complete 5) Process steps 1-4 are repeated consecutively to form new additional fiber structures composed with different geometry, alignment or fiber dimensions; 6) PDMS is molded, aligned and cured onto the glass substrate to form the microfluidic channel around the electrospun patterns; 7) Complete microfluidic channel comprising electrospun fibers visualized by cross sections of two different implementations.

ing of randomly oriented fibers that would span the entire channel. The second arrangement were $250 \times 200 \mu\text{m}^2$ pads placed with $400 \mu\text{m}$ pitch. The third pattern was composed of $250 \times 200 \mu\text{m}^2$ rectangular pads of aligned fibers with alternating perpendicular orientation. The definition of alternating fiber topographies, as shown in figure 3.19e was achieved by a subsequent round of deposition, exposure and development (step 1-4 in figure 3.18). As the photo-lithographic method does not influence previously deposited fiber layers, the possibility to sequentially iterate patterning steps allows for the design and generation of highly complex patterns. Demonstrating aligned fibers of different orientation was chosen as it is of relevance for cell locomotion and spreading of stem cells. Each of the fiber pads can be used as an individual probing area and the effect of different alignments, as well as random fiber orientation, can be studied simultaneously in one single device.

The microfluidic channels were fabricated in PDMS using standard soft lithography and included a flow based gradient generator prior to the probing channel in which the fiber patterns resided. The gradient generating network was based on the original design of Jeon et al. [185] and was demonstrated, over a range of flow speeds, to be capable of imposing a concentration gradient perpendicular to the flow in the probing channel. The microfluidic network was aligned onto the glass substrate, with the fiber patterns in the center of the probing channel, and irreversibly bonded to the glass using reactive air plasma. The bonding of the PDMS microfluidic network to the glass substrate with the patterned electrospun fiber pads was shown to be successful.

To investigate the need for patterning in the integration process, the bonding efficiency of PDMS on glass substrates uniformly covered with electrospun fibers was evaluated. The PDMS was found unable to bind to fiber covered glass substrates. The tests thus demonstrated that the fiber patterning process is not only valuable for forming multiple topographies, but also found to be essential for proper integration without affecting the PDMS processing. Defining fiber sites to reside only in areas where they do not restrict the bonding process of the PDMS microchannels is thus a key to successful assembly

After completing the development of the fabrication procedures, the functionality of the devised system was evaluated. First, it was established, using sodium

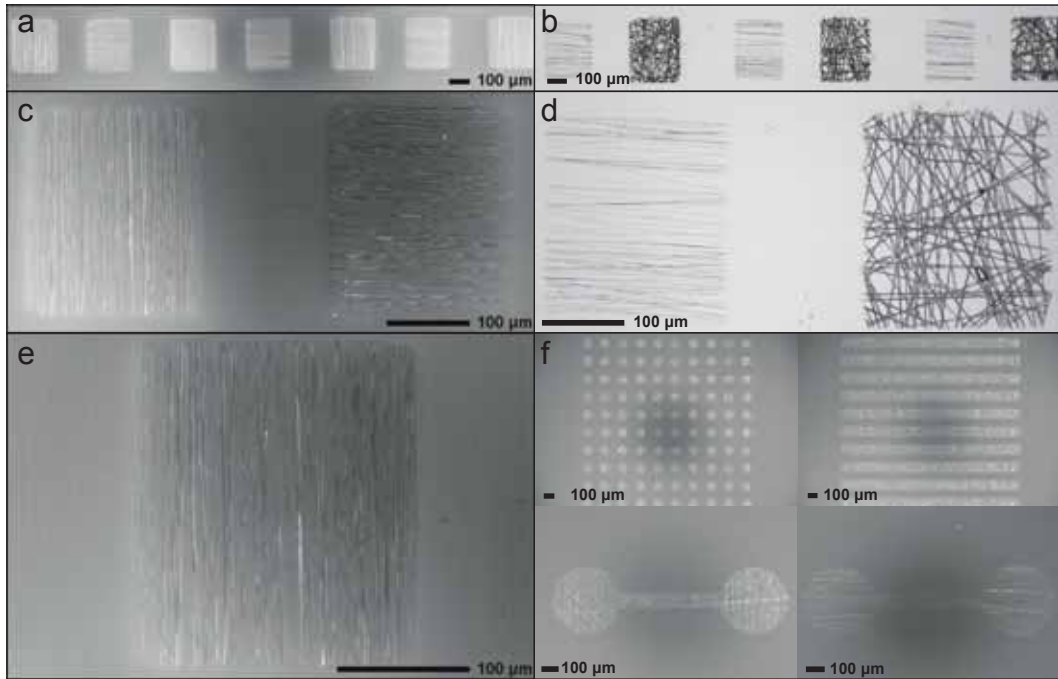


Figure 3.19: SEM micrographs and light microscopy view showing patterned fibers. a), c) and e) show alternating fiber alignment topographies perpendicular to and along the flow direction. b) and d) display alternating patterns with fibers aligned along flow in the channel and random oriented fibers. f) shows arrays of aligned fibers to demonstrate the potential scalability and versatility of pattern definition inherent to the lithography process.

fluorescein to visualize intensity profiles of the flow, that the fiber pads had negligible influence on the linear gradients, that could be produced by the gradient generating network at relevant flow rates. In order to demonstrate suitability of the system to support cell attachment and growth, 3T3 fibroblast cells were employed. Cells were introduced to the probing channel through the outlet and were able to attach successfully after two hours under static conditions (figure 3.20a). The cells were also seen to align to the underlying fiber pattern by staining for actin filaments (figure 3.20b).

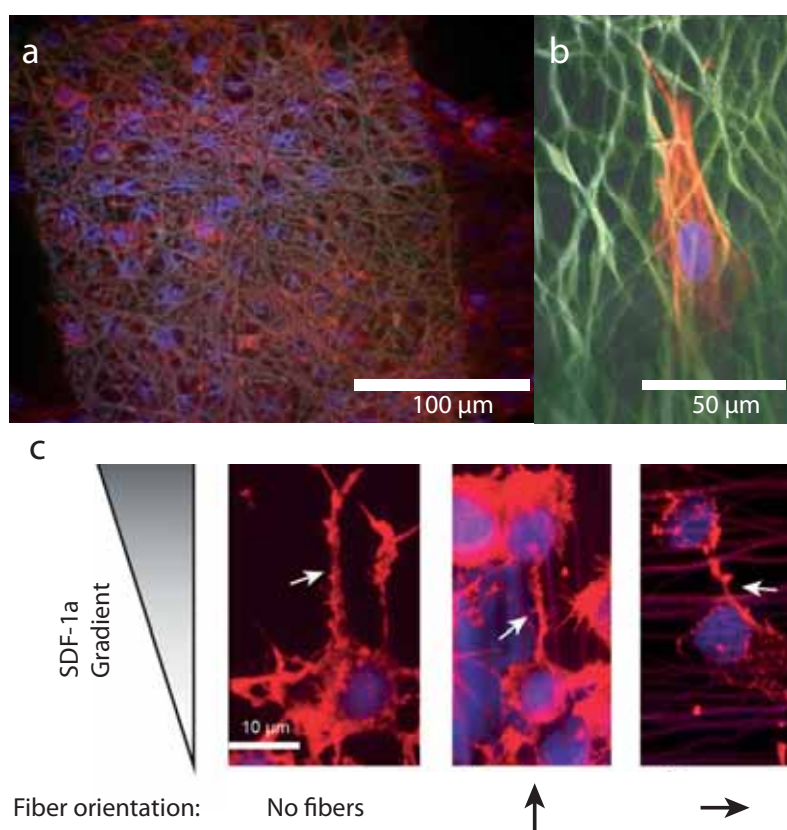


Figure 3.20: Cells after culture in microfluidic system with electrospun fibers. (a) 3T3 fibroblast cells after 24 h of culture in the microfluidic channel on electrospun fibers. (b) A single fibroblast on a fiber pad with the actin filaments partially aligned to the underlying fiber substrate. (c) Neural stem cells cultured on three different conditions: without fibers, fibers orientated in parallel and perpendicular to the gradient.

The potential of the platform was further verified by a functional investigation of neural stem cell/neural progenitor alignment in response to orientation of electrospun fibers combined with a chemo-attractant gradient generated by the microfluidic network. As chemical cue, a stromal cell-derived factor 1 alpha (SDF-1a), a small cytokine that promotes neural stem cell migration to pathological sites in the brain for regeneration [186], was used. Spatial, as well as temporal, gradients of these molecules are known to have a large effect on axon outgrowth and cell migration. Accordingly, during experiments, cells both on fibers, and on the glass between fiber pads were observed to respond to the chemical gradient through directional outgrowth along gradient. Figure 3.20 c shows three examples of different combinations of fiber orientation and SDF-1a gradient conditions. In some experiments, cell outgrowth was observed along the gradient, but perpendicular to the fibers, indicating that cells respond stronger to the chemical stimulus than the topographical. Indeed further studies are needed to elucidate the interplay between contact guidance cues and chemical gradients on the outgrowth behavior of nSCs. Nevertheless, the methodology and resulting microfluidic system presented can open the possibility for numerous investigations on the behavior of cells in well-defined fiber based microenvironments.

Chapter 4

Thermal Interface Materials in Microelectronics Packaging

4.1 Heat Transfer Across Interfaces

In microelectronics packaging, the thermal path from the chip to the ambient includes several interfaces between the different building blocks. Very often these contacting building blocks are composed of dissimilar materials. An example layout for a single chip package with a high power density chip, is outlined in figure 4.1. During device operation, most of the input electrical power supplied to the chip is turned into thermal energy, for instance through leakage currents, the switching of transistor states and associated resistances. The generated thermal energy needs to be dissipated from the chip to the ambient in order to maintain temperatures that allows for stable operation and long term reliability.

The thermal energy inside a solid state material is transported by phonons and/or free electrons, through a diffusive process. The heat flux (Q) of thermal energy in a bulk material is proportional to the temperature gradient (∇T) and the thermal conductivity (λ) through Fourier's law ($Q = \lambda \nabla T$) [187]. However, in the context of microelectronics packaging, it is often more useful to view a temperature drop (ΔT) as a product of thermal resistance ($R_{thermal}$) and the heat flux across a specific layer ($\Delta T = R_{thermal}Q$) [188]. Similarly, the interfacial thermal resistance, or total thermal interface resistance ($R_{interface}$), defines the temperature drop for

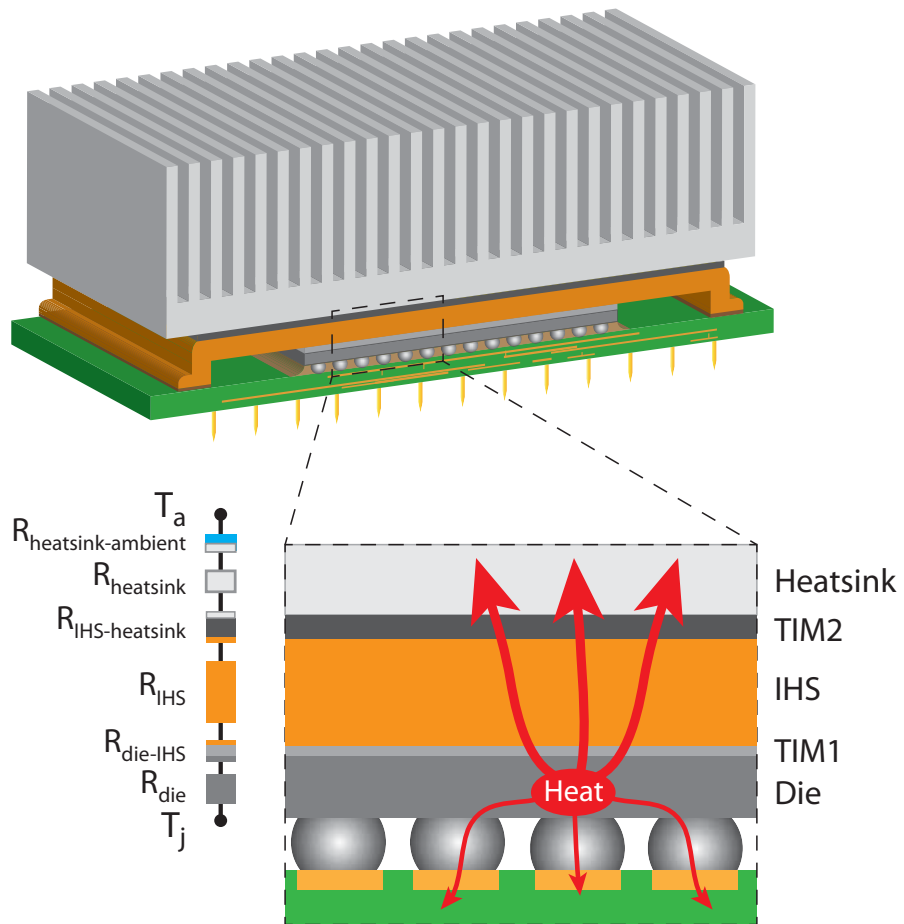


Figure 4.1: Generic FCPGA (Flip Chip Pin Grid Array) package illustrating a FC assembled die (1), a TIM1 (2) thermally connecting the die backside to the IHS (3) and a TIM2 (4) acting between the IHS and the heatsink (5).

a given heat flux across an interface ($R_{interface} = \Delta T/Q$).

For a highly dissipating device in a single chip package, the main heat conduction path is typically through the heatsink and the thermal resistance from junction-to-ambient (R_{j-a}) can be expressed as:

$$R_{j-a} = R_{die} + R_{die-IHS} + R_{IHS} + R_{IHS-heatsink} + R_{heatsink} + R_{heatsink-ambient} \quad (4.1)$$

In this simple model (equation 4.1), the resistance related to the bulk conductivity of the die (R_{die}) and the integrated heatspreader (IHS) R_{IHS} are determined by the particular system in use and comparatively small. Thus, from a thermal management perspective, more efficient heat dissipation can primarily be achieved through improving the heatsink configuration and/or by minimizing the interface resistances.

To minimize the interface resistances in a package, TIMs act to reduce the air voids and gaps that are inevitably present around the contact points of two surfaces, due to their respective microscopic roughness and relative asperity (figure 4.2). A conventional classification is that materials mounted at the interface between the die and the IHS are referred to as TIM1, while materials at the interface between the IHS and heatsink are called TIM2. The term "TIM1.5" for die-to-heatsink interfaces has also been used [189].

For heat transfer across an interface, the primary figure of merit is the total thermal interface resistance, composed of two contact resistances between the TIM and each of the contacting surfaces ($R_{contact1}$ and $R_{contact2}$) and the bulk resistance of the TIM (R_{TIM}):

$$\begin{aligned} R_{interface} &= R_{contact1} + R_{TIM} + R_{contact2} \\ &= R_{contact1} + BLT/\lambda_{TIM} + R_{contact2} \\ &= BLT/\lambda_{effective} \end{aligned}$$

The bulk resistance of the TIM can be described as the apparent thickness of the interface, called bond line thickness (BLT), divided by the thermal conductivity

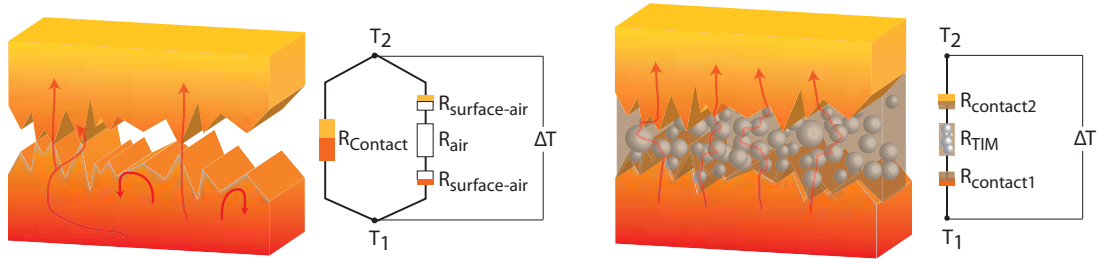


Figure 4.2: Schematic of the thermal resistance across interfaces with and without a conventional TIM material.

of the TIM (λ_{TIM}). For comparative purposes, it is also sometimes convenient to use the effective thermal conductivity ($\lambda_{\text{effective}}$), which includes the contact resistances, as a figure of merit.

Though these relations are simple, they clearly point out the challenge for attaining low total interface resistance using TIMs. This involves a trade-off between con-formability and coupling to the surfaces, to achieve low contact resistances, and high thermal conductivity to reduce the bulk contribution. Obviously factors such as interface geometry, contact pressure as well as surface materials and their properties will affect what characteristics of the TIM that present the optimal trade-off. Additionally, to maintain reliable performance the TIM must be able to cope with the thermo-mechanically induced stress, most commonly associated with contacting surfaces of mismatching coefficients of thermal expansion (CTE) and substrate warpage. For TIM1 materials, it is for instance important to provide sufficient mechanical decoupling between a metal (CTE of 15-25 ppm/K) heatsink or heatspreader and the semiconductor die (CTE of 3-5 ppm/K), so that stress induced cracking does not occur.

In summary, the fundamental challenge for TIM technologies, is how to reliably maximize the transfer of thermal energy between adjacent surfaces, with initial and boundary conditions set by microelectronic packaging. The next section will provide a brief overview of conventional TIM technologies and new TIM concepts still in research.

4.2 Thermal Interface Materials

4.2.1 Conventional Materials

There is a wide variety of commercially available TIMs that target varying requirements. In general, the parameters that are considered for TIMs include (with certain overlap) performance/cost ratio, BLT, long term reliability, compressibility, assembly processing conditions/handle-ability, re-workability, outgassing/risk of contamination, dielectric properties, insulating capability and mechanical coupling to surfaces/adhesive function.

Polymer Matrix Composites

Unmatched in usage, throughout the microelectronics industry, are the particle loaded polymer matrix based materials. This is mainly due to their low cost and uncomplicated assembly conditions together with an acceptable and fairly reliable performance. The polymer matrices are typically composed of silicone, epoxy, urethane or paraffin, while common thermally conductive filler materials are Al, Al₂O₃, ZnO, BN and Ag particles [190, 191]. The main heat transport through this class of materials rely on particle-particle contact between the conductive fillers and thus requires a particle loading that exceed the percolation threshold [192]. The most straightforward way to increase the thermal conductivity is to use a higher particle loading. The particle concentration is however limited by the drastically increased viscosity that occurs at high loading, which makes the materials difficult to apply, increases bond line thickness and leads to poor surface contact. The composition is thus trade-off between high thermal conductivity, connected with high viscosity, and low contact resistance associated with lower viscosity. Today, the highest performing polymer matrix composites, available commercially, in the form of non-crosslinked grease/paste or phase change materials are reported to have thermal conductivity around 4-6 W/mK, despite significant loading of high thermal conductivity particles [193, 194]. A thermal performance in this range is not considered by the industry to meet the requirements on thermal dissipation for future applications.

Furthermore, modelling work has indicated that the inter-particle resistances

will pose severe limits to the achievable effective thermal conductivity [195], despite using particles of very high thermal conductivity. It has been claimed that there is no significant additional improvement in the thermal conductivity of the composite, from increased thermal conductivity of the filler, when the filler is already greater than 100 times that of the polymer matrix. Instead, the aspect ratio of highly conductive fillers has been suggested to be a more potent approach to increased performance, as large aspect ratio fillers easily form connections in a conductive network [196]. Attempting to push the performance of polymer matrix materials, there have been suggestions to include particles with high aspect ratios in bi- and trimodal size distributions, including both micro and nanosized fillers [197]. However, as filler sizes move from micro to nanosize the thermal boundary resistance (also known as Kapitza resistance) tend to add a significant contribution to the total thermal resistance [192].

Of additional concern, for non-crosslinked polymer matrix composite, are the long term usage problems related to separation of the matrix and fillers and migration out from the interface. The two main degradation modes are pump-out, referring to material migrating out or to an uneven distribution creating voids at the interface, as well as dry-out, which is essentially separation of the matrix and filler components [198]. These degrading effects can, over time, result in orders of magnitude higher thermal interface resistance and are primarily attributed to the pumping action occurring due to warpage movements from thermal expansion of the substrate, package and heatsink during thermal cycles.

Solder based TIMs

Solder alloys have thermal conductivities which are an order of magnitude higher than the polymer matrix composite materials. In similarity with low viscosity polymer matrix materials, they can flow to fill the microscopic gaps of the interface, thereby minimizing the contact resistances. Despite the existence of a wide range of solders used in conventional electronic assembly, such as interconnects and die attach applications, the solder alternatives viable for thermal interface applications, are more limited. The main limiting factors are related to the assembly process temperature, environmental and health restraints and the mechanical compliance

requirements causing reliability issues. Firstly, the solder melting point needs to be below the maximum allowed temperature, not to induce degradation of the package materials that has been assembled during prior steps. This reduces possible alloys to those with a liquidus temperature below roughly 240–250 °C. At the same time the melting point should be sufficiently high to allow for reliable performance at operating temperatures, typically above 120 °C [199]. Secondly, environmental and health aspects essentially excludes the use of alloys based on lead or cadmium. Thirdly, STIMs are limited to alloys with high resistance to crack formation and propagation under dynamic and thermally induced loads, that otherwise can cause severe degradation of the thermal performance. Typically, soldered joints with low ductility are typically prone to crack formation. Additionally, insufficient mechanical decoupling puts geometrical constraints on the BLT and the interface area where solder TIM can be applied. In TIM1 applications, solders require relatively high BLT in order to maintain the stress transfer onto the die at an acceptable level [199]. High joint stiffness limits the area that can be soldered due to thermal expansion and solidification shrinkage causing increasing strain at large distance to the neutral point [200].

In an interesting study, Deppisch et al. [201] identified and evaluated 6 viable solder alloy candidates based on Sn, Bi and/or In for TIM1 application in a microprocessor package. They found that pure In, combining low mechanical yield strength (4-6 MPa) and low melting temperature (157 °C), at a BLT of ~ 200 -300 μm , was the only configuration that allowed reliable assembly and device operation without crack formation, while maintaining adequate thermal performance. Devices assembled with pure Sn as interface material, exhibited die cracking due to the combined effect of high process temperature and low ductility of the formed joint. Using eutectic composition of Sn and Bi, with significantly lower processing temperature, degraded rapidly in thermal performance due to its inherent brittleness. As a results, despite concerns regarding high price and supply, In has been used as TIM1 material in high end processors, after the transition to Pb-free solder based TIMs [202].

Escaping some of the problems, related to high reflow temperature and stress transfer, are STIMs based on low melting point alloys (LMAs). Using alloying elements such as gallium (Ga), Sn, Bi and In, the melting points range from ~ 20 –80

°C, which enables the materials to undergo phase change into a molten state during operation. The liquid state allows for complete mechanical decoupling between the surfaces and enables a very high degree of wetting, which in combination with decent thermal conductivities in the range of 10-20 W/mK, yields low total thermal interface resistance. Recently, a Ga based TIM was measured to have a thermal conductivity of 13 W/mK as well as an interface resistance of 2.6 Kmm²/W at a contact pressure of 50 kPa [203]. The main problem with Ga in pure form is that it causes severe corrosion on aluminium alloys, making it unwanted in most systems [204]. Other negative aspects of LMAs include risk of leakage to cause shorts, migration from the interface, oxidation, and corrosive effects on certain metal surfaces through progressive formation of inter-metallic species. However, some of these effects have been addressed. The risk of leakage and oxidation can be avoided by employing a gasket sealing around the interface. To minimize migration, it is also possible to incorporate a mesh-work which can act to stabilize and retain the melt. In spite of promising performance and presented countermeasures for dealing with potential issues, the overall usage of LMAs remain limited [205].

4.2.2 Emerging Technologies

The thermal challenges faced in modern electronics are considerable, and new innovative materials with related process technologies are required to meet them. Current TIM research features the use of novel nanostructured materials as well as established materials applied in non-traditional ways [10]. In general, a recent and successful trend has been to align and/or form a continuous and highly conductive phase across the interface. Without covering all, and focusing on materials aimed for interfaces of high power densities, two promising approaches are based on vertically aligned carbon allotropes and continuous metal phases.

Vertically Aligned Carbon Based Materials

Carbon structures are considered attractive as TIMs primarily due to their promise of high thermal conductivity, inherent to the properties of the hexagonal structures of sp² C=C bonds. Around 3000–3500 W/mK at room temperature, i.e. one order of magnitude higher than metals, has been experimentally measured on single

walled CNTs [187, 206, 207]. Multiple studies have therefore looked into the possibility to utilize CNTs as a high aspect ratio and highly conductive fillers in polymer matrix composites [208]. However, in general the thermal performance of such composites is still severely limited by the multiple contact resistance between individual CNTs and the surrounding matrix. Applied at an interface, the CNTs also tend to align perpendicularly towards the contacting surfaces, or at best remain randomly dispersed, which results in a diminishing contribution to the through-plane conductivity.

To overcome the alignment issue, and instead create continuous conducting channels across the interface, vertically aligned CNTs infiltrated with a polymer phase have been investigated [209]. Despite substantial increase of the through-plane conductivity due to CNT alignment, the thermal transport across interfaces has still been found limited by the dominating contact resistance between the CNTs and the connecting surfaces [210–212]. Accordingly, different strategies to reduce these contact resistance have been proposed. Tong et al. [213] demonstrated that the resistance associated with the free-end CNT tips, physically bonded by van der Waals adhesion, is $\sim 10 \text{ Kmm}^2/\text{W}$, but can be reduced through welding using a thin layer of deposited In. Ni et al. [214] instead used an azide-functionalized polymer with C-N bonds and reported that it was possible to decrease the thermal resistance of $10 \mu\text{m}$ CNT forest down to $\sim 1.4 \text{ Kmm}^2/\text{W}$, between the Si growth substrate and a Cu surface. Recently, Taphouse et al. [215] also showed that it was possible to achieve a 9-fold reduction in the thermal interface resistance ($4.6 \pm 0.5 \text{ Kmm}^2/\text{W}$) compared to dry contact for a CNT forest bonded between the growth substrate and a Cu oxide surface.

Much of the low contact resistance, contributing to a low total thermal interface resistance, can be attributed to the CVD growth directly on the substrates used in the measurements. It has thought to be a result of the melting underlayer, below the catalyst particles, that forms an intimate contact between the CNTs and the substrate [213]. However, since most applications are incompatible with the high temperature required for CNT growth, a transfer from the growth substrate is typically needed. This has proven to add substantial contributions to the contact resistances. For instance, Cross et al. [212] measured a resistance of around $10 \text{ Kmm}^2/\text{W}$ for both $30 \mu\text{m}$ and $130 \mu\text{m}$ transferred CNTs between Si and Ag

surfaces, indicating a high contact resistance and a low bulk contribution to the resistance from CNTs. In another study, Barako et al. [216] transferred 500 μm tall CNT forests using In films to bond two glass substrates and was able to obtain thermal resistances of $28 \text{ Kmm}^2/\text{W}$. Depending on the success of strategies to reduce the contact resistances for transferred VACNT TIMs, their use may be limited to relatively high BLTs.

Despite promising, there are still several obstacles for using CNTs as TIMs that remain. Firstly, the scalability of the required processing using VACNTs in TIMs in practical applications can be questioned for many of the evaluated approaches [215]. In fact, in most practical applications the achievable CNT density is low, which limits the thermal conductivity. Additionally, the thermal conductivity tend to fall rapidly with the number of defects and impurities [217], which, so far, seems to be largely unavoidable in larger scale production of CNTs.

Graphene, the basic structural element of both CNTs and graphite, has also gathered interest for practical applications in thermal management of electronics. The interest was spurred on from measurements on freely suspended graphene showing an exceptionally high thermal conductivity (up to 5000 W/mK). It has also been shown that the thermal conductivity of sufficiently large graphene flakes can exceed that of bulk graphite ($>2000 \text{ W/mK}$) [218]. However, for practical applications, it is established that the thermal conductivity of graphene decrease substantially with increasing number of layers or in contact with other materials [219]. For instance single layer graphene on silicon dioxide has been found to have a suppressed thermal conductivity of 600 W/mK , which is higher than Cu, but much lower than for suspended and clean graphene. The reduction is due to the umklapp processes, impurity and boundary scattering which are acting when the material is in contact with other surfaces [187]. Despite this, there are some results of potential interest for TIM applications.

Without alignment, Balandin and co-workers [220] reported an enhancement of 1000 % of the thermal conductivity of epoxy based composites by 5 wt% addition of liquid-phase exfoliated few layer graphene. They also found that the conductivity of silver based epoxy could be increased by $\sim 500 \%$ through the addition of 5 wt% of hybrid graphene-metal particle fillers, which had a strong coupling to the matrix material and wide size distribution from nano-to micrometer [221].

For aligned graphene, Liang et al. used vacuum filtration to prepare relatively thick multilayer graphene sheets, which were cut out and assembled so that the graphene flakes aligned across a silicon-silicon interfaces. Through laser flash measurements they found a promising bulk thermal conductivity of 75.5 W/mK of the aligned graphene sheets. However, despite using a thin In coating to improve the thermal transfer to the silicon substrate, the thermal contact resistance towards each silicon surface was 5.1 Kmm²/W, which is far from optimal for thin BLTs.

Another approach to a graphene based TIM was suggested by Zhang et al., who synthesized graphene foams with high flexibility and a three dimensional structure by using CVD at 900 °C on a sacrificial nickel foam. Under compression of 200 kPa and with a resulting foam thickness of ~2-3 μm, they found a thermal interface resistance between Cu-Cu and Si-Al interfaces of 7 and 4 Kmm²/W, respectively.

Also carbon allotropes in aligned form have been explored for use in TIM applications. For instance, Uetani et al. [222] fabricated a CF-based TIM by electrostatic flocking as a way to align pitch-based carbon fibers in the vertical direction, followed by filling the interstitial space with a flourinated rubber matrix. Showing a conductivity of 23 W/mK at a filler loading of 13 %, the composite could retain the flexibility of the rubber matrix. By using a fabrication process which is scaleable and already available in industry, they believed this approach could be realized in the near future. Unfortunately no measurements of the thermal interface resistance were reported.

Metallic materials with modified mechanical properties

A critical challenge with metal based TIMs are to deal with potential reliability issues, related to stiffness of the joint, shear creep compliance, delamination and crack propagation, without compromising the thermal performance. Efforts have therefore focused to develop materials and related processes which allows for an optimal combination of mechanical and thermal performance. To this end, several groups have studied sintering of metal particles. Dutta et al. studied liquid phase sintering of Sn and In as the high and low melting phase respectively and found that 30-50 % In content, sintered just above In melting point, was able to produce a material that was ductile under low strain conditions. The sintered material

was able to sustain strains of $>20\%$ without crack formation and had high shear strain compliance under thermal cycling conditions while maintaining a thermal conductivity of roughly half of In (~ 40 W/mK) [223]. In another study, Yu et al. [224] found that Ag nanoparticles sintered by spark plasma under hot pressing at 250°C at a pressure of 30 MPa during 30 min between two polished copper surfaces showed thermal resistance from 0.1 Kmm^2 up to $2\text{ Kmm}^2/\text{W}$. The material was claimed to be promising for power electronic applications, but there was no data reported on reliability aspects. However, for most microelectronic assemblies temperature levels above $240\text{--}260^\circ\text{C}$ are too high and typical contact pressures of heatsinks assemblies are in the order of ~ 100 kPa, which is roughly two orders of magnitude lower than for the sintering process. As an alternative route, Chliasatia et al. [225] suggested to use low temperature sintering (120°C) of Ag nanoparticles, targeting only chip hot spot locations, by inkjet printing and combined this with conventional grease in a hybrid approach. Through simulations they demonstrated the potential to improve heat dissipation through thin bond line thickness and maintain low stress induced on the die.

Yet another option, introduced by Wunderle et al. [226], is using a porous Au nanosponge structure on wafer level to enhance thermal heat transfer across interfaces by either allowing better conformation to filler particles in the applied TIM material or used in direct bonding of two surfaces with nanosponge structures at 200°C .

Another potential route to escape the mechanical drawbacks of a stiff solid joint is to modify conventional polymer matrix composite with the addition of solderable/fusible metallic filler. Intel has acquired a few patents [227, 228] regarding a polymer solder hybrid TIMs which aim to improve on the particle-particle contact limitation of traditional particle loaded polymer matrix composites. During assembly the solder component can be reflowed and thus interlink the other particles and allow formation of continuous conducting channels across the interface.

Recently, Raj et al. [229] suggested using co-electrodeposition process of Sn-graphite and Sn-SiC composites onto silicon chips for TIM applications. Their concept relies on achieving a thin BLT through deposition techniques, while using the particles to increase the thermal conductivity and to tune the CTE. However, so far, no measurements on reliability or thermal performance has been re-

ported. Furthermore, they recognized the difficulty with the wetting of Sn onto the graphite and SiC particles. By using pressure assisted solder infiltration in a thermocompression bonding equipment they presented SEM images indicating that tin covered SiC particle surfaces.

The next section will introduce the concept and three implementations of using a metal matrix polymer composite as a TIM, developed in our group. Noticeably, the material concept includes certain features that are similar to the examples presented above. This is true in particular for the latter two, as our developed composite materials rely on reflow during application, a fiber phase intended to modify the thermo-mechanical properties and fabrication with pressure assisted metal alloy infiltration.

4.3 Metal Matrix Composite Thermal Interface Material

This section presents the fabrication processes and characterization of a composite material comprised of a porous fiber network infiltrated with a continuous metallic phase aimed for TIM applications. More specifically, three specific implementations of this technology will be treated; Polyimide fibers with an In matrix (Paper F), PI fibers with a solder alloy matrix (Paper G), and finally carbonized pitch fibers with a solder alloy matrix (Paper H). Below we will introduce the material principal concept, followed by details regarding the general fabrication process and related developments, and finally summarize and discuss important results.

4.3.1 Development and Fabrication

4.3.1.1 Concept

The material concept is a two component composite system comprising a surface modified fibrous network with interconnected pores infused with a continuous metal matrix phase. The network consists of non-woven randomly oriented sub-micron fibers formed through electrospinning of a material that can serve to tune the mechanical or thermal properties of the joint.

Using polymeric fibers, as a specific implementation, the intended function of the network is to act as a carrier for the metal and serve the following main aspects:

- Decrease the shear modulus and thus lower stress transfer between interfaces
- Increase ductility and prevent crack propagation through the metal phase
- Reinforce the composite structure during reflow assembly by acting as a spacer element to control BLT and to, certain extent, impede flow of melt out from the interface while the metal phase is in liquid state
- Confine solidification volumes during reflow to reduce shrinkage

During application as a TIM, the metal phase is brought above the melting point to allow for wetting and binding of the contacting surfaces, thus creating multiple continuous metallic heat transfer paths across the interface (figure 4.3). In principle, the metal matrix can be any suitable alloy, which offers flexibility and makes the concept adaptable to different applications with varying requirements on surface metallization, cost and performance. For microelectronics packaging applications primarily the use of conventional Sn or In based solder alloys are considered eligible, in order to stay within non-harmful temperature limits during reflow.

4.3.1.2 Fabrication

Overview

The fabrication of the metal matrix polymer composite TIM consists of three consecutive steps and is outlined in figure 4.4. First electrospinning is used as a straightforward and scalable route to form a non woven mesh of macroscopically long submicron diameter fibers to act as the carrier. The electrospinning process offers well suited opportunities to alter the fiber dimensions and to achieve initial porosity in a suitable range (nm- μm and $\sim 60\text{-}90\%$) for the intended TIM composites of final thickness between 10–200 μm . The second process step is a fiber surface modification to facilitate the subsequent infiltration and to improve the coupling between the metal matrix and fibers. The final step is infiltration of a

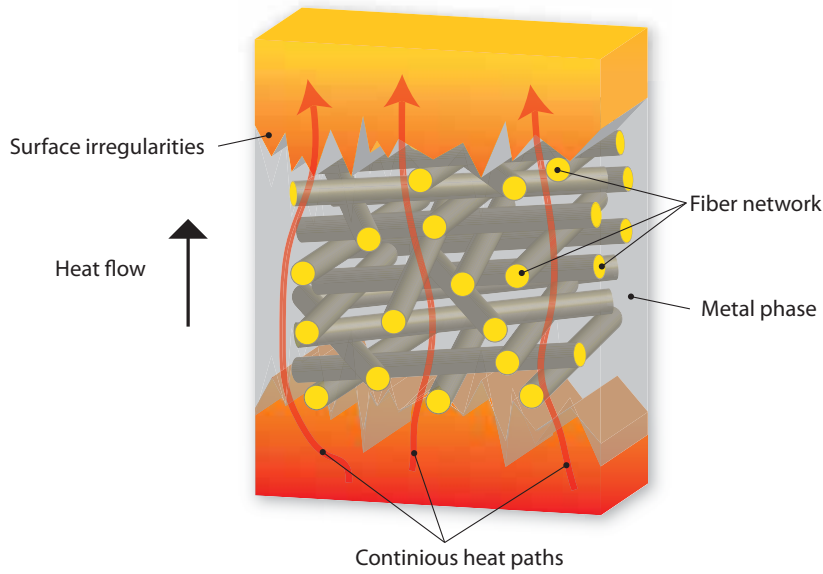


Figure 4.3: Schematic of a small segment of an interface showing the structure and functionality of the metal matrix polymer composite after assembly.

metal matrix into the fiber network. This infiltration is challenging due to the non-wettable and small fiber diameters in combination with small pore size and high porosity.

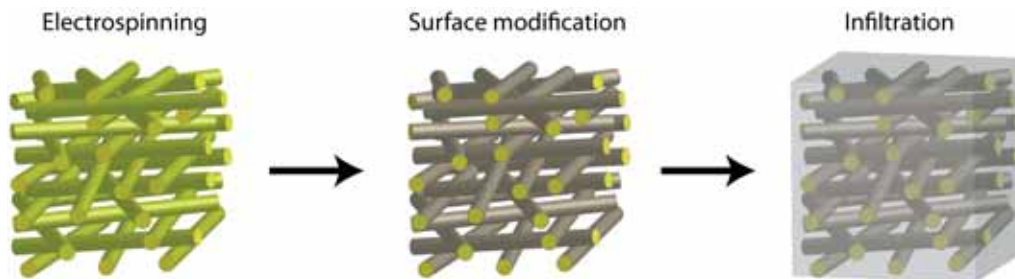


Figure 4.4: Overview of the three main fabrication process steps of the composite. The fiber carrier network is formed through electrospinning followed by surface modification of the fibers to facilitate subsequent infiltration of the interpenetrating metal matrix.

Electrospinning

The fibrous non-woven mesh was formed by electrospinning a solution containing 16 wt% PI (Huntsman Advanced Materials) in N,N-dimethylacetamide (DMAC) using 18 kV, 2 mL/h feed rate and 20 cm between cannula and collector in a commercial electrospinning unit (Nanofiber Electrospinning Unit, Kato Tech). The mesh was spun to a thickness of 50 μm on aluminum foil and heated to 320 °C for 1 hour to extort any residual solvent.

Fiber Surface Modification

Earlier investigations of an ion exchange based fiber surface modification using PI cleavage combined with chemical and thermal reduction has found that both reduction methods present promising routes to surface modification of electrospun PI fibers [230]. The ion exchange process followed by thermal or chemical reduction has also been shown to result in two distinct morphologies of nanoparticle formation on the fibers. Thermal reduction lead to nano-particles that were embedded and uniformly dispersed through the surface modified layer of the fibers and longer treatment time mainly increased the depth of the modification. Such embedded layer of Ag nanoparticles resulting from thermal reduction was also demonstrated to be suitable as a seed layer for an autocatalytic process in order to form a continuous Ag layer on the fiber surface to provide an adequate adherent interface towards an In matrix [231]. The resulting composite showed attractive thermal conductivity of 27 W/mK and low thermal contact resistance when applied as TIM between two copper surfaces. On the other hand, the chemical reduction, which used dimethylamine borane (DMAB) as reducing agent, lead to a preferential reduction and formation of the nanoparticles primarily confined to the surface with partial embedment. Ion exchange followed by DMAB reduction can thus be considered an alternative approach to the thermal reduction followed by an autocatalytic process to achieve a full surface coating suitable for improving wetting and metal matrix infiltration.

Further studies of the composite fabrication process based on chemical reduction using DMAB was therefore initiated. First the focus was to enable and optimize the imide cleavage process, which is otherwise a time consuming bottle-

neck in the composite fabrication, by determining the effect on fiber modification depth and Ag nanoparticle synthesis while varying treatment time, temperature and KOH concentration. After suitable process conditions that could enable a complete nanoparticle coating and facilitate wetting was found, we proceed to infiltrate the structure to form the final composite and evaluate its performance as a TIM.

The complete process of the investigated fiber surface modification is schematically given in figure 4.5. In order to find optimal conditions for the surface modification, i.e. to achieve a proper Ag coating of the electrospun PI to facilitate the infiltration of the metal matrix, a scan was made over temperature, concentration and time for the imide cleavage process. After immersion in up to 4 M KOH aqueous solution for 60 min at both 50 °C and 60 °C, and subsequent processing steps, visual inspection revealed only slight color changes (from bright yellow to slightly brown) on both PI film and fiber networks. Based on experience from previous experiments such color change correlates with very thin Ag coatings was therefore considered not to be of further interest to this study. Ramping up to 80 °C in the imide cleavage process proved to have a pronounced impact on the modification speed. The visual appearance of the surface modified fiber mats range from light brown to dark brown with hints of silver, while the PI film span from dark yellow all the way to solid metallic silver. The same trend is also observed during SEM inspection of the samples. SEM micrographs of the resulting morphology from different initial treatment of 1, 2 and 4 M KOH during 30 and 60 min at 80 °C on both flat PI film and fibers are given in figure 4.6. The difference between film and fiber modification is most prominent for the 2 and 4 M treatments. Comparing the 2 M samples after 60 min, (figure 4.6h and l) the film surface displays Ag particle clusters that are several hundreds of nanometers wide and particles which are 50–100 nm while the fiber surface exhibit very few particles at all. Another example is the 4 M sample after 30 min (figure 4.6c and f) where the particle grains are 105 ± 35 nm on the film compared to 50 ± 15 nm on the fibers. This indicates that the rate of modification is affected by the hierarchical structure presented by the fibers and may be explained by the larger surface area as well as a slower exchange of ions due to reduced diffusive flow inside the network. Additional contribution can be from the axial alignment of the PI chains shown to occur during electro-

spinning process [232], which can lead to decreased modification rate compared to the bulk film.

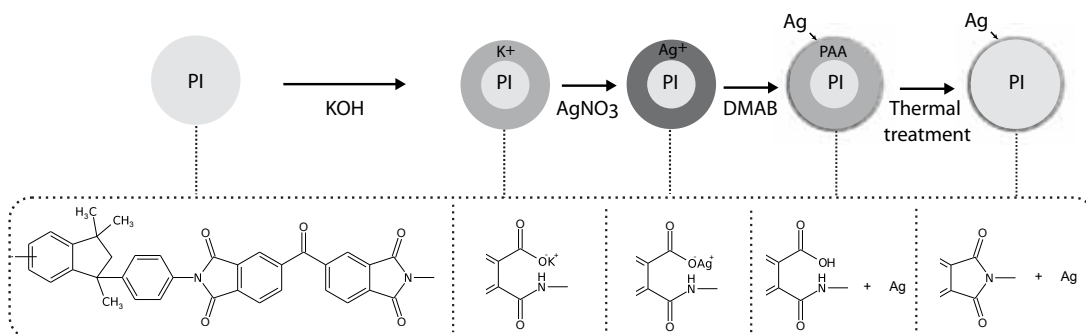


Figure 4.5: The major steps in the surface modification; washing with ethanol, imide cleavage induced from KOH, ion exchange of K^+ to Ag^+ in $AgNO_3$, Ag^+ reduction using DMAB and re-imidization through thermal treatment.

To study the depth of the modification fiber cross sections were prepared by casting samples into epoxy resin followed by preparing ultrathin sections (~ 60 nm) using a diamond knife in an ultramicrotome (PowerTome XL, Boeckeler). The ultra-thin sections were placed on 400 mesh copper grid for inspection in a TEM (Tecnai T20, FEI). Figure 4.7 displays a representative selection of fibers showing that for immersion in 4 M for 15 and 30 min as well as 1 M for 60 min the modification is mainly limited to the surface. The depth of the surface modification from 15, 30 and 60 min are measured to be 100 ± 10 nm, 190 ± 20 nm and >500 nm respectively, while corresponding values at 1 and 2 M for 60 min are 150 ± 30 nm and >500 nm. From the combined results from SEM it can be seen that both 30 min and 60 min subjection to 4 M KOH creates a Ag nanoparticle layer modification with a density that can act as an intermediate layer of higher surface energy to assist in wetting for the subsequent infiltration. However, as it is beneficial to retain the mechanical properties of PI during processing the preferred choice is selected based on TEM images as 4 M for 30 min.

The final step of the surface modification was to induce re-imidization of the layer of polyamic acid (PAA), resulting after the Ag reduction, to restore the original polymer structure of the PI carrier network. This was carried out by a thermal anneal at 350 °C for 40 min in nitrogen atmosphere. To confirm that

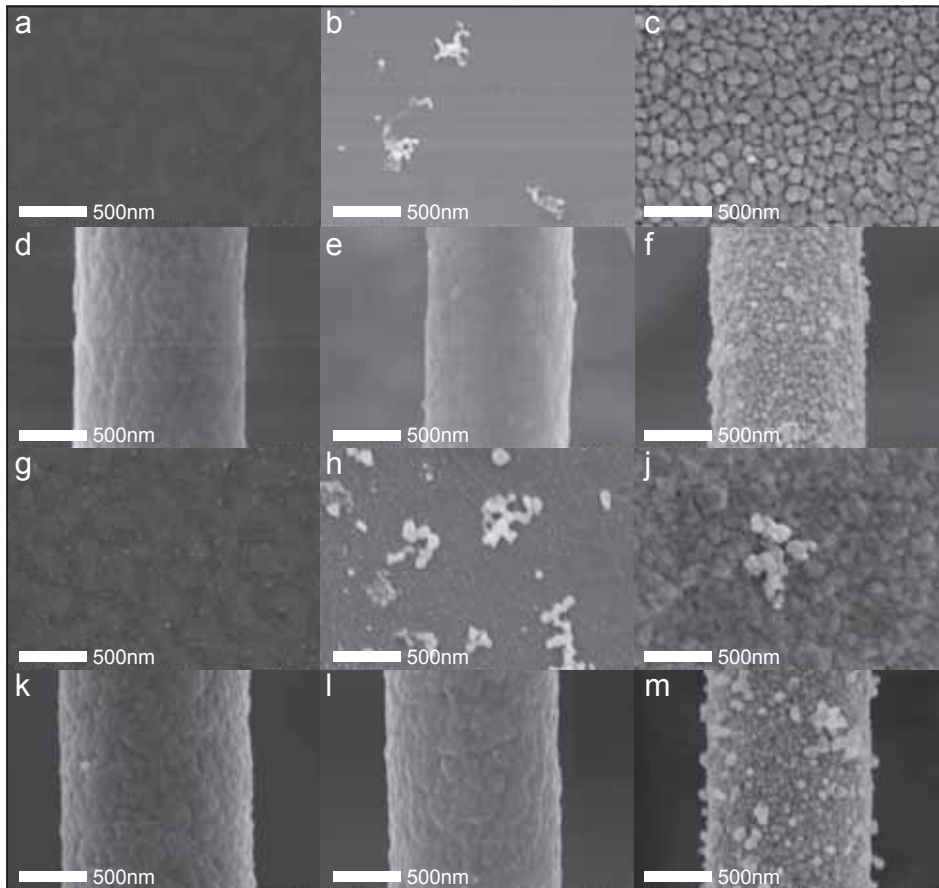


Figure 4.6: Surface modified solution cast PI film and electrospun PI fibers from immersion in 1 M (a, d, g, k), 2 M (b, e, h, l) and 4 M (c, f, j, m) KOH aqueous solution at 80 °C followed by Ag^+ ion exchange in 100 mM AgNO_3 and reduction in 1 mM DMAB at room temperature.

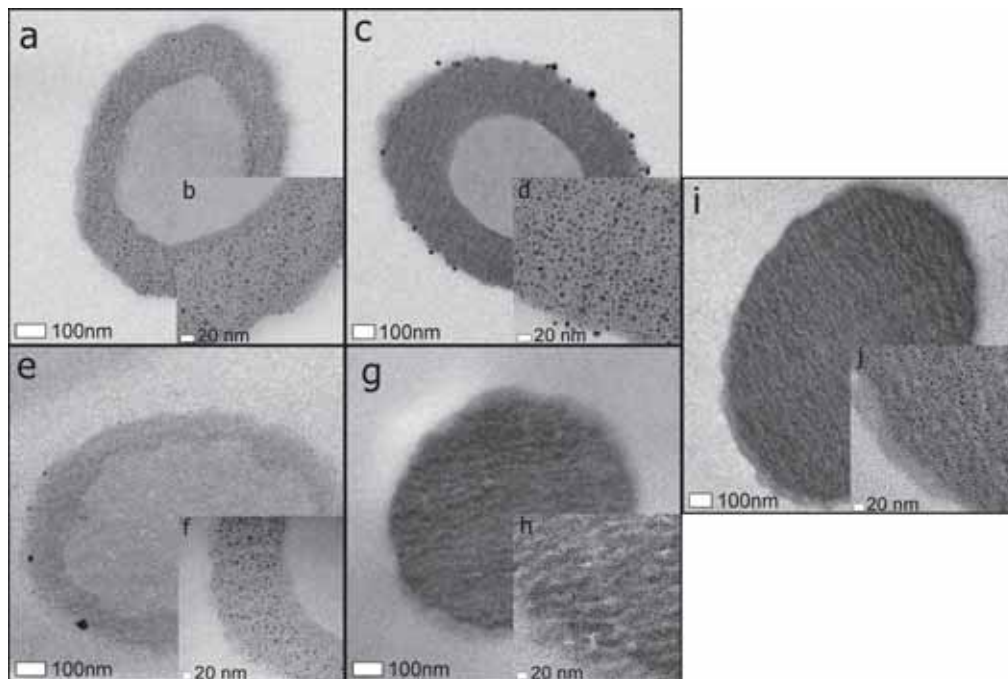


Figure 4.7: TEM cross section showing the effect of concentration and time on the modification depth of PI fibers from immersion in KOH aqueous solution of a concentration of 4 M for 15 min (a, b), 30 min (c, d), 60 min (i,j) and 60 min in 1 M (e, f) and 2 M (g, h) at 80 °C.

complete re-imidization had occurred, ATR-FTIR spectra were collected. The ATR-FTIR spectra collected from the fibers in pristine condition, after 30 min in 4 M KOH and after thermal anneal is given in figure 4.8. The spectrum of the pristine fibers displays the characteristic imide structures at 1780, 1720 and 1370 cm^{-1} [233]. After the KOH treatment there is a band broadening in the range between 1500-1700 cm^{-1} which corresponds to the superposition of the two amide peaks at 1650 and 1550 cm^{-1} . The intensities of the imide peaks after the imide cleavage are not completely eliminated, indicating that the modification depth is smaller than the probing depth of the ATR-FTIR [234], which agrees with the modification depth measured in TEM.

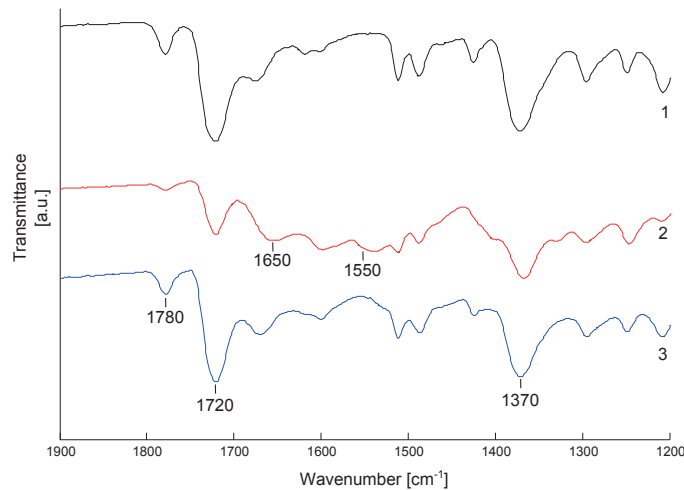


Figure 4.8: ATR-FTIR spectra showing the effect of KOH treatment and thermally induced re-imidization. (1) Pristine PI fibers (2) after 30 min in 4 M KOH at 80 °C (3) after 40 min thermal anneal at 350 °C.

The improvement in wetting of In after the Ag nanoparticle surface modification was assessed qualitatively by comparing reflow on top of pristine and modified PI film. On the surface modified PI film the melt front formed with very low contact angles while In on the pristine formed contacts with angles that were $>90^\circ$. Low contact angles, as observed on the modified PI, indicates the possibility of spontaneous infiltration driven by capillary forces. However, with further experiments it was found that the resistance for the In melt to penetrate the network was too high. By submerging plated fibers into an In melt, only a few of the top

contacting fibers of the network, could be embedded into the metal. These findings are in agreement with geometry based estimations which predicts that spontaneous infiltration cannot occur with the porous characteristics of an electrospun PI fiber network.

The following section elaborates on the difficulty infiltrating electrospun fiber structures and the need for pressure assisted infiltration, by considering the available theory of metal wetting developed for metal matrix composites.

Forced Infiltration

To better understand the challenges faced when infiltrating a non-wettable interface with metal it can be instructive to consider theory related to wetting phenomena. The theory for infiltration of liquid metal matrices into fibrous reinforcements of metal matrix materials has been treated earlier [235–237] by adapting the original wetting equations derived by Young [238]. By considering a capillary geometry and the difference in surface tension between the solid–gas ($\gamma_{\text{solid-gas}}$) and solid–liquid ($\gamma_{\text{solid-liquid}}$) as the driving force ($D_f = \gamma_{\text{solid-gas}} - \gamma_{\text{solid-liquid}} = \gamma_{\text{liquid-gas}} \cos \theta$) it is possible to express the pressure required for infiltrating pores of an effective radius r as [235]:

$$\Delta P = P_{\text{liquid}} - P_{\text{gas}} \geq \frac{2D_f}{r} \quad (4.2)$$

Equation 4.2 can thus be used as a rough estimate of the required pressure for infiltration of a liquid metal into the capillaries of the porous network, which the electrospun PI fibers arguably constitute. Input of generic values in equation 4.2 to assess the infiltration pressure for metals with no wetting ($\cos \theta = -1 \Rightarrow D_f = -\gamma_{\text{liquid-gas}} \sim 500 - 2000 \text{ mJm}^{-2}$) and micron size pores ($r \sim 10^{-6} \text{ m}$) results in values between 1–4 MPa.

Nevertheless, it has been shown that a more appropriate expression can be derived by considering the specific surface area S (which can be related to the fiber diameter and the fiber volume fraction) to describe the threshold pressure for infiltration P_{th} parallel to the fibers' axes [236]:

$$P_{th} = S\gamma_{\text{liquid-gas}} \cos \theta = \frac{-4\gamma_{\text{liquid-gas}}}{D} \frac{V_f}{1 - V_f} \cos \theta \quad (4.3)$$

where D represents fiber diameter, V_f the fiber volume fraction and θ the contact angle between fibers and the infiltrating metal. Again assuming a low degree of wetting ($\cos \theta = -1$), using diameters ranging from 1000 nm down to 100 nm and volume fractions of 40 up to 80 % the threshold pressure P_{th} is from 2.5 up to 160 MPa. Lowering the contact angle to 120° cuts the estimated pressure range in about half (1.25-80 MPa). Indeed these estimations show that it is a challenging task to achieve proper infiltration on fibrous assemblies of such dimensions, without modifying the surface to improve wettability.

Moreover, according to equation 4.3, the condition $\theta < 90^\circ$ results in $P_{th} < 0$. This indicates that spontaneous infiltration is possible along the fibers if the wetting angle is low enough. However, when infiltration takes places in normal direction to fibers it has been shown that the threshold angle (θ_{th}) for spontaneous infiltration is below 90° in most cases and depends on fiber arrangement [237]. It has been recently argued by Kaptay [236] that the equations governing wetting by liquid metal into fibrous materials needs to be modified to take into account the orientation of the fibers. By considering the geometry of a liquid front onto two parallel fibers he was able to draw principal conclusions relevant for the threshold value for the contact angle for spontaneous infiltration. Importantly it was found that even a contact angle of 0° is not sufficient for spontaneous infiltration if the ratio between inter fiber spacing (δ) to fiber diameter (D) is larger than a certain critical value $\frac{\delta}{D} > 0.155$, or similarly if $V_f < 0.68$. Considering fiber diameters around $1 \mu\text{m}$, means that the spacing between fibers need to be below 100 nm for spontaneous infiltration to occur, which is not fulfilled in the case of a typical porous electrospun PI network. Essentially, this points out that pressure assisted infiltration is the only possible approach, aside from infiltration driven through chemical reactions, to attain full infiltration for an electrospun randomly oriented fiber network, even in the situation of perfect wetting between fiber and matrix.

Recognizing the need for high pressure liquid phase infiltration, a custom in-house constructed tool for infiltration of the metal matrix into fiber networks was

used. Briefly, the process is as follows: The surface modified fibrous film is fixed and enclosed between two tool blocks forming a thin mould cavity around the fiber film. The cavity containing the film is then evacuated using a small gate connected to a vacuum pump. The mould temperature is heated to 30 °C above the liquidus temperature of the matrix, and molten matrix, coming from a melt cavity, is then slowly allowed fill the mould from both sides of the fixed film. To ensure that the matrix material penetrates into the porous fiber network, a pressure of 30 MPa is applied to the melt using a piston and maintained for several seconds. Finally, a mould insert is used to define the final composite thickness before cooling and solidification.

The excess pressure applied ($P_{\text{excess}} = \Delta P + \frac{2D_f}{r}$) during pressure assisted infiltration will serve to drive the metal liquid front, with viscosity η , through the capillaries a distance x after time t according to [235]:

$$\begin{aligned} x &= \left[\frac{r^2 t}{4\eta} \left(\Delta P + \frac{2D_f}{r} \right) \right]^{1/2} \\ \Rightarrow t &= \frac{x^2 4\eta}{r^2 \left(\Delta P + \frac{2D_f}{r} \right)} \end{aligned} \quad (4.4)$$

Using a typical viscosity of metal in liquid state ($\eta \sim 10^{-3}$ Pa sec [239]) in equation 4.4 it is quickly realized that the estimated time for a 100 μm electrospun film to be infiltrated is virtually negligible at 1 MPa of excess pressure.

During our experiments, the high pressure assisted infiltration process was found not to be sufficient on its own, to provide adequate infiltration (figure 4.9). Instead, successful formation of the composite could be achieved only when the pressure assisted infiltration was combined with the Ag nano surface modification.

4.3.1.3 Evaluation of Thermal Properties

There are multiple methods available to evaluate thermal interface resistance based on both steady-state and transient measurements. In this work the flash method, previously used to evaluate solders, sintered silver, CNT and graphene based TIM and thermal grease [189, 224, 240–242], was utilized. The theory governing the flash method for characterizing the thermal diffusivity, heat capacity and thermal

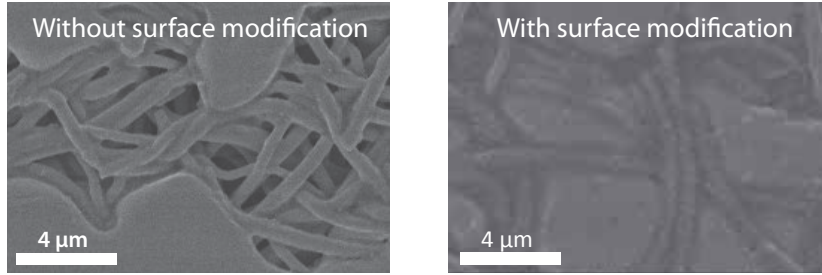


Figure 4.9: Comparing the infiltration of In into pristine and Ag nano particle surface modified PI fiber networks.

conductivity of single layer was originally formulated by Parker et al. [243], but later refined by Cowan [244] and finally extended to double and triple layer samples [245, 246].

During a typical measurement, one side of the sample under evaluation is subjected to a short energy pulse, while the resulting transient temperature response of the sample is collected on the opposite side, using an IR detector. The characteristics of the temperature response is governed by the thermal diffusivity through the sample. Under the assumption of adiabatic conditions and one dimensional heat flow, it is possible to extract the thermal diffusivity α from:

$$\alpha = \frac{1.38d^2}{\pi^2 t_{1/2}} \quad (4.5)$$

where d is the thickness of the sample and $t_{1/2}$ is the half rise time of the temperature transient. As pointed out by Cowan, to extract the sample thermal diffusivity for non-adiabatic conditions requires additional corrections. However, these refined equations are quite mathematically tedious, and therefore not presented here. Nevertheless, thermal diffusivity is related to the thermal conductivity λ via the specific heat capacity C_p and the density ρ :

$$\lambda = \rho C_p \alpha \quad (4.6)$$

The principal way to characterize the thermal interface resistance of a two-layer sample, is based on measuring the effective thermal diffusivity of the sample. Then, knowing the thermophysical properties of the layers in the stacked sample, the thermal resistance due to the contact interface (R_c) can be determined. This is best done through software using iterative algorithms and integrated mathematical model functions, but in principle the relation is illustrated by the following equation:

$$\lambda_{effective} = \rho C_p \alpha_{effective} = \frac{d_{total}}{\frac{d_1}{\lambda_1} + \frac{d_2}{\lambda_2} + R_c} \quad (4.7)$$

where d_{total} is the total thickness and d_1 , d_2 are the thickness of each of the stacked layers.

In the case of an intermediate layer, i.e. a TIM applied between two layers, which is comparably thin, so that it has negligible influence on the heat capacity and density of the sample stack in a measurement, the calculated contact resistance corresponds to the total thermal interface resistance of the TIM ($R_c = R_{interface}$). This resistance then includes the two contact resistances of the TIM and the bulk resistance of the TIM ($R_{interface} = R_{contact1} + R_{contact2} + BLT/\lambda_{TIM}$). The contact resistances of the TIM and its thermal conductivity can be thus found from linear regression of $R_{interface}$ versus BLT.

4.3.2 Indium Matrix and Polyimide Fiber Composite

To introduce an In matrix into the Ag surface modified fiber networks, pressure assisted liquid phase infiltration were carried out, as described above, using an in-house designed tool. The surface modified fiber mat had a thickness of 50 μm prior to infiltration, and thus the infiltrated composite preform thickness was controlled, using the tool, to be 50 μm after solidification. The surface of the resulting composite is shown in figure 4.10a, while a high magnification of a surface modified fiber embedded in In matrix is displayed in figure 4.10b and c. Through SEM inspection it was observed that the Ag coating remain intact and the wetting between the metallic phase and Ag coated fibers appear appropriate.

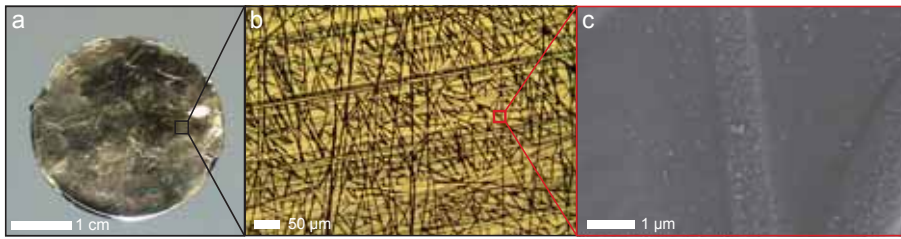


Figure 4.10: The surface of the In–MMC after infiltration.

The thermal performance of the MMC as a thermal interface material was evaluated using two different interfaces and compared to In solder. The first interface was prepared by sandwiching the preform samples between two ENIG Cu surfaces coated in an industrial process. The second interface was between a dummy Si chip with back side metallization (100 nm Ti and 300 nm Au) and a polished Cu plate, representing a Si die and a Cu IHS. Fluxless reflow was carried out for all samples while applying 200 kPa of compressive mechanical pressure to the stack. After assembly, the In preform samples resulted in BLTs $<3 \mu\text{m}$, as most of the In was pushed out from the interface during reflow. The additional mechanical support from the fibrous carrier in the MMCs gave BLTs in the range of 20–30 μm , which was roughly equal to 40–60 % of the initial fiber film thickness.

The total thermal resistances of the different assemblies are given in figure 4.11. Due to the low BLT, the total thermal interface resistance of the In samples can be mainly attributed to the contact resistances or possibly light voiding [247]. For the ENIG-ENIG interface the thermal interface resistances for In solder and the MMC were measured to be $1.6 \pm 0.15 \text{ Kmm}^2/\text{W}$ and $2.1 \pm 0.25 \text{ Kmm}^2/\text{W}$ respectively. The relatively high resistance for the In solder sample clearly shows that the major contribution for this interface is from contact resistance. The addition in total thermal interface resistance due to the fiber phase is thus, in this situation, around 30 %. The thermal resistance for the MMC corresponds to an effective thermal conductivity of $10 \pm 2 \text{ W/mK}$. For the Si-Cu interface, the thermal interface resistances for In solder and the MMC were found to be $0.25 \pm 0.10 \text{ Kmm}^2/\text{W}$ and $1 \pm 0.15 \text{ Kmm}^2/\text{W}$, respectively. The In results agree well with previous reports on fluxless bonding technology that has been demonstrated to produce minimal voiding for In solder as TIM1 material [248]. The effective thermal conductivity for

the MMC was 22 ± 6 W/mK for the Si-Cu interface. The low contact resistances for both types of samples indicate that metallurgical bonds are formed with the contacting surfaces. The relatively large difference in thermal resistance between the two interfaces is likely due to differences in surface roughness, which is substantially higher on the ENIG plated surfaces compared to a Si and polished Cu surface.

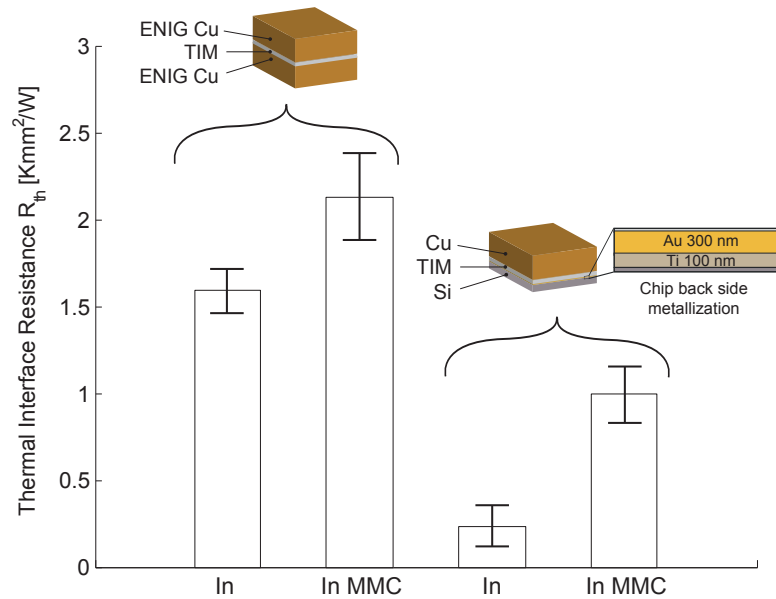


Figure 4.11: Total thermal interface resistance for In solder and the In–MMC at ENIG-ENIG and Si(Ti/Au)-Cu interfaces.

Comparing the route using chemical reduction to thermal reduction together with autocatalytic deposition to fabricate the MMC, the results are promising. Previous research [231] has shown that a MMC fabricated using thermal reduction and autocatalytic deposition resulted in a bulk conductivity of 27 W/mK and thermal contact resistances below 1 Kmm²/W between polished Cu surfaces. As the chemical reduction has fewer complex process steps involved, and the MMCs have similar performance characteristics, it can be considered to be a more attractive approach.

From a TIM perspective the MMC display solid thermal performance which is in the same range as that of In solder. Considering the higher BLT compared

to the pure In joint, which would add another $0.25 \text{ Kmm}^2/\text{W}$ ($=20 \mu\text{m} / 82 \text{ W/mK}$) of resistance, together with the lower In content, the MMC preform can be considered a competitive alternative.

4.3.3 Solder Alloy Matrix and Polyimide Fiber Composite

As a continued development from the indium composite, we next investigated the possibility to infiltrate the surface modified fiber network with standard solder alloy. After modifying the infiltration process to function properly at higher temperatures, a new type of solder alloy matrix nano polymer composite (SMNPC) could be successfully fabricated. Similar to the In–MMC, the SMNPC uses the nano Ag surface functionalized highly porous electrospun non-woven polyimide fiber network, but the matrix material is now Sn95.5Ag3.8Cu0.7 alloy. The result of the fabrication steps can be seen in figure 4.12.

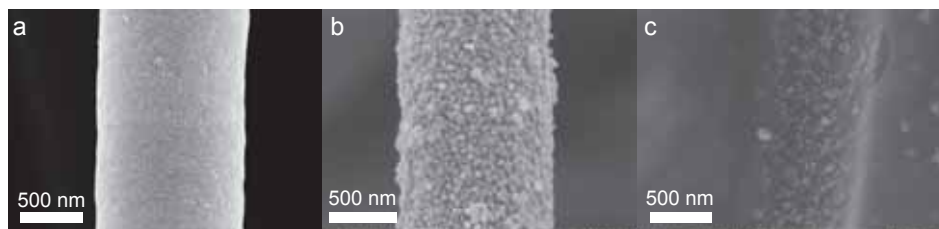


Figure 4.12: Electrospun polyimide fiber(a), Ag nanoparticle surface modified PI (b) and a fiber embedded in the SMNPC surface after matrix infiltration (c).

When assembled as a thermal interface or die attach material and reflowed, the target for the SMNPC is to form a structure that has continuous heat transfer paths through the SnAgCu matrix and a fiber phase that can act to lower the stiffness of the joint. Therefore, to assess the influence of the embedded fiber phase on the mechanical properties, the elastic modulus of composite was evaluated and compared to pure alloy in tensile tests. The results are summarized in figure 4.13. Figure 4.13a shows a comparison of the stress-strain relation for the Sn-Ag-Cu alloy and the SMNPC up to 0.2 % strain. From the slope of the stress strain relation the elastic modulus was estimated for Sn-Ag-Cu film and the SMNPC to be $23.4 \pm 2.3 \text{ GPa}$ and $8.1 \pm 1.1 \text{ GPa}$, respectively (figure 4.13 b). The measurements

thus indicate that the introduction of the polymer fiber phase can reduce the elastic modulus by 65 % with respect to the matrix bulk value. The relatively large effect on modulus seem reasonable considering the fracture surface (figure 4.13 c and d), which displays a combination of light fiber pull-out occurs and fibers that break at the interface. The result is also comparable to reports on Sn-based interpenetrating phase composites for which a 23 % reduction in elastic modulus and a 34 % reduction in shear modulus was observed at 20 volume percent polymer inclusion [249, 250].

In literature, the bulk value for Sn_{95.5}Ag_{3.8}Cu_{0.7} alloy is reported to be ~ 46 GPa at room temperature [251]. However, the Sn-Ag-Cu film used in this work has been processed under high pressure and could possess slightly different alloy composition, grain structure and porosity, which have been shown elsewhere to lead to relatively large differences in mechanical properties [251, 252]. It is also probable that the differences compared to bulk values measured for the SAC film are due to size effects, which can play an important role for the mechanical properties of thin metal foils [253].

To investigate the in situ effects on thermal performance of the fiber phase in the composite, a xenon flash methodology was used. The interface resistance of the composite was evaluated and compared to pure SnAgCu alloy as a reference. To enable measurements of relevant in situ values, the sample under test were sandwiched and reflowed under a compressive pressure of 200 kPa between ENIG coated copper pieces. After assembly, the BLT of the assembled SMNPC ranged from 35 μm up to 65 μm , which show that the fiber phase was compressed 30-40 % during reflow with 200 kPa compressive pressure. Glass spacers were used to control the BLT of the reference test assemblies with SnAgCu alloy film.

The total thermal interface resistance for the composite and SnAgCu alloy, as a function of BLT is given in figure 4.14a. The measured through-plane, effective through-plane and in-plane thermal conductivity for the SMNPC and SnAgCu alloy are summarized figure 4.14. For the thermal resistance measurements of the SnAgCu alloy, the reciprocal of the slope of the least square fit, corresponds to a conductivity of 64 W/mK. The intersection with the y-axis of the extrapolation shows that the contact resistance is below 1 Kmm^2/W for each surface contact. The slope of the total thermal interface resistance for the SMNPC indicates that

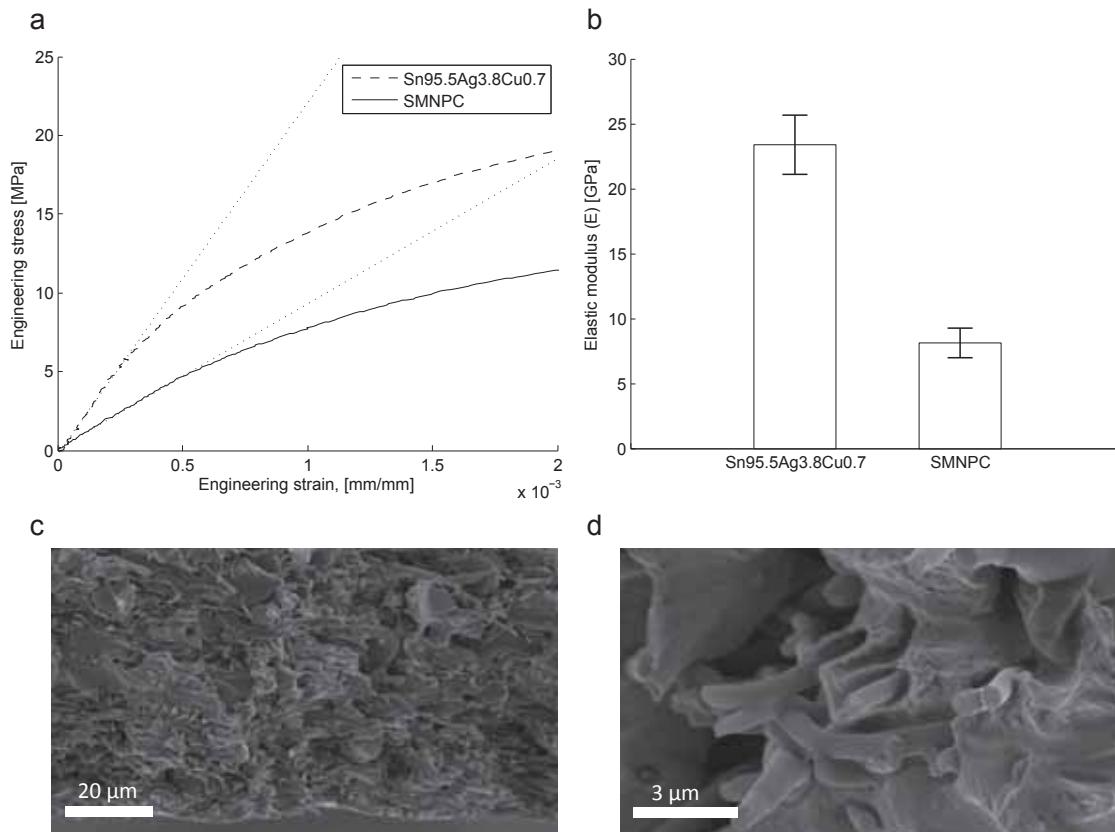


Figure 4.13: Mechanical characteristics measured for SnAgCu alloy and the SMNPC. Engineering stress-strain relation below 0.2 % strain (a), and elastic modulus (b) measured for SnAgCu alloy and SMNPC preforms, $n = 3$. SEM micrographs of the fracture surface of a SMNPC sample (c,d).

the throughplane thermal conductivity (i.e. in the thermal conductivity transverse to the fibers), is approximately 22 W/mK. The fiber phase in the composite thus results in a through-plane conductivity which has roughly 35 % of the bulk conductivity of the SnAgCu matrix. However, due to compression of fibers during the fabrication process, it is not likely that such conductivity is also valid for much higher thickness of the SMNPC. Instead, it could be expected that compression of very high thickness of the fiber network would eventually seal off an increasing amount of continuous high conducting matrix paths. Such an effect could lead to an increase in thermal resistance which is higher than the linear extrapolation predicts, and thus a steeper slope corresponding to lower thermal conductivity. The contact resistance for the SMNPC is found to be in the same range as that of the pure SnAgCu joint, and thus relatively unaffected by the fiber reinforcement.

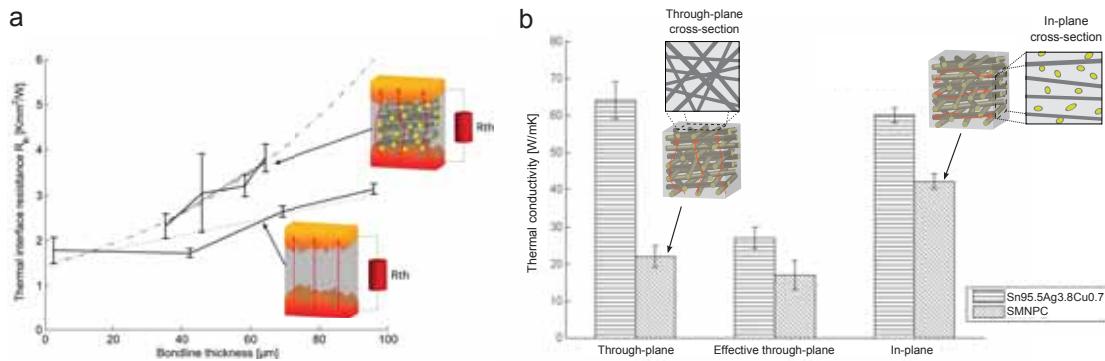


Figure 4.14: Total thermal interface resistance as a function of BLT directly after bonding of the SMNPC and pure SnAgCu alloy between ENIG coated Cu (a). The measured thermal conductivity of the SMNPC compared to SnAgCu alloy.

Nevertheless, the most important figure of merit for thermal interface materials and die attach, due to thin BLT, is the total thermal resistance across the interface. Over the tested thickness range, the total thermal interface resistance was found to be between 2.2-3.7 Kmm²/W and 1.6-2.8 Kmm²/W for the SMNPC and pure SnAgCu alloy respectively. This corresponds to an average effective through-plane thermal conductivity of 17 ± 4 W/mK for the composite, which is around 60 % of the 27 ± 3 W/mK measured for the reference alloy. The effective difference in heat transfer is thus much less than what appears from considering only through-plane

thermal conductivity.

In-plane thermal conductivity is becoming increasingly relevant for TIMs as it directly influences the ability to accommodate for high heat flux areas of active devices [254]. To measure the in-plane conductivity of the composite, xenon flash methodology, with a special fixture which evaluates the time response for in-plane heat transport, was utilized. The conductivity of the SnAgCu alloy was measured to 60 ± 2 W/mK, which is in reasonable agreement with the measured value when sandwiched between copper pieces. The measurements also agree with previous reported values for SnAgCu alloy in literature [255]. The in-plane conductivity of the SMNPC was found to be 42 ± 2 W/mK, which is about 70 % of the bulk matrix value. Thus an anisotropic thermal conductivity with almost 50 % higher in-plane conductivity compared to through-plane is found for the composite. A possible explanation for this is that the cross section of the low conducting fibers running in parallel direction to the heat will exhibit a smaller area compared to transverse fibers (see the through-plane cross-section in-plane cross in figure 4.14).

Furthermore, the measured data for in-plane and through-plane thermal conductivity of the SMNPC can be compared to model estimations of the thermal conductivity, using an isoflux and isogradient configuration, in combination with the rule of mixtures. Considering the case when the orientation of the conductive material is perpendicular to the thermal gradient, i.e. the isoflux case, the lower limit for the thermal conductivity of the composite (λ_c) can be estimated according to:

$$\lambda_c = \left(\frac{\phi_f}{\lambda_f} + \frac{1 - \phi_f}{\lambda_m} \right)^{-1} \quad (4.8)$$

where ϕ_f is the volume filler fraction and λ_f and λ_m are the respective thermal conductivities of the filler and the matrix. For the other case, the isogradient configuration, i.e. when the conductive portion is oriented in parallel with the thermal gradient, the upper limit of the thermal conductivity of the composite (λ_c) can be estimated according to:

$$\lambda_c = \lambda_f \phi_f + \lambda_m (1 - \phi_f) \quad (4.9)$$

Using $\phi_f = 30\%$ (estimated from density measurements), $\lambda_f = 0.5$ W/mK (polyimide fibers) and $\lambda_m = 60$ W/mK (Sn–Ag–Cu alloy), the isoflux and isogradient configurations and the rule of mixtures estimate $\lambda_c = 1.6$ W/mK and $\lambda_c = 42$ W/mK for the lower and upper limit of the thermal conductivity. The upper limit appears to agree well with the measured in-plane thermal conductivity, indicating that the composite structure is close to that of the isogradient configuration in the in-plane direction. The thermal conductivity of the through-plane direction is in-between the isoflux and isogradient, indicating that the structure is effectively a combination of the two configurations. Both these results are in agreement with what can be expected because of the in-plane fiber alignment in the composite.

Another crucial aspect for materials aimed for TIM and die attach applications is the thermomechanical reliability. For STIMs reliability problems can be of similar nature as that of conventional solders, such as crack formation, fatigue and embrittlement caused by the formation of intermetallic compounds. Most often, such processes eventually lead to a drastic drop or change in mechanical and/or thermal properties, which can cause a critical failure of the system [256]. In addition to being one of the most important properties, to maintain for a thermal interface and die attach materials for reliable operation, thermal resistance is very sensitive to structural changes. Therefore, to evaluate the thermo-mechanical reliability of the SMNPC, we carried out thermal cycling under harsh conditions (40 to 115°C @ 2 cycles per hour) while periodically monitoring the relative change in thermal resistance. The results are presented in figure 4.15.

After 1000 cycles, the thermal resistance of the SMNPC was found largely unaffected, which indicate that the joints were kept reasonably intact through the thermal cycling. Most of the samples stayed within 20% of the initial resistance, which is within the variation of the accuracy for some of the measurements with very low initial thermal resistance. One sample showed an increase in the range of 20-40%. However, as this increase occurred already after 100 cycles, and did not change drastically for the next 900 cycles, it is likely due to some initial

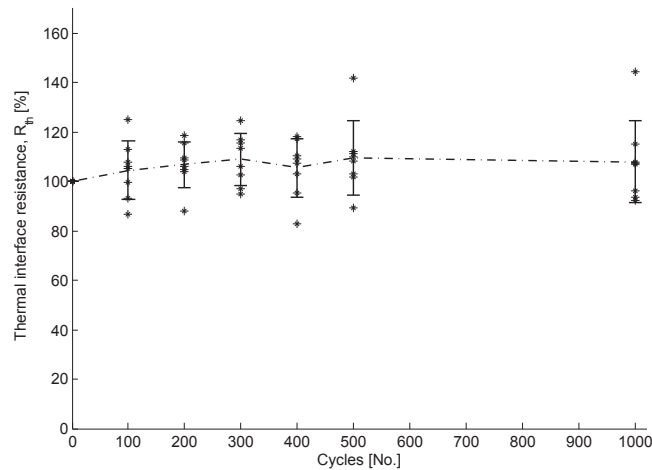


Figure 4.15: Change in thermal resistance during thermal cycling. The error bars indicate the standard deviation of the average of 8 samples measured.

defect of the particular sample, rather than a continuous degradation mechanism. The result thus indicate that the evolution of intermetallic compounds formed, which can be quite complex for SnAgCu alloy on surfaces containing Au, Ni and Cu species [257], is such that the performance is not severely affected. As high levels of intermetallic compounds are well known to cause brittle joints [258], the formation is in this case likely relatively low.

The finding of reliable thermal performance during thermal cycling for a material with high flexibility, presented here, is in agreement with a study by Li et al. [259]. In their study it was shown that conductive adhesive with added flexible molecules into the epoxy matrix dramatically reduced the thermomechanical stress and better maintained electrical resistance. A study by Hua et al. [199] investigating thermal cycling of solders for TIM1 applications has shown that pure Sn is unsuitable to use, as it can cause die cracking. In the same article, it was also discussed that the ideal solder for TIM1 applications should be ductile enough in order to absorb the thermally induced strain during thermal cycling. In this regard, the SMNPC can potentially be a useful alternative.

The reliability of the performance of conventional grease based materials is well known to be subject to pump out and dry-out which can cause degradation of the thermal performance. Studies conducting thermal cycling of greases have

however ambiguously shown both large increase and slight reduction of the thermal resistance over time [260]. The material behavior during thermal cycling of the SMNPC are hence more similar to that of phase change- and gel-based TIMs, reported in literature, which display stable performance over time [260].

To summarize, the results have shown that the SMNPC concept can combine the characteristics of low elastic modulus together with high thermal conductivity. The elastic modulus, which was significantly lowered from that of pure SnAgCu alloy, indicates the potential of the concept to enable the use this low-cost alloy for TIM and die attach applications. When taking into account the low thermal resistance, on par with pure solder, and reliable performance during thermal cycling, the SMNPC appears as a competitive alternative to both high cost In and particle laden polymer matrix materials.

4.3.4 Solder Alloy Matrix and Carbon Fiber Composite

As have been described earlier, carbon fibers has been used in composite for TIM applications. We next sought to investigate the characteristics of a composite using carbon fibers, instead of polymer fibers. The possibilities of increased conductivity and lowered CTE may be attractive in applications, where more rigid materials, rather than flexible interfaces, are applicable. Additionally, the use of continuous CFs to form composite solder for TIM applications has, to the best of our knowledge, not been previously reported in the literature.

A strategy based on electrospinning to fabricate a carbon fiber based Sn–Ag–Cu alloy matrix composite (CF-TIM) was developed, and shown in the flow chart in figure 4.16. Mesophase pitch (ARS) was selected as a precursor to be electrospun for the carbon fiber formation due to its polynuclear ring structure, that has previously been shown to allow for the formation of highly organized crystalline carbon structures via high temperature annealing [261]. However, in our initial experiments, the ARS was found to be very difficult to electrospin directly into fibers. Instead, the soluble portion of mesophase pitch (*s*-ARS) obtained from N,N-dimethyl acetamide (DMAc) solvent extraction was used together with polyimide (PI), to render a solution which could be electrospun. The main steps in the preparation of the CF-TIM, was consequently via solvent extraction of mesophase-pitch,

electrospinning, stabilization, carbonization, sputter coating and pressure assisted liquid-phase infiltration.

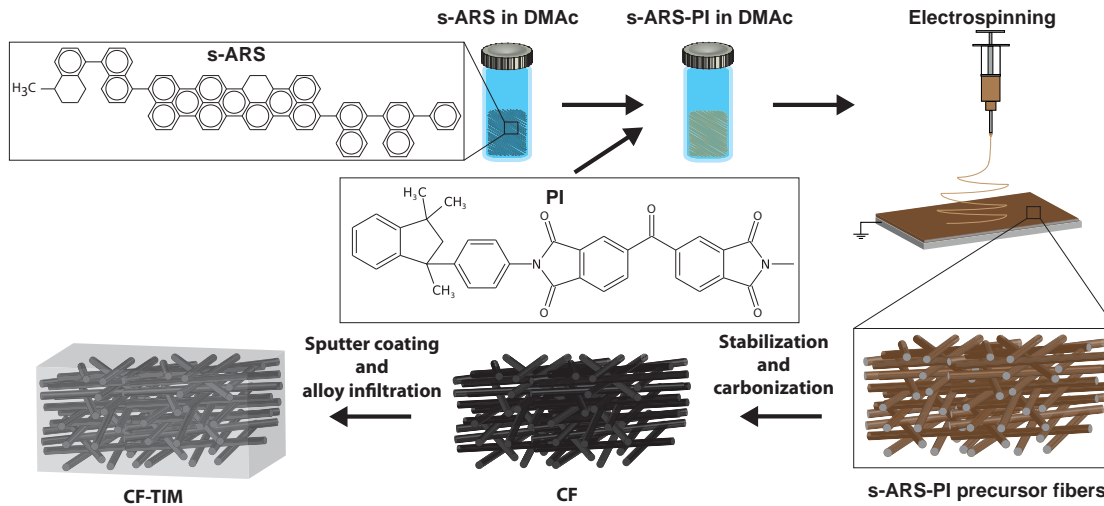


Figure 4.16: Schematic of the modified fabrication of the CF-TIM. The preparation includes solvent extraction, electrospinning, stabilization, carbonization, sputter coating with titanium and gold, and liquid Sn–Ag–Cu alloy infiltration.

From the electrospinning process, the resulting nonwoven fibers had diameters in the range of $12\ \mu\text{m}$ (figure 4.17a). After electrospinning, the fiber mats were preheated to 310°C , followed by carbonization at 1000°C in a nitrogen atmosphere to form final CFs (figure 4.17b,c). The carbonization treatment caused the fiber mats and individual fibers to shrink significantly.

Further analysis of the CFs, through transmission electron microscopy, X-ray diffraction and raman indicated the effects on the microstructure from the processes occurring during the carbonization, such as dehydrogenation, condensation, hydrogen transfer and isomerization, and molecular rearrangement. The TEM images, indicated that each fiber had a disordered internal arrangement after the carbonization at 1000°C . A disordered arrangement of the carbon was confirmed using X-ray diffraction, in which the main peak was seen to be only slightly shifted towards the (002) peak at $2\theta = 23^\circ$, and an a small emerging (10) peak was observed around $2\theta = 42^\circ$. Raman spectra showed the same trend in the form of clear peaks from both the G band and the D band at $1600\ \text{cm}^{-1}$ and $1328\ \text{cm}^{-1}$.

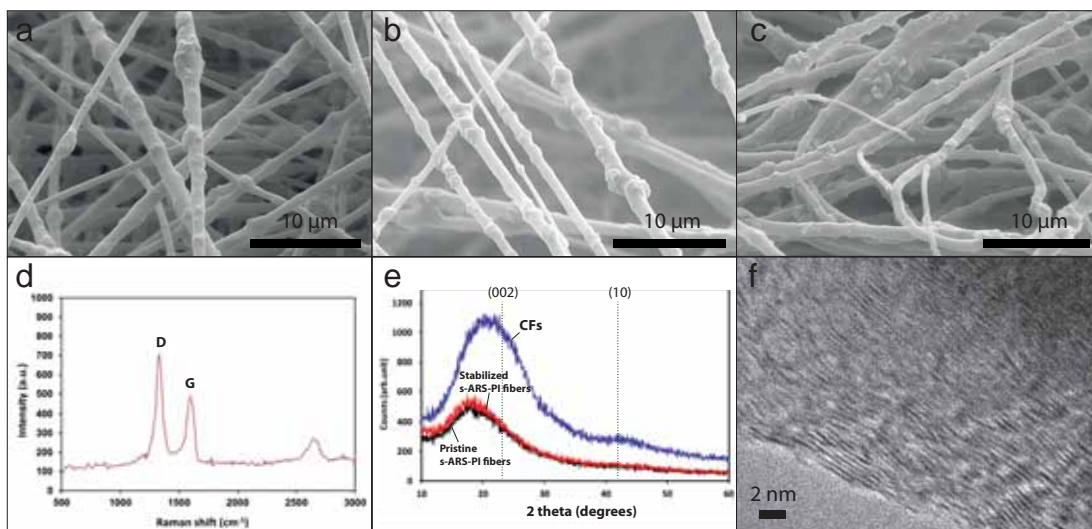


Figure 4.17: SEM images of the electrospun precursor fibers after electrospinning (a), stabilization (b) and carbonization at 1000 °C (c, f). The collected Raman spectra of the carbon fibers (d) and the measured XRD profile of the precursor, stabilized and carbon fibers (e).

The appearance of a large D band indicate that the carbon structure has a high number of defects and is disordered in nature [262]. The intensity ratio of D band to G band (I_D/I_G) of the as prepared carbon nanofibers was found to be 1.46, which is comparably low to high crystalline carbon. Nevertheless, the observed microstructure of the CFs is considered well known and comparable to what has been reported for low temperature carbonization processes [263, 264].

To evaluate the in-plane bulk thermal conductivity of CFs produced from 1000°C annealing, a transient in-plane measurement system (Hotdisk) was used. A slab module with a diameter of 4 mm was utilized and sandwiched between two CF film samples being measured during the measurement. Styrofoam was used as an insulator to minimize heat losses to the ambient. Using this technique, the porous CF films with a thickness of $50 \pm 5 \mu\text{m}$ were found to have a thermal conductivity of 4 W/mK. Due to the high porosity of the carbon fibrous network the measured thermal conductivity is relatively low compared to other carbon based materials. Nevertheless, the individual CFs can be expected to have significantly higher thermal conductivity than the measured 4 W/mK. The measured thermal

conductivity of mesophase pitch derived CFs are comparable to other CFs/carbon materials produced at 1000°C and reported in the literature. For instance, Wang et al.[265] found that the thermal conductivity of PAN-based CFs carbonized at 1000°C was 5 to 10 W/mK through measurements using the 3ω -method on individual fibers with a diameter of 7 μm . Li et al. [266] reported the use of PAN based CFs with a thermal conductivity of ~ 4 W/mK for radiation shielding applications.

Before liquid phase infiltration, to form the composite, the CFs were first sputter coated with 120 nm Ti and 60 nm Au, in order to facilitate proper wetting. The coated CFs were infiltrated with a SnAgCu matrix in molten stage under 30 MPa pressure, again, in the custom built infiltration equipment.

The results from the thermal evaluation of the composite are summarized in figure 4.18. The in-plane thermal conductivity was evaluated by measuring with an in-plane measurement fixture for the flash method, and was found to be around 40 ± 2 W/mK, with a marginal effect of high temperature over the range of 50-90°C. The through-plane thermal conductivity was evaluated by measuring the total thermal resistance while varying the thickness of the composite sandwiched and reflowed between ENIG coated copper plates. The effective through-plane thermal conductivity of CF-TIM was found to be 20 ± 3 W/mK over the range of 50 to 90°C at 65 μm BLT. The total thermal interface resistance was measured to be 27 Kmm^2/W at BLTs between 65 and 160 μm . Extrapolation of the results towards zero BLT indicates a contact resistance below 1 Kmm^2/W .

To assess the reliability of the joint formed with CF-TIM, thermal cycling of the test assemblies was carried out. The temperature was cycled between -40 and 115 °C in accordance with global standards for the microelectronics industry (JEDEC standard), for 1000 cycles while periodically evaluating the thermal resistance. It was found that the thermal resistances remain largely unaffected after 1000 cycles, indicating that reliable joints have been formed for all different sample thicknesses. The observable trend of a few percent increases in thermal resistance is within the accuracy of the measurements.

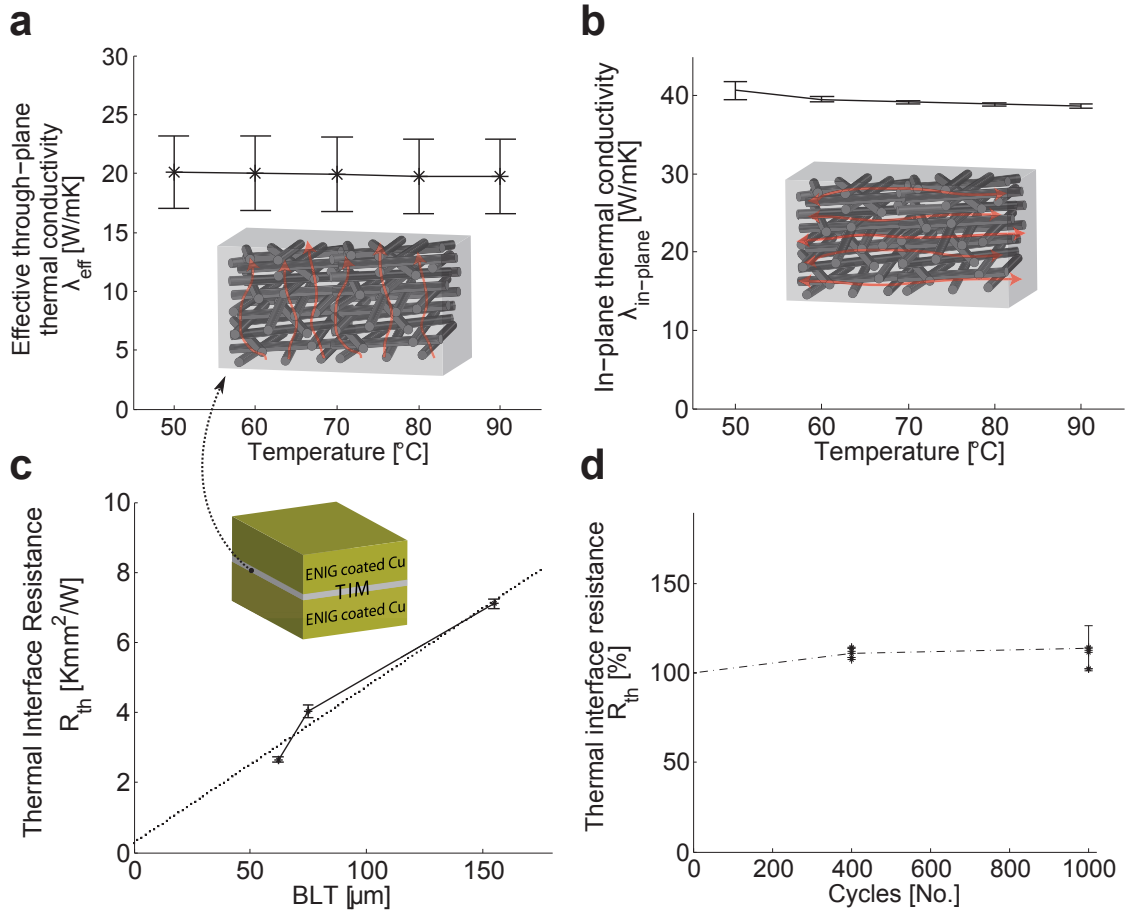


Figure 4.18: A summary of the results from the thermal characterization of the CF-TIM. (a) Effective through-plane thermal conductivity of CF-TIM between 50 and 90° C at a BLT of 65 mm. (b) In-plane thermal conductivity of CF-TIM. (c) Total thermal interface resistance of CF-TIM at various BLTs. (d) The relative change in thermal resistance of the CF-TIM after thermal cycling up to 1000 cycles.

4.3.5 Summary and discussion

Three specific implementations of the fiber based MMC technology has been developed and characterized. In the development of the In–MMC, the potential of using the chemical reduction method for surface modification of the fibers was demonstrated. The addition of a fiber phase was shown to have a relatively small effect on the thermal interface resistance. The internal microstructure of the composite introduced by the continuous submicron fibers can also be expected to modify breakdown phenomena such as crack propagation during deformation and fatigue. This in combination with well defined BLTs and restricting possible leakage during assembly, makes the composite an attractive option.

From a TIM perspective, perhaps even more interesting than a composite with an In matrix, is the cost-effective alternative of using a Sn-based alloy matrix. Earlier attempts to implement Sn-based alloys has been reported to fail due to die cracking caused by excessive stress transfer from CTE mismatch across the stiff interface during assembly [199]. By demonstrating a significant reduction in elastic modulus compared to a pure SAC alloy, the SMNPC developed here has potential to solve these issues. One such example could be for TIM1 applications, as a lead-free replacement of current indium solutions. Another example is bonding of large chip surfaces ($>100 \text{ mm}^2$), for which it can be problematic to use pure solder due to delamination and cracking.

For a better understanding of the stress transfer across an interface, it can be illustrative to consider the one-dimensional equation for the shear stress (τ_{max}) present at the edge of the structure between two bonded materials. Taking the example of a IHS and a die, of given thickness (t_{ihs} and t_{die}) and elastic modulus (E_{ihs}, E_{die}), bonded with a TIM of Young's modulus in shear of E_{TIM} , and neglecting bending effects of the structure, the relation is [267]:

$$\tau_{max} = (\alpha_{ihs} - \alpha_{die})\Delta T \sqrt{\frac{E_{TIM}}{BLT}} \gamma \tanh\left(\sqrt{\frac{E_{TIM}}{BLT}} \frac{1}{\gamma} L_{1/2}\right) \quad (4.10)$$

$$\gamma = \frac{E_{die}t_{die}E_{ihs}t_{ihs}}{E_{die}t_{die} + E_{ihs}t_{ihs}} \quad (4.11)$$

where $L_{1/2}$ is half of the length of the bonded structure and ΔT is the temperature

difference to the stress free state.

As can be seen from equation 4.10 both the modulus of the TIM and the BLT has a large effect on the stress. The relation thus indicates that reducing the modulus of the TIM joint could permit lower BLT, larger bond length, higher assembly temperatures or a combination thereof, while maintaining acceptable levels of stress. In turn, lower BLT can lead to more competitive thermal performance, as well as lower material consumption, potentially important in the case of In. Large bond length permits for larger surfaces to be bonded, which may be of relevance for TIM2 materials, or for larger die sizes. Allowing for higher assembly temperatures can enable the use of low cost alloys of high melting point and high elastic modulus as TIM materials. Furthermore, the life-time of a joint is proportional to the total accumulated stress, for instance over multiple thermal cycles. Hence, lowering the induced maximum stress of each cycle can improve the reliability of the joint substantially.

In the case of small mismatch in thermal expansion between joining surfaces and/or at relatively high BLTs, so that the stress levels are kept within limits, the bulk thermal conductivity of the TIM becomes more important. Therefore, using carbon fibers with significantly higher thermal conductivity compared to polymer fibers, were investigated as the fiber phase in a SAC based matrix. The wetting and infiltration of the SnAgCu alloy into carbon fibers was mitigated by sputter coating with Ti and Au. Our measurements showed that the improvement in thermal conductivity of the CF composite was limited compared to the use of polymer fibers. The result is likely explained by a poor phonon-coupling between the matrix and the fibers, as well as the limited crystallinity of the carbon fibers. Consequently, to enable higher performance, further development is needed to improve the interface between the carbon and metal phase in combination with carbonization/graphitization of the fibers at higher temperatures. The improvement using carbon fibers was instead seen for higher BLTs, where the CF TIM did not show the trend of lower conductivity, in the same manner as the SMNPC. Potentially, this can be explained by the higher rigidity of the carbon network which thus is less compressible than the polymer. The CF-TIM can therefore retain a continuous conductive network at higher BLT, when there is a higher number of fiber layers present.

Of further relevance for the CF-TIM, is that the CTE of carbon is very low, and the introduction of the carbon fibers will lead to a lower CTE of the composite compared to the alloy matrix. For applications with brittle and CTE-matching surfaces, the opportunity of tailoring the CTE of the CF-TIM could be of relevance. Potentially this could complement efforts of tailoring the CTE of heatsinks to that of semiconducting and thermoelectric materials that uses Cu and Al MMCs with filler additions [268, 269].

As a summary, figure 4.19 and table 4.3.5 presents the total thermal interface resistance as a function of BLT, for the materials developed in this thesis and for other high performing and emerging TIM materials discussed earlier. For comparison, also single contact resistances are plotted and given in table 4.3.5. In general, the thermal performance of the three MMC composites appear competitive across BLTs from below 20 to around 150 μm . The performance of the composites are equivalent to a material with low contact resistance of around 1 Kmm^2/W ($R_{c1} + R_{c2}$) with a conductivity between 20-40 W/mK (given by the dashed gray lines). Crudely, this is also the same range as has been reported for other metal based TIMs. Aligned carbon based materials, i.e. VACNT and graphene, typically has higher total thermal resistance compared to metal based TIMs, even though they, after additional modifications, can offer some improvement with respect to conventional grease and phase-change material. Considering only the thermal resistance, combining VACNT growth directly on silicon chips, with specific surface modification towards Cu, appear promising as a TIM1 structure. However, the high-temperature required for direct growth may severely limit possible applications for this approach.

A few of the reported single thermal contact resistance values for interfaces, indicates that there is still room for some improvements for TIM materials. However, to reach thermal resistances that are much lower, is very challenging. It will require a combination of very high conductivity and low contact resistance material interfaces which, until now, very few emerging technologies have demonstrated. Interfaces using metallic wetting and bonding are, so far, the most successful way to accomplish low contact resistance, under the boundary conditions set by electronics packaging. On the other hand, carbon based materials are considered to be an attractive option due to their high conductivity, but typically have high contact

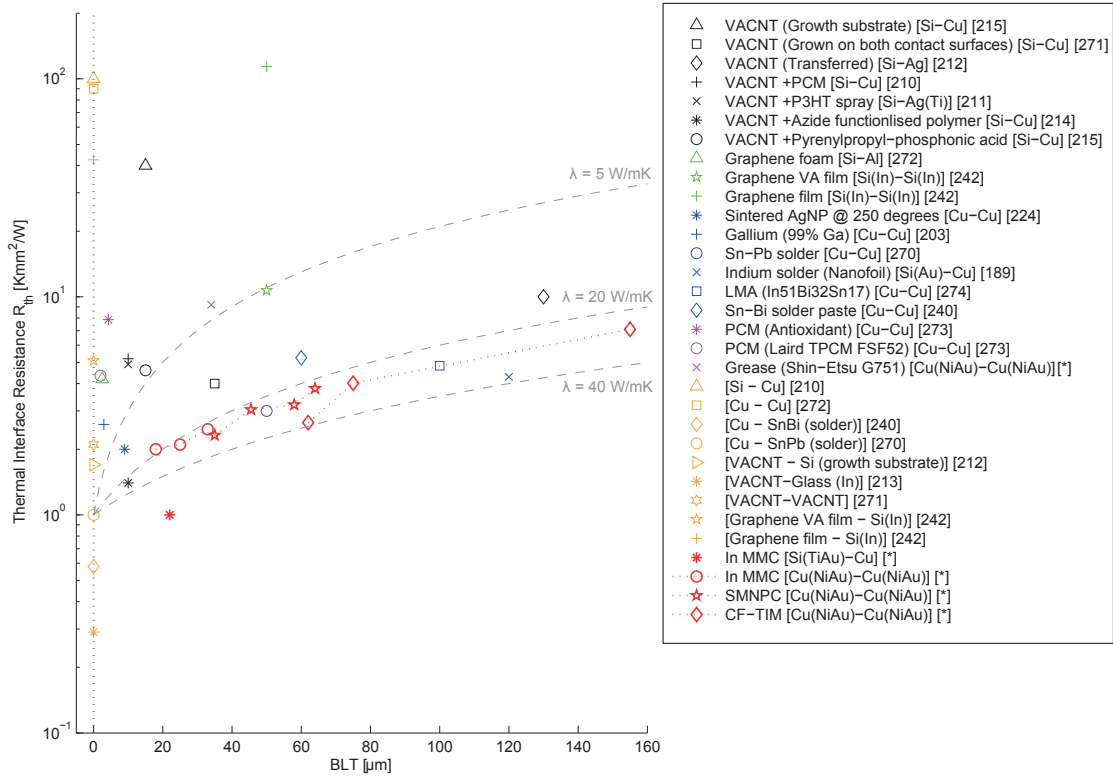


Figure 4.19: Summary of total thermal interface resistances as a function of BLT, reported in this thesis and in literature; VACNT based (Black), Graphene based (Green), Metal based (Blue), Conventional TIMs (Magenta) and the MMC TIMs from this thesis (Red). For comparison, single contact resistances (R_c) are plotted (Orange) and the grey dashed lines correspond to materials with a thermal conductivity of 5, 20 and 40 W/mK, with a total contact resistance of 1 Kmm²/W. For clarity, error bars have been excluded and only average reported total thermal interface resistance values are marked.

Thermal Interface Materials in Microelectronics Packaging

Table 4.1: Total thermal interface resistances for different TIMs reported in this thesis and in literature.

TIM	R_{TIM} [Kmm ² /W]	BLT [μm]	Interface	Method	Ref.
In-MMC	~1	22	Si(TiAu)-Cu	A	*
VACNT + Azide functionalised polymer	1.4	10	Si-Cu	D	[214]
Sintered AgNp @ 250degC	2	9	Cu-Cu	A	[224]
In-MMC	2.0-2.5	18-33	Cu(NiAu)-Cu(NiAu)	A	*
Gallium (99 % Ga)	2.6	1	Cu-Cu	D	[203]
Sn-Pb solder	3	50	Cu-Cu	A	[270]
SMNPC	2.3-3.8	35-64	Cu(NiAu)-Cu(NiAu)	A	*
CF-TIM	2.7-7.1	62-155	Cu(NiAu)-Cu(NiAu)	A	*
VACNT (Grown on both contact surfaces)	4	35	Si-Cu	B	[271]
Graphene foam	4.2	3	Si-Al	C	[272]
Indium solder (Nanofilm)	4.3	120	Si(Au)-Cu	A	[189]
PCM (Laird TPCM FSF52)	4.4	2	Cu-Cu	C	[273]
VACNT + Pyrenylpropyl-phosphonic acid	4.6	15	Si-Cu	B	[215]
LMA (In51Bi32Sn17)	4.8	100	Cu-Cu	A	[274]
VACNT + P3HT spray	4.9	10	Si-Ag(Ti)	B	[211]
VACNT + PCM	5.2	10	Si-Cu	C	[210]
Sn-Bi solder paste	5.3	60	Cu-Cu	A	[240]
Graphene VA Film	10.7	50	Si(In)-Si(In)	A	[242]
PCM (Antioxidant)	7.9	4	Cu-Cu	C	[273]
Grease (Shin Etsu G751)	9.2	34	Cu(NiAu)-Cu(NiAu)	A	*
VACNT transferred	10	30	Si-Ag	B	[212]
VACNT (Growth substrate)	40	15	Si-Cu	B	[215]
Graphene film	114	50	Si(In)-Si(In)	A	[242]
CNT-Cu-CNT TIM	319	207	Cu-Cu	A	[275]

*Results from this thesis

A - Flash technique

B - Photoacoustic technique

C - ASTM D5470

D - Customized setup

Table 4.2: Single contact resistances reported in this thesis and in literature.

Single Contact	R_c [Kmm ² /W]	Method	Ref.
VACNT-Glass (In)	~0.3	D	[213]
Cu-SnBi	~0.6	C	[240]
Cu(NiAu)-In	<1	A	*
Cu(NiAu)-SnAgCu	<1	A	*
Cu-SnPb	~1	A	[270]
VACNT-Si (Growth substrate)	1.7	B	[212]
VACNT-VACNT	2.1	B	[271]
Graphene VA film - Si(In)	5.1	A	[242]
Graphene film - Si(In)	42.5	A	[242]
Cu-Cu	90	C	[272]
Si-Cu	100	A	[210]

*Results from this thesis

A - Flash technique

B - Photoacoustic technique

C - ASTM D5470

D - Customized setup

resistance. Hence, combining the two comes across as an interesting alternative, and is what was attempted with the CF-TIM. Even though our success thus far has been limited, it is believed that the MMC structure combined with continuous, and possibly vertically aligned, carbon phases is a relevant path for continued efforts.

Chapter 5

Conclusions and Outlook

This thesis has explored the utilization of electrospun materials and associated fiber surface modifications within two fields: fibrous architectures as cell culture substrates and fiber networks as carrier phases in a novel MMC TIM technology.

The first part of this thesis focused on the use of electrospun PU scaffolds for stem cells and neural cells. First, we studied plasma treatments as a modification of the fiber scaffold surfaces and considered the effects on fiber surface morphology, surface chemistry and wettability, as well as the associated influence on stem cell proliferation, differentiation and migration. The plasma modified fiber interface was found to enhance the possibility for hESC culture expansion on randomly oriented electrospun fibers, but without apparent effects on the directed migration of nSCs along aligned fiber samples. The surface chemical and morphological changes induced from the plasma did not affect the differentiation of nSCs. Instead, the similar differentiation found across all samples suggested that the influence of the cell media was dominant. We also explored the use of electrospun scaffolds with varying fiber diameter as substrates for fully differentiated primary cells, i.e. specific neural cells, in the form of neurons and astrocytes. Scaffolds of PU fibers, just larger than 1 μm in diameter, with a physically adsorbed PoLam coating, were shown to induce complex astrocyte cell morphologies that resemble the *in vivo* appearance to a higher degree than standard planar surfaces. Culturing astrocytes on these electrospun topographies was also observed to substantially limit the up-regulation of protein expression associated with astrocyte stress and activation. Such stress related protein expression has traditionally been recognized

as a consequence of the highly artificial environment that conventional *in vitro* culture substrates constitute. These positive effects suggest the usefulness of electrospun structures as 3D topographical culture substrates to complement or, to a certain extent, replace two-dimensional *in vitro* culture substrates for astrocytes. Consequently, our findings leave a number of interesting directions for future studies, such as re-evaluating various traditional *in vitro* assays and introducing cells in co-culture with astrocytes on the fiber scaffolds. In our continued studies, a reduced stress related protein expression was also confirmed for the contaminating astrocytes in neuronal cultures on the electrospun scaffolds. Additionally, for neuronal cultures, we found that fibers of thinner diameter, i.e. around 500 nm, which in other studies have been associated with increased directional differentiation towards neuronal fate [90, 98], was favorable in terms of neurite outgrowth. Combined with the high porosity, leading to formation of three-dimensional neuronal networks, the electrospun fibers also offer attractive features that are beyond that of current conventional substrates for *in vitro* studies of neurons. Furthermore, recognizing the need to be able to generate and study complex cell micro-environments, a process based on direct photolithography to integrate patterned electrospun PU topographies within micro-fluidic systems was developed. Using this technique we demonstrated a platform that may be used for well-controlled investigations of the interplay between reactions of cells to topography, induced from fiber patterns, and the cues from gradients of soluble substances.

The second part of the thesis described the development of a novel MMC TIM concept using continuous electrospun fibers as a reinforcement, and consecutively explored three specific implementations of this technology: In-MMC, SMNPC and CF-TIM. After a general introduction to material interfaces as crucial bottlenecks in thermal management of microelectronics, and reviewing emerging TIM technologies, the fabrication process of the proposed MMCs was presented. As a part of the fabrication, a chemical reduction based synthesis of Ag nanoparticles through imide cleavage and ion exchange was optimized and found suitable as a surface modification of electrospun PI fibers, to facilitate infiltration of a metal matrix. The Ag-nanoparticle surface modification of PI-fibers, followed by infiltration of Indium and SnAgCu alloy matrix, was then used to fabricate the In-MMC and SMNPC. The addition of a polymer fibre phase was shown to have a

relatively small effect on the total thermal interface resistance, compared to solid solder joints based on the respective matrix material. The intended function of the internal microstructure introduced by the polymer fibers is modification of the thermo-mechanical behavior, to address reliability issues such as crack propagation during solidification, deformation and fatigue, and to limit the leakage during assembly. In this regard, the SMNPC showed a reduction in the elastic modulus compared to solid SAC alloy, which indicates the possibility to use this composite to bond materials with CTE mismatch. This is believed to be relevant for TIM1 applications or other semiconductor-metal contacts, as a tin-based alternative to indium. The CF-TIM was developed for interfaces where shear stress is of less concern, and based on the hypothesis that the thermal conductivity could be increased by switching to a fiber phase based on carbonized mesophase-pitch/PI. Despite no clear reduction in the total thermal interface resistance of the composite could be measured, it may provide other advantages, such as reaching higher BLTs and tuning the CTE. Further studies should investigate methods to improve the interface between the carbon and metal phase in combination with carbonization/graphitization of the fibers at higher temperatures.

Comparing the thermal performance of the three composites to other TIMs reported in literature, the technology appears promising and motivates continued development. There are several aspects that future work could consider. This includes: improving the understanding of how the fiber type and volume affects the thermo-mechanical properties of the composite; studying reflow conditions and formation of intermetallics at the fiber-matrix interface and at the contacting surfaces; utilizing exothermic reactions between thin layers of metals (e.g. Al and Ni) as a localized heating source for reflow; alternative matrix alloys such as SnZn for application at Al surfaces; and investigating reliability aspects of the composites applied at large interfaces with and CTE mismatch.

Given the data in this thesis, we conclude that electrospun micro- and nanofibers can play functional roles in future advanced materials for biological and engineering applications.

Acknowledgements

First of all, I would like to express my gratitude to my supervisor and examiner Prof. Johan Liu, for giving me the opportunity to work in an exciting, challenging and creative research environment. His continuous guidance and trust are deeply appreciated. I also want to thank my co-supervisors Lilei Ye and Marina Voinova for their contributions, patience and fruitful discussions.

I want to thank my former and present colleagues at the BioNano Systems Laboratory: Murali Murugesan, Di Jiang, Si Chen, Yifeng Fu, Xin Luo, Nan Wang, Wei Mu, Michel Edwards, Teng Wang, Zhili Hu and many others for their collaboration, support and interesting discussions on all kinds of topics. I especially owe a great deal to Björn Carlberg, for his appreciated friendship, entertaining discussions, guidance, and invaluable input on numerous problems faced along the way.

I am deeply indebted to Till "the German Edition" Puschmann. He entered my life as a neuroscientist bubbling with ideas, and is now one of my dearest friends. Without his contributions, both scientific and in my personal life, nothing would have been the same.

The work in this thesis would not have been possible without the contributions and support from fellow researchers at the Sahlgrenska Academy; Nina Erkenstam, Georg Kuhn and Milos Pekny, as well as Patric Wallin and Julie Gold from the Department of Applied Physics at Chalmers. I have really enjoyed working with all of you.

I want to thank Carl-Magnus Kihlman for his help creating various parts for my experiments and the staff of the Nanofabrication Laboratory for providing excellent research facilities.

My friends Sumedh "sum of all bolometers" Mahashabde and Tom "scary vegetarian shoes" Yager deserve special thanks for enduring my company in our lunch league.

Last but not least, I deeply thank my beloved Carolina Johansson and my family for their love, support and encouragement.

This work was supported by EU programs "Thema-CNT", "Smartpower", "Nanotherm", the Swedish National Science Foundation (VR) under the project "Thermoelectric Nanostructures for On-Chip Cooling" with contract no. 2009-5042 and EU Eranet program "Nanotim" with contract no. 2011-02075 funded by Vinnova. This work was also supported by the Vinnova IT-hälsa program on "Nanoscaffolds for control of stem cell division, differentiation and migration" with contract No. 2009-00227. This work was carried out within the Sustainable Production Initiative and the Production Area of Advance at Chalmers.

References

- [1] M. Rahaman and J. Mao, "Stem cell-based composite tissue constructs for regenerative medicine," *Biotechnology and Bioengineering*, vol. 91, no. 3, pp. 261–284, 2005.
- [2] P. De Coppi, G. Bartsch, M. M. Siddiqui, T. Xu, C. C. Santos, L. Perin, G. Mostoslavsky, A. C. Serre, E. Y. Snyder, J. J. Yoo, M. E. Furth, S. Soker, and A. Atala, "Isolation of amniotic stem cell lines with potential for therapy," *Nature Biotechnology*, vol. 25, pp. 100–106, Jan. 2007.
- [3] J. Holst, S. Watson, M. S. Lord, S. S. Eamegdool, D. V. Bax, L. B. Nivison-Smith, A. Kondyurin, L. Ma, A. F. Oberhauser, A. S. Weiss, and J. E. J. Rasko, "Substrate elasticity provides mechanical signals for the expansion of hemopoietic stem and progenitor cells," *Nature Biotechnology*, vol. 28, pp. 1123–1128, Oct. 2010.
- [4] M. P. Lutolf, P. M. Gilbert, and H. M. Blau, "Designing materials to direct stem-cell fate," *Nature*, vol. 462, pp. 433–441, Nov. 2009.
- [5] J. W. Haycock, "3d cell culture: A review of current approaches and techniques," in *3D Cell Culture* (J. W. Haycock, ed.), vol. 695 of *Methods in Molecular Biology*, pp. 1–15, Humana Press, 2011.
- [6] J. A. Burdick and G. Vunjak-Novakovic, "Engineered microenvironments for controlled stem cell differentiation," *Tissue Engineering Part A*, vol. 15, pp. 205–219, Feb. 2009.
- [7] S. Sakore and B. Chakraborty, "In vitro in vivo correlation (IVIVC): a strategic tool in drug development," *J Bioequiv Availab S*, vol. 3, p. 2, 2011.
- [8] F. Pampaloni, E. G. Reynaud, and E. H. K. Stelzer, "The third dimension bridges the gap between cell culture and live tissue," *Nature Reviews Molecular Cell Biology*, vol. 8, pp. 839–845, Oct. 2007.
- [9] J. Bell and J. Haycock, "Next generation nerve guides: Materials, fabrication, growth factors, and cell delivery," *Tissue Engineering - Part B: Reviews*, vol. 18, no. 2, pp. 116–128, 2012.
- [10] A. L. Moore and L. Shi, "Emerging challenges and materials for thermal management of electronics," *Materials Today*, vol. 17, pp. 163–174, May 2014.
- [11] ITRS, "International technology roadmap for semiconductors - emerging research materials summary," 2013.
- [12] iNEMI, "iNEMI 2011 research priorities," 2011.
- [13] ITRS, "International technology roadmap for semiconductors 2009 edition - assembly and packaging," 2009.
- [14] S. Garimella, A. Fleischer, J. Murthy, A. Keshavarzi, R. Prasher, C. Patel, S. Bhavnani, R. Venkatasubramanian, R. Mahajan, Y. Joshi, B. Sammakia, B. Myers, L. Chorosinski, M. Baelmans, P. Sathyamurthy, and P. Raad, "Thermal challenges in next-generation electronic systems," *IEEE Transactions on Components and Packaging Technologies*, vol. 31, no. 4, pp. 801–815, 2008.
- [15] E. Pop, "Energy dissipation and transport in nanoscale devices," *Nano Research*, vol. 3, no. 3, pp. 147–169, 2010.

- [16] R. Mahajan, D. Mallik, R. Sankman, K. Radhakrishnan, C. Chiu, and J. He, “Advances and challenges in flip-chip packaging,” in *Custom Integrated Circuits Conference, 2006. CICC '06. IEEE*, pp. 703–709, Sept. 2006.
- [17] E. Pop, S. Sinha, and K. Goodson, “Heat generation and transport in nanometer-scale transistors,” *Proceedings of the IEEE*, vol. 94, pp. 1587–1601, Aug. 2006.
- [18] Y. Zhao, T. Semenic, and A. Bhunia, “Advanced packaging and thermal management for high power density GaN devices,” in *2013 IEEE Compound Semiconductor Integrated Circuit Symposium (CSICS)*, pp. 1–4, Oct. 2013.
- [19] S. E. Saddow and A. Agarwal, *Advances in Silicon Carbide Processing and Applications*. Artech House, Jan. 2004.
- [20] Y. Fu, N. Nabiollahi, T. Wang, S. Wang, Z. Hu, B. Carlberg, Y. Zhang, X. Wang, and J. Liu, “A complete carbon-nanotube-based on-chip cooling solution with very high heat dissipation capacity,” *Nanotechnology*, vol. 23, p. 045304, Feb. 2012.
- [21] K. Shahil and A. Balandin, “Graphene-multilayer graphene nanocomposites as highly efficient thermal interface materials,” *Nano Letters*, vol. 12, no. 2, pp. 861–867, 2012.
- [22] W. Lin, J. Yuan, and B. Sundn, “Review on graphite foam as thermal material for heat exchangers,” in *World Renewable Energy Congress 2011, WREC 2011*, 2011.
- [23] Z. Yan, G. Liu, J. M. Khan, and A. A. Balandin, “Graphene quilts for thermal management of high-power GaN transistors,” *Nature Communications*, vol. 3, p. 827, May 2012.
- [24] D. H. Reneker and I. Chun, “Nanometre diameter fibres of polymer, produced by electrospinning,” *Nanotechnology*, vol. 7, no. 3, pp. 216–223, 1996.
- [25] N. Bhardwaj and S. C. Kundu, “Electrospinning: A fascinating fiber fabrication technique,” *Biotechnology Advances*, vol. 28, pp. 325–347, May 2010.
- [26] D. Li and Y. Xia, “Electrospinning of nanofibers: Reinventing the wheel?,” *Advanced Materials*, vol. 16, pp. 1151–1170, July 2004.
- [27] W. E. Teo and S. Ramakrishna, “A review on electrospinning design and nanofibre assemblies,” *Nanotechnology*, vol. 17, pp. R89–R106, July 2006.
- [28] X. Lu, C. Wang, and Y. Wei, “Onedimensional composite nanomaterials: Synthesis by electrospinning and their applications,” *Small*, vol. 5, pp. 2349–2370, Sept. 2009.
- [29] S. Agarwal, J. H. Wendorff, and A. Greiner, “Use of electrospinning technique for biomedical applications,” *Polymer*, vol. 49, pp. 5603–5621, Dec. 2008.
- [30] A. Greiner, S. Agarwal, and J. H. Wendorff, *Electrospinning : Materials, Processing, and Applications*. Hoboken, NJ, USA: Wiley-VCH, 2012.
- [31] L. Persano, A. Camposeo, C. Tekmen, and D. Pisignano, “Industrial upscaling of electrospinning and applications of polymer nanofibers: A review,” *Macromolecular Materials and Engineering*, vol. 298, pp. 504–520, May 2013.
- [32] N. E. Zander, “Hierarchically structured electrospun fibers,” *Polymers*, vol. 5, pp. 19–44, Jan. 2013.
- [33] C. J. Luo, S. D. Stoyanov, E. Stride, E. Pelan, and M. Edirisinghe, “Electrospinning versus fibre production methods: from specifics to technological convergence,” *Chemical Society reviews*, vol. 41, pp. 4708–4735, July 2012.
- [34] D. H. Reneker, A. L. Yarin, H. Fong, and S. Koombhongse, “Bending instability of electrically charged liquid jets of polymer solutions in electrospinning,” *Journal of Applied Physics*, vol. 87, pp. 4531–4547, May 2000.
- [35] S. Ramakrishna, *An Introduction to Electrospinning and Nanofibers*. World Scientific, Jan. 2005.
- [36] R. M. Nezarati, M. B. Eifert, and E. Cosgriff-Hernandez, “Effects of humidity and solution

- viscosity on electrospun fiber morphology,” *Tissue engineering. Part C, Methods*, vol. 19, pp. 810–819, Oct. 2013.
- [37] S. D. Vrieze, T. V. Camp, A. Nelvig, B. Hagstrm, P. Westbroek, and K. D. Clerck, “The effect of temperature and humidity on electrospinning,” *Journal of Materials Science*, vol. 44, pp. 1357–1362, Mar. 2009.
- [38] C. L. Casper, J. S. Stephens, N. G. Tassi, D. B. Chase, and J. F. Rabolt, “Controlling surface morphology of electrospun polystyrene fibers: effect of humidity and molecular weight in the electrospinning process,” *Macromolecules*, vol. 37, pp. 573–578, Jan. 2004.
- [39] D. Sun, C. Chang, S. Li, and L. Lin, “Near-field electrospinning,” *Nano Letters*, vol. 6, pp. 839–842, Apr. 2006.
- [40] X. Zhou, Z. Dai, S. Liu, J. Bao, and Y.-G. Guo, “Ultra-uniform SnOx/carbon nanohybrids toward advanced lithium-ion battery anodes,” *Advanced Materials*, vol. 26, pp. 3943–3949, June 2014.
- [41] S. Jiang, H. Hou, A. Greiner, and S. Agarwal, “Tough and transparent nylon-6 electrospun nanofiber reinforced melamineformaldehyde composites,” *ACS Applied Materials & Interfaces*, vol. 4, pp. 2597–2603, May 2012.
- [42] M. Shin, J. H. Song, G.-H. Lim, B. Lim, J.-J. Park, and U. Jeong, “Highly stretchable polymer transistors consisting entirely of stretchable device components,” *Advanced Materials*, vol. 26, pp. 3706–3711, June 2014.
- [43] L. Persano, C. Dagdeviren, Y. Su, Y. Zhang, S. Girardo, D. Pisignano, Y. Huang, and J. A. Rogers, “High performance piezoelectric devices based on aligned arrays of nanofibers of poly(vinylidene fluoride-co-trifluoroethylene),” *Nature Communications*, vol. 4, p. 1633, Mar. 2013.
- [44] J.-P. Chen and Y. Chiang, “Bioactive electrospun silver nanoparticles-containing polyurethane nanofibers as wound dressings,” *Journal of Nanoscience and Nanotechnology*, vol. 10, no. 11, pp. 7560–7564, 2010.
- [45] P. Jungebluth, E. Alici, S. Baiguera, K. L. Blanc, P. Blomberg, B. Bozky, C. Crowley, O. Einarsson, K.-H. Grinnemo, T. Gudbjartsson, S. L. Guyader, G. Henriksson, O. Hermanson, J. E. Juto, B. Leidner, T. Lilja, J. Liska, T. Luedde, V. Lundin, G. Moll, B. Nilsson, C. Roderburg, S. Strmblad, T. Sutlu, A. I. Teixeira, E. Watz, A. Seifalian, and P. Macchiarelli, “Tracheobronchial transplantation with a stem-cell-seeded bioartificial nanocomposite: a proof-of-concept study,” *The Lancet*, Nov. 2011.
- [46] D. Fon, K. Zhou, F. Ercole, F. Fehr, S. Marchesan, M. R. Minter, P. J. Crack, D. I. Finkelstein, and J. S. Forsythe, “Nanofibrous scaffolds releasing a small molecule BDNF-mimetic for the re-direction of endogenous neuroblast migration in the brain,” *Biomaterials*, vol. 35, pp. 2692–2712, Mar. 2014.
- [47] L. Binan, C. Tendey, G. De Crescenzo, R. El Ayoubi, A. Ajji, and M. Jolicoeur, “Differentiation of neuronal stem cells into motor neurons using electrospun poly-l-lactic acid/gelatin scaffold,” *Biomaterials*, vol. 35, pp. 664–674, Jan. 2014.
- [48] C. Wang and M. Wang, “Electrospun multifunctional tissue engineering scaffolds,” *Frontiers of Materials Science*, vol. 8, pp. 3–19, Mar. 2014.
- [49] D. I. Braghirolli, D. Steffens, and P. Pranke, “Electrospinning for regenerative medicine: a review of the main topics,” *Drug Discovery Today*, vol. 19, pp. 743–753, June 2014.
- [50] J. Matthews, G. Wnek, D. Simpson, and G. Bowlin, “Electrospinning of collagen nanofibers,” *Biomacromolecules*, vol. 3, no. 2, pp. 232–238, 2002.
- [51] A. Alessandrino, B. Marelli, C. Arosio, S. Fare, M. Tanzi, and G. Freddi, “Electrospun silk fibroin mats for tissue engineering,” *Engineering in Life Sciences*, vol. 8, no. 3, pp. 219–225, 2008.
- [52] C. Ki, J. Kim, J. Hyun, K. Lee, M. Hattori, D. Rah, and Y. Park, “Electrospun three-dimensional silk fibroin nanofibrous scaffold,” *Journal of Applied Polymer Science*, vol. 106,

no. 6, pp. 3922–3928, 2007.

- [53] Z. Ma, M. Kotaki, and S. Ramakrishna, “Electrospun cellulose nanofiber as affinity membrane,” *Journal of Membrane Science*, vol. 265, no. 1-2, pp. 115–123, 2005.
- [54] D. Grafahrend, K.-H. Heffels, M. V. Beer, P. Gasteier, M. Mller, G. Boehm, P. D. Dalton, and J. Groll, “Degradable polyester scaffolds with controlled surface chemistry combining minimal protein adsorption with specific bioactivation,” *Nature Materials*, vol. 10, pp. 67–73, Jan. 2011.
- [55] X. Zong, K. Kim, D. Fang, S. Ran, B. S. Hsiao, and B. Chu, “Structure and process relationship of electrospun bioabsorbable nanofiber membranes,” *Polymer*, vol. 43, pp. 4403–4412, July 2002.
- [56] D. Reneker, W. Kataphinan, A. Theron, E. Zussman, and A. Yarin, “Nanofiber garlands of polycaprolactone by electrospinning,” *Polymer*, vol. 43, no. 25, pp. 6785–6794, 2002.
- [57] D. C. Miller, A. Thapa, K. M. Haberstroh, and T. J. Webster, “Endothelial and vascular smooth muscle cell function on poly(lactic-co-glycolic acid) with nano-structured surface features,” *Biomaterials*, vol. 25, pp. 53–61, Jan. 2004.
- [58] X. Xin, M. Hussain, and J. J. Mao, “Continuing differentiation of human mesenchymal stem cells and induced chondrogenic and osteogenic lineages in electrospun PLGA nanofiber scaffold,” *Biomaterials*, vol. 28, pp. 316–325, Jan. 2007.
- [59] P. Taepaiboon, U. Rungsardthong, and P. Supaphol, “Drug-loaded electrospun mats of poly(vinyl alcohol) fibres and their release characteristics of four model drugs,” *Nanotechnology*, vol. 17, no. 9, pp. 2317–2329, 2006.
- [60] S. Baker, N. Atkin, P. Gunning, N. Granville, K. Wilson, D. Wilson, and J. Southgate, “Characterisation of electrospun polystyrene scaffolds for three-dimensional in vitro biological studies,” *Biomaterials*, vol. 27, no. 16, pp. 3136–3146, 2006.
- [61] Z. Ma, M. Kotaki, T. Yong, W. He, and S. Ramakrishna, “Surface engineering of electrospun polyethylene terephthalate (PET) nanofibers towards development of a new material for blood vessel engineering,” *Biomaterials*, vol. 26, pp. 2527–2536, May 2005.
- [62] C. A. Bashur, R. D. Shaffer, L. A. Dahlgren, S. A. Guelcher, and A. S. Goldstein, “Effect of fiber diameter and alignment of electrospun polyurethane meshes on mesenchymal progenitor cells,” *Tissue Engineering Part A*, vol. 15, pp. 2435–2445, Sept. 2009.
- [63] H. Bergmeister, C. Grasl, I. Walter, R. Plasenzotti, M. Stoiber, C. Schreiber, U. Losert, G. Weigel, and H. Schima, “Electrospun small-diameter polyurethane vascular grafts: In-growth and differentiation of vascular-specific host cells,” *Artificial Organs*, vol. 36, no. 1, pp. 54–61, 2012.
- [64] D. N. Rockwood, R. E. Akins Jr., I. C. Parrag, K. A. Woodhouse, and J. F. Rabolt, “Culture on electrospun polyurethane scaffolds decreases atrial natriuretic peptide expression by cardiomyocytes in vitro,” *Biomaterials*, vol. 29, pp. 4783–4791, Dec. 2008.
- [65] M. P. Lutolf and J. A. Hubbell, “Synthetic biomaterials as instructive extracellular microenvironments for morphogenesis in tissue engineering,” *Nature Biotechnology*, vol. 23, pp. 47–55, Jan. 2005.
- [66] L. Tian, M. Prabhakaran, X. Ding, D. Kai, and S. Ramakrishna, “Emulsion electrospun vascular endothelial growth factor encapsulated poly(l-lactic acid-co-caprolactone) nanofibers for sustained release in cardiac tissue engineering,” *Journal of Materials Science*, vol. 47, no. 7, pp. 3272–3281, 2012.
- [67] H. Yoshimoto, Y. Shin, H. Terai, and J. Vacanti, “A biodegradable nanofiber scaffold by electrospinning and its potential for bone tissue engineering,” *Biomaterials*, vol. 24, no. 12, pp. 2077–2082, 2003.
- [68] T. Sun, S. Mai, D. Norton, J. Haycock, A. Ryan, and S. MacNeil, “Self-organization of skin cells in three-dimensional electrospun polystyrene scaffolds,” *Tissue Engineering*, vol. 11,

- no. 7-8, pp. 1023–1033, 2005.
- [69] J. Stankus, J. Guan, and W. Wagner, “Fabrication of biodegradable elastomeric scaffolds with sub-micron morphologies,” *Journal of Biomedical Materials Research - Part A*, vol. 70, no. 4, pp. 603–614, 2004.
- [70] Q. P. Pham, U. Sharma, and A. G. Mikos, “Electrospinning of polymeric nanofibers for tissue engineering applications: A review,” *Tissue Engineering*, vol. 12, pp. 1197–1211, May 2006.
- [71] X. Yang, J. D. Shah, and H. Wang, “Nanofiber enabled layer-by-layer approach toward three-dimensional tissue formation,” *Tissue Engineering. Part A*, vol. 15, pp. 945–956, Apr. 2009.
- [72] B. M. Baker, R. P. Shah, A. M. Silverstein, J. L. Esterhai, J. A. Burdick, and R. L. Mauck, “Sacrificial nanofibrous composites provide instruction without impediment and enable functional tissue formation,” *Proceedings of the National Academy of Sciences of the United States of America*, vol. 109, pp. 14176–14181, Aug. 2012.
- [73] P. Roach, T. Parker, N. Gadegaard, and M. Alexander, “Surface strategies for control of neuronal cell adhesion: A review,” *Surface Science Reports*, vol. 65, pp. 145–173, June 2010.
- [74] M. M. Stevens and J. H. George, “Exploring and engineering the cell surface interface,” *Science*, vol. 310, pp. 1135–1138, Nov. 2005.
- [75] P. Clark, P. Connolly, A. Curtis, J. Dow, and C. Wilkinson, “Cell guidance by ultrafine topography in vitro,” *Journal of Cell Science*, vol. 99, no. 1, pp. 73–77, 1991.
- [76] D. E. Discher, P. Janmey, and Y.-l. Wang, “Tissue cells feel and respond to the stiffness of their substrate,” *Science*, vol. 310, pp. 1139–1143, Nov. 2005.
- [77] D. Discher, D. Mooney, and P. Zandstra, “Growth factors, matrices, and forces combine and control stem cells,” *Science*, vol. 324, no. 5935, pp. 1673–1677, 2009.
- [78] A. J. Engler, S. Sen, H. L. Sweeney, and D. E. Discher, “Matrix elasticity directs stem cell lineage specification,” *Cell*, vol. 126, pp. 677–689, Aug. 2006.
- [79] B. Alberts, D. Bray, K. Hopkin, A. Johnson, J. Lewis, M. Raff, K. Roberts, and P. Walter, *Essential Cell Biology*. Garland Science, 2004.
- [80] T. Ebendal, “The relative roles of contact inhibition and contact guidance in orientation of axons extending on aligned collagen fibrils in vitro,” *Experimental Cell Research*, vol. 98, pp. 159–169, Mar. 1976.
- [81] S. Sell, C. Barnes, M. Smith, M. McClure, P. Madurantakam, J. Grant, M. McManus, and G. Bowlin, “Extracellular matrix regenerated: tissue engineering via electrospun biomimetic nanofibers,” *Polymer International*, vol. 56, pp. 1349–1360, Sept. 2007.
- [82] P. Roach, D. Eglin, K. Rohde, and C. Perry, “Modern biomaterials: A review - bulk properties and implications of surface modifications,” *Journal of Materials Science: Materials in Medicine*, vol. 18, no. 7, pp. 1263–1277, 2007.
- [83] C. Mummery, A. v. d. Stolpe, B. Roelen, and H. Clevers, *Stem Cells: Scientific Facts and Fiction*. Academic Press, May 2014.
- [84] R. D. Fields, *The Other Brain: From Dementia to Schizophrenia, How New Discoveries about the Brain Are Revolutionizing Medicine and Science*. Simon and Schuster, Dec. 2009.
- [85] M. Nedergaard, B. Ransom, and S. A. Goldman, “New roles for astrocytes: redefining the functional architecture of the brain,” *Trends in neurosciences*, vol. 26, pp. 523–530, Oct. 2003.
- [86] T. A. Fiocco, C. Agulhon, and K. D. McCarthy, “Sorting out astrocyte physiology from pharmacology,” *Annual Review of Pharmacology and Toxicology*, vol. 49, no. 1, pp. 151–174, 2009.

- [87] M. T. Heneka, “The other brain,” *The Journal of Clinical Investigation*, vol. 120, p. 1789, June 2010.
- [88] N. A. Oberheim, T. Takano, X. Han, W. He, J. H. C. Lin, F. Wang, Q. Xu, J. D. Wyatt, W. Pilcher, J. G. Ojemann, B. R. Ransom, S. A. Goldman, and M. Nedergaard, “Uniquely hominid features of adult human astrocytes,” *The Journal of neuroscience: the official journal of the Society for Neuroscience*, vol. 29, pp. 3276–3287, Mar. 2009.
- [89] W. C. Low, P.-O. Rujitanaroj, D.-K. Lee, P. B. Messersmith, L. W. Stanton, E. Goh, and S. Y. Chew, “Nanofibrous scaffold-mediated REST knockdown to enhance neuronal differentiation of stem cells,” *Biomaterials*, vol. 34, pp. 3581–3590, May 2013.
- [90] J. Wang, R. Ye, Y. Wei, H. Wang, X. Xu, F. Zhang, J. Qu, B. Zuo, and H. Zhang, “The effects of electrospun TSF nanofiber diameter and alignment on neuronal differentiation of human embryonic stem cells,” *Journal of Biomedical Materials Research Part A*, vol. 100A, pp. 632–645, Mar. 2012.
- [91] R. J. Zdrahala and I. J. Zdrahala, “Biomedical applications of polyurethanes: A review of past promises, present realities, and a vibrant future,” *Journal of Biomaterials Applications*, vol. 14, pp. 67–90, July 1999.
- [92] K. Stokes, A. Coury, and P. Urbanski, “Autooxidative degradation of implanted polyether polyurethane devices,” *Journal of Biomaterials Applications*, vol. 1, pp. 411–448, Jan. 1986.
- [93] A. Tiwari, H. Salacinski, A. M. Seifalian, and G. Hamilton, “New prostheses for use in bypass grafts with special emphasis on polyurethanes,” *Cardiovascular Surgery*, vol. 10, pp. 191–197, June 2002.
- [94] J. Santerre, K. Woodhouse, G. Laroche, and R. Labow, “Understanding the biodegradation of polyurethanes: From classical implants to tissue engineering materials,” *Biomaterials*, vol. 26, pp. 7457–7470, Dec. 2005.
- [95] D. N. Rockwood, K. A. Woodhouse, J. D. Fromstein, D. B. Chase, and J. F. Rabolt, “Characterization of biodegradable polyurethane microfibers for tissue engineering,” *Journal of Biomaterials Science. Polymer Edition*, vol. 18, no. 6, pp. 743–758, 2007.
- [96] J. Meng, Z. Han, H. Kong, X. Qi, C. Wang, S. Xie, and H. Xu, “Electrospun aligned nanofibrous composite of MWCNT/polyurethane to enhance vascular endothelium cells proliferation and function,” *Journal of Biomedical Materials Research Part A*, vol. 95, no. 1, pp. 312–320, 2010.
- [97] R. Chen, L. Qiu, Q. Ke, C. He, and X. Mo, “Electrospinning thermoplastic polyurethane-contained collagen nanofibers for tissue-engineering applications,” *Journal of Biomaterials Science, Polymer Edition*, vol. 20, no. 11, pp. 1513–1536, 2009.
- [98] B. Carlberg, M. Z. Axell, U. Nannmark, J. Liu, and H. G. Kuhn, “Electrospun polyurethane scaffolds for proliferation and neuronal differentiation of human embryonic stem cells,” *Biomedical Materials*, vol. 4, p. 045004, Aug. 2009.
- [99] M. J. Dalby, N. Gadegaard, R. Tare, A. Andar, M. O. Riehle, P. Herzyk, C. D. W. Wilkinson, and R. O. C. Oreffo, “The control of human mesenchymal cell differentiation using nanoscale symmetry and disorder,” *Nature Materials*, vol. 6, pp. 997–1003, Dec. 2007.
- [100] S. Levenberg, “Differentiation of human embryonic stem cells on three-dimensional polymer scaffolds,” *Proceedings of the National Academy of Sciences*, vol. 100, pp. 12741–12746, Oct. 2003.
- [101] A. S. Badami, M. R. Kreke, M. S. Thompson, J. S. Riffle, and A. S. Goldstein, “Effect of fiber diameter on spreading, proliferation, and differentiation of osteoblastic cells on electrospun poly(lactic acid) substrates,” *Biomaterials*, vol. 27, pp. 596–606, Feb. 2006.
- [102] P. Alves, J. Coelho, J. Haack, A. Rota, A. Bruinink, and M. Gil, “Surface modification and characterization of thermoplastic polyurethane,” *European Polymer Journal*, vol. 45, pp. 1412–1419, May 2009.

- [103] S. Laishun, "Characterization of the flame retardancy of EVA copolymer by plasma grafting of acrylic acid," *European Polymer Journal*, vol. 36, pp. 2611–2615, Dec. 2000.
- [104] J. Tyczkowski, I. Krawczyk-Kys, S. Kuberski, and P. Makowski, "Chemical nature of adhesion: Plasma modified styrenebutadiene elastomer and polyurethane adhesive joints," *European Polymer Journal*, vol. 46, pp. 767–773, Apr. 2010.
- [105] N. Gomathi, A. Sureshkumar, and S. Neogi, "RF plasma-treated polymers for biomedical applications," *Current Science*, vol. 94, no. 11, pp. 1478–1486, 2008.
- [106] P. Chu, J. Chen, L. Wang, and N. Huang, "Plasma-surface modification of biomaterials," *Materials Science and Engineering: R: Reports*, vol. 36, pp. 143–206, Mar. 2002.
- [107] Y. Tamada and Y. Ikada, "Cell adhesion to plasma-treated polymer surfaces," *Polymer*, vol. 34, no. 10, pp. 2208–2212, 1993.
- [108] C. Amstein and P. Hartman, "Adaptation of plastic surfaces for tissue culture by glow discharge," *Journal of Clinical Microbiology*, vol. 2, no. 1, pp. 46–54, 1975.
- [109] P. Favia, L. Lopez, E. Sardella, R. Gristina, M. Nardulli, and R. d'Agostino, "Low temperature plasma processes for biomedical applications and membrane processing," *Desalination*, vol. 199, pp. 268–270, Nov. 2006.
- [110] M. R. Sanchis, O. Calvo, O. Fenollar, D. Garcia, and R. Balart, "Surface modification of a polyurethane film by low pressure glow discharge oxygen plasma treatment," *Journal of Applied Polymer Science*, vol. 105, pp. 1077–1085, Aug. 2007.
- [111] D. J. Wilson, N. P. Rhodes, and R. L. Williams, "Surface modification of a segmented polyetherurethane using a low-powered gas plasma and its influence on the activation of the coagulation system," *Biomaterials*, vol. 24, pp. 5069–5081, Dec. 2003.
- [112] N. P. Rhodes, D. J. Wilson, and R. L. Williams, "The effect of gas plasma modification on platelet and contact phase activation processes," *Biomaterials*, vol. 28, pp. 4561–4570, Nov. 2007.
- [113] H. Schlicht, H. J. Haugen, R. Sabetrasekh, and E. Wintermantel, "Fibroblastic response and surface characterization of o(2)-plasma-treated thermoplastic polyetherurethane.," *Biomedical materials*, vol. 5, no. 2, p. 25002, 2010.
- [114] Y.-H. Li and Y.-D. Huang, "The study of collagen immobilization on polyurethane by oxygen plasma treatment to enhance cell adhesion and growth," *Surface and Coatings Technology*, vol. 201, pp. 5124–5127, Feb. 2007.
- [115] Y. Zhang, S. Myung, H. Choi, I. Kim, and J. Choi, "Optimum conditions for the surface modification of polyurethane by oxygen plasma treatment," *JOURNAL OF INDUSTRIAL AND ENGINEERING CHEMISTRY*, vol. 8, pp. 236–240, May 2002.
- [116] H.-S. Choi, Y.-S. Kim, Y. Zhang, S. Tang, S.-W. Myung, and B.-C. Shin, "Plasma-induced graft co-polymerization of acrylic acid onto the polyurethane surface," *Surface and Coatings Technology*, vol. 182, pp. 55–64, Apr. 2004.
- [117] K. D. Andrews, J. A. Hunt, and R. A. Black, "Effects of sterilisation method on surface topography and in-vitro cell behaviour of electrostatically spun scaffolds," *Biomaterials*, vol. 28, pp. 1014–1026, Feb. 2007.
- [118] K. Wong, M. Zinke-Allmang, W. Wan, J. Zhang, and P. Hu, "Low energy oxygen ion beam modification of the surface morphology and chemical structure of polyurethane fibers," *Nuclear Instruments and Methods in Physics Research Section B: Beam Interactions with Materials and Atoms*, vol. 243, pp. 63–74, Jan. 2006.
- [119] A. Chen, K. Kaviani, A. W. Rempel, S. Kalluri, W. H. Steier, Y. Shi, Z. Liang, and L. R. Dalton, "Optimized oxygen plasma etching of polyurethane-based electro-optic polymer for low loss optical waveguide fabrication," *Journal of The Electrochemical Society*, vol. 143, pp. 3648–3651, Nov. 1996.
- [120] W. S. Choi, J. W. Bae, H. R. Lim, Y. K. Joung, J.-C. Park, I. K. Kwon, and K. D. Park,

- “RGD peptide-immobilized electrospun matrix of polyurethane for enhanced endothelial cell affinity,” *Biomedical Materials*, vol. 3, p. 044104, Dec. 2008.
- [121] H. Kwang, H. Gu, J. Su, J.-Y. Baek, K. Dong, Y. Park, and S. Lee, “Hydrophilic electrospun polyurethane nanofiber matrices for hMSC culture in a microfluidic cell chip,” *Journal of Biomedical Materials Research - Part A*, vol. 90, no. 2, pp. 619–628, 2009.
- [122] S. H. Hsu and W.-C. Chen, “Improved cell adhesion by plasma-induced grafting of -lactide onto polyurethane surface,” *Biomaterials*, vol. 21, pp. 359–367, Feb. 2000.
- [123] Y. Ozdemir, N. Hasirci, and K. Serbetci, “Oxygen plasma modification of polyurethane membranes,” *Journal of Materials Science: Materials in Medicine*, vol. 13, no. 12, pp. 1147–1151, 2002.
- [124] J. Yuan, J. Zhu, C. H. Zhu, J. Shen, and S. C. Lin, “Platelet adhesion on a polyurethane surface grafted with a zwitterionic monomer of sulfobetaine via a jeffamine spacer,” *Polymer International*, vol. 53, pp. 1722–1728, Nov. 2004.
- [125] J. Zheng, A. He, J. Li, J. Xu, and C. C. Han, “Studies on the controlled morphology and wettability of polystyrene surfaces by electrospinning or electrospraying,” *Polymer*, vol. 47, pp. 7095–7102, Sept. 2006.
- [126] A. B. D. Cassie and S. Baxter, “Wettability of porous surfaces,” *Transactions of the Faraday Society*, vol. 40, p. 546, 1944.
- [127] B. Carlberg, T. Wang, and J. Liu, “Direct photolithographic patterning of electrospun films for defined nanofibrillar microarchitectures,” *Langmuir*, vol. 26, pp. 2235–2239, Feb. 2010.
- [128] J. H. Lee, H. W. Jung, I.-K. Kang, and H. B. Lee, “Cell behaviour on polymer surfaces with different functional groups,” *Biomaterials*, vol. 15, no. 9, pp. 705–711, 1994.
- [129] M. Lampin, R. Warocquier-Clout, C. Legris, M. Degrange, and M. F. Sigot-Luizard, “Correlation between substratum roughness and wettability, cell adhesion, and cell migration,” *Journal of Biomedical Materials Research*, vol. 36, no. 1, pp. 99–108, 1997.
- [130] R. Tzoneva, N. Fauchoux, and T. Groth, “Wettability of substrata controls cell-substrate and cell-cell adhesions,” *Biochimica et Biophysica Acta (BBA) - General Subjects*, vol. 1770, pp. 1538–1547, Nov. 2007.
- [131] R. D. Cardwell, L. A. Dahlgren, and A. S. Goldstein, “Electrospun fibre diameter, not alignment, affects mesenchymal stem cell differentiation into the tendon/ligament lineage,” *Journal of tissue engineering and regenerative medicine*, Oct. 2012.
- [132] J. Y. Martin, Z. Schwartz, T. W. Hummert, D. M. Schraub, J. Simpson, J. Lankford, D. D. Dean, D. L. Cochran, and B. D. Boyan, “Effect of titanium surface roughness on proliferation, differentiation, and protein synthesis of human osteoblast-like cells (MG63),” *Journal of Biomedical Materials Research*, vol. 29, no. 3, pp. 389–401, 1995.
- [133] Y. Arima and H. Iwata, “Effect of wettability and surface functional groups on protein adsorption and cell adhesion using well-defined mixed self-assembled monolayers,” *Biomaterials*, vol. 28, pp. 3074–3082, July 2007.
- [134] S. H. Keshel, S. N. K. Azhdadi, A. Asefnezhad, M. Sadraeian, M. Montazeri, and E. Biazar, “The relationship between cellular adhesion and surface roughness for polyurethane modified by microwave plasma radiation,” *International Journal of Nanomedicine*, vol. 6, pp. 641–647, 2011.
- [135] J. Curran, R. Chen, and J. Hunt, “Controlling the phenotype and function of mesenchymal stem cells in vitro by adhesion to silane-modified clean glass surfaces,” *Biomaterials*, vol. 26, pp. 7057–7067, Dec. 2005.
- [136] B. Lei, X. Chen, Y. Wang, N. Zhao, C. Du, and L. Fang, “Surface nanoscale patterning of bioactive glass to support cellular growth and differentiation,” *Journal of biomedical materials research. Part A*, vol. 94, pp. 1091–1099, Sept. 2010.

- [137] M. V. Jose, V. Thomas, Y. Xu, S. Bellis, E. Nyairo, and D. Dean, “Aligned bioactive multi-component nanofibrous nanocomposite scaffolds for bone tissue engineering,” *Macromolecular bioscience*, vol. 10, pp. 433–444, Apr. 2010.
- [138] C. Bao, W. Chen, M. D. Weir, W. Thein-Han, and H. H. K. Xu, “Effects of electrospun sub-micron fibers in calcium phosphate cement scaffold on mechanical properties and osteogenic differentiation of umbilical cord stem cells,” *Acta biomaterialia*, vol. 7, pp. 4037–4044, Nov. 2011.
- [139] F. Zamani, M. Amani-Tehran, M. Latifi, and M. A. Shokrgozar, “The influence of surface nanoroughness of electrospun PLGA nanofibrous scaffold on nerve cell adhesion and proliferation,” *Journal of Materials Science: Materials in Medicine*, Mar. 2013.
- [140] T.-W. Chung, D.-Z. Liu, S.-Y. Wang, and S.-S. Wang, “Enhancement of the growth of human endothelial cells by surface roughness at nanometer scale,” *Biomaterials*, vol. 24, pp. 4655–4661, Nov. 2003.
- [141] M. Massumi, M. Abasi, H. Babaloo, P. Terraf, M. Safi, M. Saeed, J. Barzin, M. Zandi, and M. Soleimani, “The effect of topography on differentiation fates of matrigel-coated mouse embryonic stem cells cultured on PLGA nanofibrous scaffolds,” *Tissue engineering. Part A*, vol. 18, pp. 609–620, Mar. 2012.
- [142] J. Xie, S. M. Willerth, X. Li, M. R. Macewan, A. Rader, S. E. Sakiyama-Elbert, and Y. Xia, “The differentiation of embryonic stem cells seeded on electrospun nanofibers into neural lineages,” *Biomaterials*, vol. 30, pp. 354–362, Jan. 2009.
- [143] L. Ghasemi-Mobarakeh, M. P. Prabhakaran, M. Morshed, M.-H. Nasr-Esfahani, and S. Ramakrishna, “Electrospun poly(epsilon-caprolactone)/gelatin nanofibrous scaffolds for nerve tissue engineering,” *Biomaterials*, vol. 29, pp. 4532–4539, Dec. 2008.
- [144] G. T. Christopherson, H. Song, and H.-Q. Mao, “The influence of fiber diameter of electrospun substrates on neural stem cell differentiation and proliferation,” *Biomaterials*, vol. 30, pp. 556–564, Feb. 2009.
- [145] Y.-J. Ren, S. Zhang, R. Mi, Q. Liu, X. Zeng, M. Rao, A. Hoke, and H.-Q. Mao, “Enhanced differentiation of human neural crest stem cells towards the schwann cell lineage by aligned electrospun fiber matrix,” *Acta Biomaterialia*, 2013.
- [146] K. Baranes, N. Chejanovsky, N. Alon, A. Sharoni, and O. Shefi, “Topographic cues of nanoscale height direct neuronal growth pattern,” *Biotechnology and Bioengineering*, vol. 109, no. 7, pp. 1791–1797, 2012.
- [147] H. B. Wang, M. E. Mullins, J. M. Cregg, A. Hurtado, M. Oudega, M. T. Trombley, and R. J. Gilbert, “Creation of highly aligned electrospun poly-l-lactic acid fibers for nerve regeneration applications,” *Journal of neural engineering*, vol. 6, p. 016001, Feb. 2009.
- [148] E. Cukierman, R. Pankov, D. Stevens, and K. Yamada, “Taking cell-matrix adhesions to the third dimension,” *Science*, vol. 294, no. 5547, pp. 1708–1712, 2001.
- [149] W. Mueller-Klieser, “Three-dimensional cell cultures: From molecular mechanisms to clinical applications,” *American Journal of Physiology - Cell Physiology*, vol. 273, no. 4 42-4, pp. C1109–C1123, 1997.
- [150] D. Walpita and E. Hay, “Studying actin-dependent processes in tissue culture,” *Nature Reviews Molecular Cell Biology*, vol. 3, no. 2, pp. 137–141, 2002.
- [151] G. Kim and W. Kim, “Highly porous 3d nanofiber scaffold using an electrospinning technique,” *Journal of Biomedical Materials Research. Part B, Applied Biomaterials*, vol. 81, pp. 104–110, Apr. 2007.
- [152] J. Lee, M. J. Cuddihy, and N. A. Kotov, “Three-dimensional cell culture matrices: State of the art,” *Tissue Engineering Part B: Reviews*, vol. 14, pp. 61–86, Mar. 2008.
- [153] A. W. Lund, B. Yener, J. P. Stegemann, and G. E. Plopper, “The natural and engineered 3d microenvironment as a regulatory cue during stem cell fate determination,” *Tissue*

Engineering Part B: Reviews, vol. 15, pp. 371–380, Sept. 2009.

- [154] J. T. Borenstein, E. J. Weinberg, B. K. Orrick, C. Sundback, M. R. Kaazempur-Mofrad, and J. P. Vacanti, “Microfabrication of three-dimensional engineered scaffolds,” *Tissue Engineering*, vol. 13, pp. 1837–1844, Aug. 2007.
- [155] E. Carletti, A. Motta, and C. Migliaresi, “3d cell culture,” *Methods*, vol. 695, no. 2, pp. 41–51, 2011.
- [156] T. Elkayam, S. Amitay-Shaprut, M. Dvir-Ginzberg, T. Harel, and S. Cohen, “Enhancing the drug metabolism activities of c3a a human hepatocyte cell line by tissue engineering within alginate scaffolds,” *Tissue Engineering*, vol. 12, pp. 1357–1368, May 2006.
- [157] E. East, J. Golding, and J. Phillips, “A versatile 3d culture model facilitates monitoring of astrocytes undergoing reactive gliosis,” *Journal of Tissue Engineering and Regenerative Medicine*, vol. 3, no. 8, pp. 634–646, 2009.
- [158] C. Hwang, S. Sant, M. Masaeli, N. Kachouie, B. Zamanian, S.-H. Lee, and A. Khademhosseini, “Fabrication of three-dimensional porous cell-laden hydrogel for tissue engineering,” *Biofabrication*, vol. 2, no. 3, 2010.
- [159] K. S. Rho, L. Jeong, G. Lee, B.-M. Seo, Y. J. Park, S.-D. Hong, S. Roh, J. J. Cho, W. H. Park, and B.-M. Min, “Electrospinning of collagen nanofibers: Effects on the behavior of normal human keratinocytes and early-stage wound healing,” *Biomaterials*, vol. 27, pp. 1452–1461, Mar. 2006.
- [160] H. Koh, T. Yong, C. Chan, and S. Ramakrishna, “Enhancement of neurite outgrowth using nano-structured scaffolds coupled with laminin,” *Biomaterials*, vol. 29, no. 26, pp. 3574–3582, 2008.
- [161] J. Gerardo-Nava, T. Fhrmann, K. Klinkhammer, N. Seiler, J. Mey, D. Klee, M. Mller, P. Dalton, and G. Brook, “Human neural cell interactions with orientated electrospun nanofibers in vitro,” *Nanomedicine*, vol. 4, no. 1, pp. 11–30, 2009.
- [162] N. Schaub and R. Gilbert, “Controlled release of 6-aminonicotinamide from aligned, electrospun fibers alters astrocyte metabolism and dorsal root ganglia neurite outgrowth,” *Journal of Neural Engineering*, vol. 8, no. 4, 2011.
- [163] R. Delgado-Rivera, S. L. Harris, I. Ahmed, A. N. Babu, R. P. Patel, V. Ayres, D. Flowers, and S. Meiners, “Increased FGF-2 secretion and ability to support neurite outgrowth by astrocytes cultured on polyamide nanofibrillar matrices,” *Matrix biology: journal of the International Society for Matrix Biology*, vol. 28, pp. 137–147, Apr. 2009.
- [164] W. N. Chow, D. G. Simpson, J. W. Bigbee, and R. J. Colello, “Evaluating neuronal and glial growth on electrospun polarized matrices: bridging the gap in percussive spinal cord injuries,” *Neuron glia biology*, vol. 3, pp. 119–126, May 2007.
- [165] H. Cao, G. Marcy, E. L. K. Goh, F. Wang, J. Wang, and S. Y. Chew, “The effects of nanofiber topography on astrocyte behavior and gene silencing efficiency,” *Macromolecular Bioscience*, vol. 12, pp. 666–674, Mar. 2012.
- [166] S. Kim, C. Shin, S. Min, S.-M. Jung, and H. Shin, “In vitro evaluation of the effects of electrospun PCL nanofiber mats containing the microalgae spirulina (arthrospira) extract on primary astrocytes,” *Colloids and Surfaces B: Biointerfaces*, vol. 90, no. 1, pp. 113–118, 2012.
- [167] J. Qu, D. Wang, H. Wang, Y. Dong, F. Zhang, B. Zuo, and H. Zhang, “Electrospun silk fibroin nanofibers in different diameters support neurite outgrowth and promote astrocyte migration,” *Journal of Biomedical Materials Research. Part A*, vol. 101, pp. 2667–2678, Sept. 2013.
- [168] R. M. Smeal and P. A. Tresco, “The influence of substrate curvature on neurite outgrowth is cell type dependent,” *Experimental Neurology*, vol. 213, pp. 281–292, Oct. 2008.
- [169] S. Krause, M. V. Maffini, A. M. Soto, and C. Sonnenschein, “The microenvironment

- determines the breast cancer cells' phenotype: organization of MCF7 cells in 3d cultures," *BMC cancer*, vol. 10, p. 263, 2010.
- [170] D. Wlodkowic and J. Cooper, "Tumors on chips: Oncology meets microfluidics," *Current Opinion in Chemical Biology*, vol. 14, no. 5, pp. 556–567, 2010.
- [171] N. Raof, W. Raja, J. Castracane, and Y. Xie, "Bioengineering embryonic stem cell microenvironments for exploring inhibitory effects on metastatic breast cancer cells," *Biomaterials*, vol. 32, no. 17, pp. 4130–4139, 2011.
- [172] N. Elliott and F. Yuan, "A review of three-dimensional in vitro tissue models for drug discovery and transport studies," *Journal of Pharmaceutical Sciences*, vol. 100, no. 1, pp. 59–74, 2011.
- [173] A. Sica, C. Porta, E. Riboldi, and M. Locati, "Convergent pathways of macrophage polarization: The role of b cells," *European journal of immunology*, vol. 40, pp. 2131–2133, Aug. 2010.
- [174] C. Goodman, *Mechanisms and molecules that control growth cone guidance*, vol. 19. 1996.
- [175] J. Gurdon and P.-Y. Bourillot, "Morphogen gradient interpretation," *Nature*, vol. 413, no. 6858, pp. 797–803, 2001.
- [176] T. Bogenrieder and M. Herlyn, "Axis of evil: Molecular mechanisms of cancer metastasis," *Oncogene*, vol. 22, no. 43, pp. 6524–6536, 2003.
- [177] S. Kim, H. J. Kim, and N. L. Jeon, "Biological applications of microfluidic gradient devices," *Integrative Biology*, vol. 2, no. 11-12, p. 584, 2010.
- [178] E. Dahan, V. Bize, T. Lehnert, J.-D. Horisberger, and M. Gijs, "Rapid fluidic exchange microsystem for recording of fast ion channel kinetics in xenopus oocytes," *Lab on a Chip - Miniaturisation for Chemistry and Biology*, vol. 8, no. 11, pp. 1809–1818, 2008.
- [179] C.-Y. Chen, A. Wo, and D.-S. Jong, "A microfluidic concentration generator for dose-response assays on ion channel pharmacology," *Lab on a Chip - Miniaturisation for Chemistry and Biology*, vol. 12, no. 4, pp. 794–801, 2012.
- [180] L. Matlock-Colangelo, D. Cho, C. L. Pitner, M. W. Frey, and A. J. Baeumner, "Functionalized electrospun nanofibers as bioseparators in microfluidic systems," *Lab on a Chip*, vol. 12, no. 9, p. 1696, 2012.
- [181] D. Yang, X. Niu, Y. Liu, Y. Wang, X. Gu, L. Song, R. Zhao, L. Ma, Y. Shao, and X. Jiang, "Electrospun nanofibrous membranes: A novel solid substrate for microfluidic immunoassays for HIV," *Advanced Materials*, vol. 20, no. 24, pp. 4770–4775, 2008.
- [182] S. Pagliara, A. Camposeo, A. Polini, R. Cingolani, and D. Pisignano, "Electrospun light-emitting nanofibers as excitation source in microfluidic devices," *Lab on a Chip - Miniaturisation for Chemistry and Biology*, vol. 9, no. 19, pp. 2851–2856, 2009.
- [183] Y. Liu, D. Yang, T. Yu, and X. Jiang, "Incorporation of electrospun nanofibrous PVDF membranes into a microfluidic chip assembled by PDMS and scotch tape for immunoassays," *Electrophoresis*, vol. 30, no. 18, pp. 3269–3275, 2009.
- [184] D. Cho, L. Matlock-Colangelo, C. Xiang, P. Asiello, A. Baeumner, and M. Frey, "Electrospun nanofibers for microfluidic analytical systems," *Polymer*, vol. 52, no. 15, pp. 3413–3421, 2011.
- [185] N. Jeon, S. Dertinger, D. Chiu, I. Choi, A. Stroock, and G. Whitesides, "Generation of solution and surface gradients using microfluidic systems," *Langmuir*, vol. 16, no. 22, pp. 8311–8316, 2000.
- [186] J. Imitola, K. Raddassi, K. I. Park, F.-J. Mueller, M. Nieto, Y. D. Teng, D. Frenkel, J. Li, R. L. Sidman, C. A. Walsh, E. Y. Snyder, and S. J. Khoury, "Directed migration of neural stem cells to sites of CNS injury by the stromal cell-derived factor 1/CXC chemokine receptor 4 pathway," *Proceedings of the National Academy of Sciences*, vol. 101, pp. 18117–18122, Dec. 2004.

- [187] A. A. Balandin, “Thermal properties of graphene and nanostructured carbon materials,” *Nature Materials*, vol. 10, pp. 569–581, Aug. 2011.
- [188] G. Jiang, L. Diao, and K. Kuang, *Advanced Thermal Management Materials*. Springer Science & Business Media, Sept. 2012.
- [189] J. S. Subramanian, P. Rodgers, J. Newson, T. Rude, Z. He, E. Besnoin, T. P. Weihs, V. Evely, and M. Pecht, “Room temperature soldering of microelectronic components for enhanced thermal performance,” in *Thermal, Mechanical and Multi-Physics Simulation and Experiments in Micro-Electronics and Micro-Systems, 2005. EuroSimE 2005. Proceedings of the 6th International Conference on*, pp. 681–686, IEEE, 2005.
- [190] J. Liu, T. Wang, B. Carlberg, and M. Inoue, “Recent progress of thermal interface materials,” in *Electronics System-Integration Technology Conference, 2008. ESTC 2008. 2nd*, pp. 351–358, Sept. 2008.
- [191] F. Sarvar, D. Whalley, and P. Conway, “Thermal interface materials - a review of the state of the art,” in *Electronics Systemintegration Technology Conference, 2006. 1st*, vol. 2, pp. 1292–1302, Sept. 2006.
- [192] R. Prasher, “Thermal interface materials: Historical perspective, status, and future directions,” *Proceedings of the IEEE*, vol. 94, pp. 1571–1586, Aug. 2006.
- [193] Y. Yao, J. N. Tey, Z. Li, J. Wei, K. Bennett, A. McNamara, Y. Joshi, R. Tan, S. Ling, and C.-P. Wong, “High-quality vertically aligned carbon nanotubes for applications as thermal interface materials,” *IEEE Transactions on Components, Packaging and Manufacturing Technology*, vol. 4, pp. 232–239, Feb. 2014.
- [194] S. Narumanchi, M. Mihalic, K. Kelly, and G. Eesley, “Thermal interface materials for power electronics applications,” in *Thermal and Thermomechanical Phenomena in Electronic Systems, 2008. ITherm 2008. 11th Intersociety Conference on*, pp. 395–404, May 2008.
- [195] R. Prasher, “Rheology based modeling and design of particle laden polymeric thermal interface materials,” *IEEE Transactions on Components and Packaging Technologies*, vol. 28, no. 2, pp. 230–237, 2005.
- [196] G.-W. Lee, M. Park, J. Kim, J. I. Lee, and H. G. Yoon, “Enhanced thermal conductivity of polymer composites filled with hybrid filler,” *Composites Part A: Applied Science and Manufacturing*, vol. 37, pp. 727–734, May 2006.
- [197] N. Nabiollahi, J. Liu, Z. Hilli, Y. Zhang, Y. Cong, Z. Cheng, and M. Inoue, “FEM simulation of bimodal and trimodal thermally conductive adhesives,” in *Nanotechnology, 2009. IEEE-NANO 2009. 9th IEEE Conference on*, pp. 422–425, July 2009.
- [198] N. Islam, S. Lee, M. Jimarez, J. Lee, and J. Galloway, “TIM degradation in flip chip packages,” in *2008 11th IEEE Intersociety Conference on Thermal and Thermomechanical Phenomena in Electronic Systems, I-Therm*, pp. 259–265, 2008.
- [199] F. Hua, C. Deppisch, and T. Fitzgerald, “Indium as thermal interface material for high power devices,” *Advancing Microelectronics*, vol. 33, no. 4, pp. 16–17, 2006.
- [200] R. Tummala, *Fundamentals of Microsystems Packaging*. McGraw-Hill Professional, 1 ed., May 2001.
- [201] C. Deppisch, T. Fitzgerald, A. Raman, F. Hua, C. Zhang, P. Liu, and M. Miller, “The material optimization and reliability characterization of an indium-solder thermal interface material for CPU packaging,” *JOM Journal of the Minerals, Metals and Materials Society*, vol. 58, no. 6, pp. 67–74, 2006.
- [202] M. Renavikar, “Materials technology for environmentally green micro electronic packagin,” *Intel Technology Journal*, vol. 12, pp. 1–15, Feb. 2008.
- [203] Y. Gao and J. Liu, “Gallium-based thermal interface material with high compliance and wettability,” *Applied Physics A: Materials Science & Processing*, vol. 107, no. 3, pp. 701–708, 2012.

- [204] Y.-G. Deng and J. Liu, “Corrosion development between liquid gallium and four typical metal substrates used in chip cooling device,” *Applied Physics A: Materials Science & Processing*, vol. 95, no. 3, pp. 907–915, 2009.
- [205] X. C. Tong, *Advanced Materials for Thermal Management of Electronic Packaging*. No. 30 in Springer Series in Advanced Microelectronics, Springer Science & Business Media, Jan. 2011.
- [206] E. Pop, D. Mann, Q. Wang, K. Goodson, and H. Dai, “Thermal conductance of an individual single-wall carbon nanotube above room temperature,” *Nano Letters*, vol. 6, no. 1, pp. 96–100, 2006.
- [207] P. Kim, L. Shi, A. Majumdar, and P. McEuen, “Thermal transport measurements of individual multiwalled nanotubes,” *Physical Review Letters*, vol. 87, no. 21, pp. 2155021–2155024, 2001.
- [208] M. J. Biercuk, M. C. Llaguno, M. Radosavljevic, J. K. Hyun, A. T. Johnson, and J. E. Fischer, “Carbon nanotube composites for thermal management,” *Applied Physics Letters*, vol. 80, pp. 2767–2769, Apr. 2002.
- [209] H. Huang, C. H. Liu, Y. Wu, and S. Fan, “Aligned carbon nanotube composite films for thermal management,” *Advanced Materials*, vol. 17, pp. 1652–1656, July 2005.
- [210] J. Xu and T. S. Fisher, “Enhancement of thermal interface materials with carbon nanotube arrays,” *International Journal of Heat and Mass Transfer*, vol. 49, pp. 1658–1666, May 2006.
- [211] J. H. Taphouse, T. L. Bougher, V. Singh, P. P. S. S. Abadi, S. Graham, and B. A. Cola, “Carbon nanotube thermal interfaces enhanced with sprayed on nanoscale polymer coatings,” *Nanotechnology*, vol. 24, p. 105401, Mar. 2013.
- [212] R. Cross, B. A. Cola, T. Fisher, X. Xu, K. Gall, and S. Graham, “A metallization and bonding approach for high performance carbon nanotube thermal interface materials,” *Nanotechnology*, vol. 21, p. 445705, Nov. 2010.
- [213] T. Tong, Y. Zhao, L. Delzeit, A. Kashani, M. Meyyappan, and A. Majumdar, “Dense vertically aligned multiwalled carbon nanotube arrays as thermal interface materials,” *Components and Packaging Technologies, IEEE Transactions on*, vol. 30, pp. 92–100, Mar. 2007.
- [214] Y. Ni, H. L. Khanh, Y. Chalopin, J. Bai, P. Lebarry, L. Divay, and S. Volz, “Highly efficient thermal glue for carbon nanotubes based on azide polymers,” *Applied Physics Letters*, vol. 100, p. 193118, May 2012.
- [215] J. H. Taphouse, O. L. Smith, S. R. Marder, and B. A. Cola, “A pyrenylpropyl phosphonic acid surface modifier for mitigating the thermal resistance of carbon nanotube contacts,” *Advanced Functional Materials*, vol. 24, pp. 465–471, Jan. 2014.
- [216] M. Barako, Y. Gao, A. Marconnet, M. Asheghi, and K. E. Goodson, “Solder-bonded carbon nanotube thermal interface materials,” in *2012 13th IEEE Intersociety Conference on Thermal and Thermomechanical Phenomena in Electronic Systems (ITherm)*, pp. 1225–1233, May 2012.
- [217] M. T. Pettes and L. Shi, “Thermal and structural characterizations of individual single, double, and multiwalled carbon nanotubes,” *Advanced Functional Materials*, vol. 19, pp. 3918–3925, Dec. 2009.
- [218] S. Ghosh, D. L. Nika, E. P. Pokatilov, and A. A. Balandin, “Heat conduction in graphene: experimental study and theoretical interpretation,” *New Journal of Physics*, vol. 11, p. 095012, Sept. 2009.
- [219] S. Ghosh, W. Bao, D. L. Nika, S. Subrina, E. P. Pokatilov, C. N. Lau, and A. A. Balandin, “Dimensional crossover of thermal transport in few-layer graphene,” *Nature Materials*, vol. 9, pp. 555–558, July 2010.
- [220] K. M. Shahil, V. Goyal, and A. Balandin, “Thermal properties of graphene: Applications

- in thermal interface materials,” *ECS Transactions*, vol. 35, pp. 193–199, Apr. 2011.
- [221] V. Goyal and A. A. Balandin, “Thermal properties of the hybrid graphene-metal nano-micro-composites: applications in thermal interface materials,” *Applied Physics Letters*, vol. 100, no. 7, p. 073113, 2012.
- [222] K. Uetani, S. Ata, S. Tomonoh, T. Yamada, M. Yumura, and K. Hata, “Elastomeric thermal interface materials with high through-plane thermal conductivity from carbon fiber fillers vertically aligned by electrostatic flocking,” *Advanced Materials*, vol. 26, pp. 5857–5862, Sept. 2014.
- [223] I. Dutta, R. Raj, P. Kumar, T. Chen, C. Nagaraj, J. Liu, M. Renavikar, and V. Wakharkar, “Liquid phase sintered solders with indium as minority phase for next generation thermal interface material applications,” *Journal of Electronic Materials*, vol. 38, no. 12, pp. 2735–2745, 2009.
- [224] H. Yu, L. Li, and Y. Zhang, “Silver nanoparticle-based thermal interface materials with ultra-low thermal resistance for power electronics applications,” *Scripta Materialia*, vol. 66, pp. 931–934, June 2012.
- [225] V. Chliasia, F. Zhou, Y. Sun, L. Huang, and H. Wang, “Design optimization of custom engineered silver-nanoparticle thermal interface materials,” in *Thermal and Thermomechanical Phenomena in Electronic Systems, 2008. ITherm 2008. 11th Intersociety Conference on*, pp. 419–427, May 2008.
- [226] B. Wunderle, M. Klein, L. Dietrich, M. Ras, R. Mrossko, D. May, R. Schacht, H. Oppermann, B. Michel, and H. Reichl, “Advances in thermal interface technology: mono-metal interconnect formation, processing and characterisation,” in *Thermal and Thermomechanical Phenomena in Electronic Systems (ITherm), 2010 12th IEEE Intersociety Conference on*, pp. 1–10, June 2010.
- [227] S. Jayaraman, P. A. Koning, and A. Dani, “Phase change material containing fusible particles as thermally conductive ...,” Aug. 2005. U.S. Classification: 428/323 International Classification: :B23B005/16.
- [228] S. Jayaraman, P. A. Koning, and A. Dani, “Polymer matrices for polymer solder hybrid materials,” June 2011. U.S. Classification: 156/325.
- [229] P. Raj, P. Gangidi, N. Nataraj, N. Kumbhat, G. Jha, R. Tummala, and N. Brese, “Co-electrodeposited solder composite films for advanced thermal interface materials,” *IEEE Transactions on Components, Packaging and Manufacturing Technology*, vol. 3, pp. 989–996, June 2013.
- [230] B. Carlberg, L.-L. Ye, and J. Liu, “Surfaceconfined synthesis of silver nanoparticle composite coating on electrospun polyimide nanofibers,” *Small*, vol. 7, pp. 3057–3066, Nov. 2011.
- [231] B. Carlberg, L.-L. Ye, and J. Liu, “Polymer-metal nanofibrous composite for thermal management of microsystems,” *Materials Letters*, vol. 75, pp. 229–232, 2012.
- [232] A. Bianco, G. Iardino, A. Manuelli, C. Bertarelli, and G. Zerbi, “Strong orientation of polymer chains and small photochromic molecules in polyamide 6 electrospun fibers,” *ChemPhysChem*, vol. 8, pp. 510–514, Mar. 2007.
- [233] Y. Li, Q. Lu, X. Qian, Z. Zhu, and J. Yin, “Preparation of surface bound silver nanoparticles on polyimide by surface modification method and its application on electroless metal deposition,” *Applied Surface Science*, vol. 233, pp. 299–306, June 2004.
- [234] W. Yu and T.-M. Ko, “Surface characterizations of potassium-hydroxide-modified upilex-s polyimide at an elevated temperature,” *European Polymer Journal*, vol. 37, pp. 1791–1799, Sept. 2001.
- [235] F. Delannay, L. Froyen, and A. Deruyttere, “The wetting of solids by molten metals and its relation to the preparation of metal-matrix composites,” *Journal of Materials Science*, vol. 22, no. 1, pp. 1–16, 1987.

- [236] G. Kaptay, “The threshold pressure of infiltration into fibrous preforms normal to the fibers’ axes,” *Composites Science and Technology*, vol. 68, no. 1, pp. 228–237, 2008.
- [237] G. Kaptay and T. Brczy, “On the asymmetrical dependence of the threshold pressure of infiltration on the wettability of the porous solid by the infiltrating liquid,” *Journal of Materials Science*, vol. 40, no. 9-10, pp. 2531–2535, 2005.
- [238] T. Young, “An essay on the cohesion of fluids,” *Philosophical Transactions of the Royal Society Trans. R. Soc.*, vol. 95, 1805.
- [239] M. F. Culpin, “The viscosity of liquid indium and liquid tin,” *Proceedings of the Physical Society. Section B*, vol. 70, pp. 1069–1078, Nov. 1957.
- [240] R. Zhang, J. Cai, Q. Wang, J. Li, Y. Hu, H. Du, and L. Li, “Thermal resistance analysis of sn-bi solder paste used as thermal interface material for power electronics applications,” *Journal of Electronic Packaging*, vol. 136, pp. 011012–011012, Feb. 2014.
- [241] V. Khuu, M. Osterman, A. Bar-Cohen, and M. Pecht, “Considerations in the use of the laser flash method for thermal measurements of thermal interface materials,” *IEEE Transactions on Components, Packaging and Manufacturing Technology*, vol. 1, pp. 1015–1028, July 2011.
- [242] Q. Liang, X. Yao, W. Wang, Y. Liu, and C. P. Wong, “A three-dimensional vertically aligned functionalized multilayer graphene architecture: An approach for graphene-based thermal interfacial materials,” *ACS Nano*, vol. 5, pp. 2392–2401, Mar. 2011.
- [243] W. J. Parker, R. J. Jenkins, C. P. Butler, and G. L. Abbott, “Flash method of determining thermal diffusivity, heat capacity, and thermal conductivity,” *Journal of Applied Physics*, vol. 32, pp. 1679–1684, Sept. 1961.
- [244] R. D. Cowan, “Pulse method of measuring thermal diffusivity at high temperatures,” *Journal of Applied Physics*, vol. 34, pp. 926–927, Apr. 1963.
- [245] H. Lee, *Thermal Diffusivity in Layered Dispersed Composites*. Ph. D. dissertation, Purdue University, 1975.
- [246] T. Y. R. Lee, A. B. Donaldson, and R. E. Taylor, “Thermal diffusivity of layered composites,” in *Thermal Conductivity 15* (V. V. Mirkovich, ed.), pp. 135–148, Springer US, Jan. 1978.
- [247] C.-P. Chiu, J. G. Maveety, and Q. A. Tran, “Characterization of solder interfaces using laser flash metrology,” *Microelectronics Reliability*, vol. 42, pp. 93–100, Jan. 2002.
- [248] T. Chaowasakoo, T. H. Ng, J. Songninluck, M. Stern, and S. Ankireddi, “Indium solder as a thermal interface material using fluxless bonding technology,” in *Semiconductor Thermal Measurement and Management Symposium, 2009. SEMI-THERM 2009. 25th Annual IEEE*, pp. 180–185, Mar. 2009.
- [249] R. Seifert and G. Wassermann, “Composite materials made of metals and polymers - 1.,” *Zeitschrift fuer Metallkunde/Materials Research and Advanced Techniques*, vol. 72, no. 6, pp. 381–390, 1981.
- [250] R. Seifert and G. Wassermann, “Fiber-reinforced composite materials of metals and polymers - 2.,” *Zeitschrift fuer Metallkunde/Materials Research and Advanced Techniques*, vol. 72, no. 12, pp. 854–864, 1981.
- [251] A. Schubert, H. Walter, R. Dudek, B. Michel, G. Lefranc, J. Otto, and G. Mitic, “Thermo-mechanical properties and creep deformation of lead-containing and lead-free solders,” in *International Symposium on Advanced Packaging Materials: Processes, Properties and Interfaces, 2001. Proceedings*, pp. 129–134, 2001.
- [252] H. S. Kim and M. B. Bush, “The effects of grain size and porosity on the elastic modulus of nanocrystalline materials,” *Nanostructured Materials*, vol. 11, pp. 361–367, May 1999.
- [253] M. Klein, A. Hadrboletz, B. Weiss, and G. Khatibi, “The size effect on the stress-strain, fatigue and fracture properties of thin metallic foils,” *Materials Science and Engineering:*

- A, vol. 319321, pp. 924–928, Dec. 2001.
- [254] A. Bar-Cohen and P. Wang, “On-chip thermal management and hot-spot remediation,” in *Nano-Bio-Electronic, Photonic and MEMS Packaging*, pp. 349–429, Springer, 2010.
- [255] J. Bilek, J. K. Atkinson, and W. A. Wakeham, “Thermal conductivity of molten lead-free solders,” *International Journal of Thermophysics*, vol. 27, pp. 92–102, Jan. 2006.
- [256] M. Abtew and G. Selvaduray, “Lead-free solders in microelectronics,” *Materials Science and Engineering R: Reports*, vol. 27, no. 5, pp. 95–141, 2000.
- [257] A. Zribi, A. Clark, L. Zavalij, P. Borgesen, and E. J. Cotts, “The growth of intermetallic compounds at sn-ag-cu solder/cu and sn-ag-cu solder/ni interfaces and the associated evolution of the solder microstructure,” *Journal of Electronic Materials*, vol. 30, pp. 1157–1164, Sept. 2001.
- [258] P. G. Harris and K. S. Chaggar, “The role of intermetallic compounds in lead-free soldering,” *Soldering & Surface Mount Technology*, vol. 10, pp. 38–52, Dec. 1998.
- [259] H. Li, K.-S. Moon, Y. Li, L. Fan, J. Xu, and C. Wong, “Reliability enhancement of electrically conductive adhesives in thermal shock environment,” in *Proceedings - Electronic Components and Technology Conference*, vol. 1, pp. 165–169, 2004.
- [260] J. Due and A. Robinson, “Reliability of thermal interface materials: A review,” *Applied Thermal Engineering*, vol. 50, no. 1, pp. 455–463, 2013.
- [261] J. Klett, R. Hardy, E. Romine, C. Walls, and T. Burchell, “High-thermal-conductivity, mesophase-pitch-derived carbon foams: effect of precursor on structure and properties,” *Carbon*, vol. 38, no. 7, pp. 953–973, 2000.
- [262] M. B. Vázquez-Santos, E. Geissler, K. Lszl, J.-N. Rouzaud, A. Martínez-Alonso, and J. M. Tascn, “Comparative XRD, raman, and TEM study on graphitization of PBO-derived carbon fibers,” *The Journal of Physical Chemistry C*, vol. 116, pp. 257–268, Jan. 2012.
- [263] P. Morgan, *Carbon Fibers and Their Composites*. Taylor & Francis Group, 2005.
- [264] H. O. Pierson, *Handbook of Carbon, Graphite, Diamond, and Fullerenes: Properties, Processing, and Applications*. Noyes Publications, Jan. 1993.
- [265] J. Wang, B. Song, X. Zhang, Y. Song, and G. Wu, “Simultaneous measurements of thermal properties of individual carbon fibers,” *International Journal of Thermophysics*, vol. 32, pp. 974–983, May 2011.
- [266] B. Li, Y. Feng, G. Qian, J. Zhang, Z. Zhuang, and X. Wang, “The effect of gamma ray irradiation on PAN-based intermediate modulus carbon fibers,” *Journal of Nuclear Materials*, vol. 443, pp. 26–31, Nov. 2013.
- [267] T. Taylor and F. L. Yuan, “Thermal stress and fracture in shear-constrained semiconductor device structures,” *IRE Transactions on Electron Devices*, vol. 9, pp. 303–308, May 1962.
- [268] D. B. Miracle, “Metal matrix composites from science to technological significance,” *Composites Science and Technology*, vol. 65, pp. 2526–2540, Dec. 2005.
- [269] E. Della Gaspera, R. Tucker, K. Star, E. H. Lan, Y. S. Ju, and B. Dunn, “Copper-based conductive composites with tailored thermal expansion,” *ACS applied materials & interfaces*, vol. 5, pp. 10966–10974, Nov. 2013.
- [270] J. Bai, Z. Zhang, G.-Q. Lu, and D. Hasselman, “Measurement of solder/copper interfacial thermal resistance by the flash technique,” *International Journal of Thermophysics*, vol. 26, no. 5, pp. 1607–1615, 2005.
- [271] B. A. Cola, J. Xu, C. Cheng, X. Xu, T. S. Fisher, and H. Hu, “Photoacoustic characterization of carbon nanotube array thermal interfaces,” *Journal of Applied Physics*, vol. 101, p. 054313, Mar. 2007.
- [272] X. Zhang, K. K. Yeung, Z. Gao, J. Li, H. Sun, H. Xu, K. Zhang, M. Zhang, Z. Chen,

- M. M. F. Yuen, and S. Yang, "Exceptional thermal interface properties of a three-dimensional graphene foam," *Carbon*, vol. 66, pp. 201–209, Jan. 2014.
- [273] Y. Aoyagi and D. D. L. Chung, "Antioxidant-based phase-change thermal interface materials with high thermal stability," *Journal of Electronic Materials*, vol. 37, pp. 448–461, Apr. 2008.
- [274] E. Yang, H. Guo, J. Guo, J. Shang, and M. Wang, "Thermal performance of low-melting-temperature alloy thermal interface materials," *Acta Metallurgica Sinica (English Letters)*, vol. 27, pp. 290–294, Apr. 2014.
- [275] H. Wang, J. Y. Feng, X. J. Hu, and K. M. Ng, "Reducing thermal contact resistance using a bilayer aligned CNT thermal interface material," *Chemical Engineering Science*, vol. 65, pp. 1101–1108, Feb. 2010.

